# Modelling and Simulation of the Cardiovascular System and the Istanbul Heart Ventricular Assist Device

by

**Khunsha Mehmood**

A Dissertation Submitted to the
Graduate School of Sciences and Engineering
in Partial Fulfillment of the Requirements for
the Degree of

Doctor of Philosophy

in

Mechanical Engineering

KOÇ ÜNİVERSİTESİ

2024

**Modelling and Simulation of the Cardiovascular System and the Istanbul Heart Ventricular Assist Device**

Koç University

Graduate School of Sciences and Engineering

This is to certify that I have examined this copy of a doctoral dissertation by

**Khunsha Mehmood**

and have found that it is complete and satisfactory in all respects,
and that any and all revisions required by the final
examining committee have been made.

Committee Members:

_____

Prof. Dr. İsmail Lazoğlu

_____

Prof. Dr. Deniz Süha Küçükaksu

_____

Prof. Dr. Vedat Bakuy

_____

Prof. Dr. Özlem Yalçın

_____

Assoc. Prof. Dr. Levent Beker

Date: _____

*This thesis is dedicated to my father, Amjad Mehmood, whose sacrifices and love are engraved in the pages of this work, forevermore.*

# ABSTRACT

**Modelling and Simulation of the Cardiovascular System and the Istanbul Heart Ventricular Assist Device**
**Khunsha Mehmood**
**Doctor of Philosophy in Mechanical Engineering**
**2024**

Heart transplantation rates are limited due to high donor heart rejection rates and the rising number of heart failure (HF) patients due to a growing and ageing population. Left Ventricular Assist Devices (LVADs) are increasingly being implanted as a buttress against advanced-stage heart failure. However, they are associated with a multitude of complications. LVAD design and development is a thorough process involving many steps before they can acquire approval from regulatory bodies, involving virtual testing in-silico, verification of the results in-vitro, validation of performance in animals, i.e., in-vivo, and ultimately clinical trials. As we progress along its different phases, the development process becomes more complex, less controllable, and more costly. Under such circumstances, reliable pre-clinical evaluation becomes imperative. The current work makes use of two pre-clinical models namely numerical modelling and mock circulatory loops. An intuitive and knowledge-based approach to numerical modelling is adopted whereby model components are connected in a topological manner without explicitly coding model equations. Mathworks' Simscape$^{TM}$ modelling environment is used to develop a comprehensive and real-time executable model of the cardiovascular system (CVS) and the Istanbul Heart (iHeart) VAD. The CVS model is developed by combining existing models and the VAD model is an analytically-derived model calibrated using iHeart VAD's characteristic data. A baseline is established by calibrating the CVS model with healthy heart parameters. Parameters for Dilated Cardiomyopathy (DCM), a subset of Heart Failure with Reduced Ejection Fraction (HFrEF), are collected from published patient data and disease modelling is conducted using statistically pooled values. To simulate iHeart VAD support, it is anatomized to the left ventricle apex and the ascending aorta in Simscape$^{TM}$. CVS-VAD modelling is applied for in-silico

adaptation of hemodynamic ramp testing, an invasive clinical procedure which can potentially support clinical decision-making before conducting such an invasive procedure by exploring the possibility of improvements preemptively. It is also used to conduct a full factorial design of experiments to study the functional relationships between CVS parameters and LVAD suction speed which can be used to guide the development of suction detection and avoidance control algorithms. CVS-VAD model is also used to develop a numerical-hydraulic hybrid mock circulatory loop to study the behaviour of the iHeart VAD in-vitro. The adopted modelling approach results in a more realistic replication of the physiological environment an LVAD is exposed to. A comprehensive framework for the pre-clinical evaluation of mechanical circulatory support devices is provided. Due to its object-oriented and modular nature, the featured model can be readily modified for other cardiovascular diseases. In addition to facilitating LVAD research, the presented work provides a teaching tool for understanding the pathophysiology of heart failure, diagnosis rationale, and degree of assist requirements. Utilization of in-silico and in-vitro approaches provide complementary information, allowing device behaviour and performance prediction and enhancing model accuracy.

# ÖZETÇE

**Kardiyovasküler Sistem ve İstanbul Kalp Ventriküler Destek Cihazının Modellenmesi ve Simülasyonu**
**Khunsha Mehmood**
**Makina Mühendisliği, Doktora**
**2024**

Kalp nakli oranları, donör kalp reddi oranlarının yüksek olması ve artan ve yaşlanan nüfusa bağlı olarak kalp yetmezliği (KY) hastalarının sayısındaki artış sebebiyle sınırlıdır. Sol Ventrikül Destek Cihazları (SVDC'lar), ileri evre kalp yetmezliğine karşı bir destek olarak giderek daha fazla implante edilmektedir ancak, birçok komplikasyonla ilişkilendirilmişlerdir. SVDC tasarımı ve geliştirmesi, düzenleyici kurumlardan onay almadan önce, in-siliko sanal testler, in-vitro sonuçların doğrulanması, hayvanlarda performansın doğrulanması ve son olarak klinik denemeleri içeren cok adimli kapsamlı bir süreçtir. Farklı aşamalarda ilerledikçe, geliştirme süreci daha karmaşık, daha az kontrol edilebilir ve daha maliyetli hale gelir. Bu tür koşullar altında, güvenilir ön klinik calismalari kaçınılmaz hale gelir. Mevcut çalışma, sayısal modelleme ve mock circulatory loops olmak üzere iki ön klinik modelden faydalanmaktadır. Sayısal modellemede sezgisel ve bilgiye dayalı bir yaklaşım benimsenir; burada model bileşenleri, model denklemlerini açıkça kodlamadan topolojik bir şekilde bağlanır. Mathworks'ün Simscape modelleme ortamı, kardiyovasküler sistem (CVS) ve İstanbul Kalp (iHeart) VAD'ın kapsamlı ve gerçek zamanlı yürütülebilir bir modelini geliştirmek için kullanılmıştır. CVS modeli, mevcut modellerin birleştirilmesiyle geliştirilirken, VAD modeli, iHeart VAD'ın karakteristik verileri kullanılarak kalibre edilmiş analitik bir modeldir. CVS modelinin sağlıklı kalp parametreleriyle kalibre edilmesiyle bir başlangıç noktası oluşturulur. Genişlemiş Kardiyomiyopati (DCM) için parametreler, Azalmış Ejeksiyon Fraksiyonlu Kalp Yetersizliği (HFrEF) alt kümesi için yayınlanmış hasta verilerinden toplanır ve hastalık modellemesi istatistiksel olarak havuzlanmış değerler kullanılarak gerçekleştirilir. iHeart VAD desteğini simüle etmek için, Simscape'te sol ventrikül apeksine ve çıkan aorta anatomize edilir. CVS-VAD modellemesi, invazifklinik bir prosedür olan hemodinamik ramp testinin

in-siliko adaptasyonu için uygulanır;böyle invazif bir prosedürü gerçekleştirmeden önce klinik karar verme sürecini destekleyebilir ve iyileştirmelerin mümkün olup olmadığını önceden araştırarak potansiyel olarak klinik kararları destekleyebilir. Ayrıca, CVS parametreleri ile SVDC emiş hızı arasındaki işlevsel ilişkileri incelemek için tam faktöriyel deney tasarımı yapmak için kullanılır. Emiş tespiti ve avoidance control algorithmin geliştirilmesine rehberlik etmek için kullanılabilir. CVS-VAD modeli ayrıca, iHeart VAD'ın in-vitro davranışını incelemek için numerical-hydraulic hybrid mock circulatory loop geliştirmek için de kullanılır. Benimsenen modelleme yaklaşımı, bir SVDC'nın maruz kaldığı fizyolojik ortamın daha gerçekçi bir şekilde çoğaltılmasına yol açar. Mekanik dolaşım desteği cihazlarının ön klinik değerlendirmesi için kapsamlı bir çerçeve sunulmaktadır. Nesne yönelimli ve modüler yapısı nedeniyle öne çıkan model, kolayca diğer kardiyovasküler hastalıklar için de değiştirilebilir. SVDC araştırmalarını kolaylaştırmanın yanı sıra, sunulan çalışma kalp yetmezliği patofizyolojisini anlama, tanı kriterleri ve yardım gereksinimleri derecesini anlama konusunda bir öğretim aracı sağlar. İn-siliko ve in-vitro yaklaşımların kullanılması, cihaz davranışı ve performans öngörüsü sağlar ve model doğruluğunu artırarak tamamlayıcı bilgiler sunar.

# ACKNOWLEDGMENTS

I would like to extend my heartfelt gratitude to my supervisor Prof. Dr. Ismail Lazoglu whose continuous support, timely guidance, and insightful suggestions served as invaluable assets in my doctoral journey. I would also like to thank my honorable committee members Prof. Dr. Deniz Suha Kucukaksu, Prof. Dr. Vedat Bakuy, Prof. Dr. Ozlem Yalcin, and Asst. Prof. Dr. Levent Beker, for taking the time to read my work and generously providing their knowledge and expertise. I am also grateful to my colleagues at the Manufacturing and Automation Research Center Hammad ur Rahman, Farouk Abdulhamid, Omer Subasi, and Atacan Oral, who have been great companions in what can often feel like a lonely journey.

I could not have undertaken this endeavor without my friends Munam Arshad, Ayesha Gulzar, Palwisha Akhtar, Esra Akman, Azmatullah, and Denizhan Korkut, for they have always been there to share in my joys and sorrows and have always been in my corner. I would also like to extend my deepest gratitude to Qasim Khadim and Serban Gheta for offering their mentorship and friendship when I needed it most.

Words cannot express my gratitude for my family. I am indebted to my parents for their unflinching support and unconditional love, and grateful to my sisters for cheering me on. I would be remiss in not mentioning my cats who have been a constant source of joy and emotional support. Last but not the least, I am extremely grateful to my husband, Farjad Zafar, whose love, patience, and understanding were instrumental in the completion of this work.

# TABLE OF CONTENTS

# LIST OF TABLES

# LIST OF FIGURES

# ABBREVIATIONS

| | |
|---|---|
| ADC | Analogue to Digital Class |
| Ao | Aorta |
| AoP | Aortic Pressure |
| ASD | Atrial Septal Defect |
| AV | Aortic Valve |
| BP | Blood Pressure |
| BTR | Bridge to Recovery |
| BTT | Bridge to Transplant |
| CO | Cardiac Output |
| CVD | Cardiovascular Disease |
| CVP | Central Venous Pressure |
| CVS | Cardiovascular System |
| DCM | Dilated Cardiomyopathy |
| DoE | Design of Experiments |
| ER | Eccentric Remodelling |
| EF | Ejection Fraction |
| FGPA | Field Programmable Graphic Array |
| HF | Heart Failure |
| HFpEF | Heart Failure with Preserved Ejection Fraction |
| HIL | Hardware in the loop |
| HMCL | Hybrid Mock Circulatory Loops |
| HR | Heart Rate |

| | |
|---|---|
| HRT | Hemodynamic Ramp Testing |
| HRAEs | Hemocompatibility Related Adverse Events |
| HVAD | HeartWare Ventricular Assist Device |
| iHeart | Istanbul Heart |
| LAP | Left Atrial Pressure |
| LHF | Left Heart Failure |
| LPM | Lumped Parameter Models |
| LSQ | Least Square |
| LV | Left Ventricle |
| LVADs | Left Ventricular Assist Devices |
| LVCO | Left Ventricular Cardiac Output |
| LVEDV | Left Ventricular End Diastolic Volume |
| LVESV | Left Ventricular End Systolic Volume |
| LVP | Left Ventricular Pressure |
| LVV | Left Ventricular Volume |
| MAP | Mean Atrial Pressure |
| MCS | Mechanical Circulatory Support Systems |
| MLBX | MicroLabBox |
| MLR | Multiple Linear Regression |
| MRI | Magnetic Resonance Imaging |
| NLHW | Nonlinear Hammerstein-Wiener |
| P-V | Pressure-Volume |
| PCWP | Pulmonary Capillary Wedge Pressure |
| PVR | Pulmonary Vascular Resistance |
| PWM | Pulse Width Modulation |

| | |
|---|---|
| RBP | Rotary Blood Pumps |
| RHF | Right Heart Failure |
| RTI | Real Time Interface |
| SISO | Single Input Single Output |
| SV | Stroke Volume |
| TAG | Transaortic Gradient |
| VAD | Ventricular Assist Device |
| VSD | Ventricular Septal Defect |

# Chapter 1

# INTRODUCTION

## *1.1 Background*

Left Ventricular Assist Devices (LVADs) are mechanical circulatory support systems (MCS) that supplant the function of the native left ventricle of a weakened heart. These small but revolutionary therapeutic devices have been around since the mid 1960s with Dr. DeBakey first successfully implanting an LVAD in a 37-year old patient for post-cardiotomy support in 1966 [10]. Since then, LVADs have evolved through generations (Figure 1.1). 1$^{st}$ Gen LVADs were pneumatically or electrically-driven pulsatile devices. The first LVAD comprised a polyurethane pump housed in a titanium frame, with inflow-outflow valves and pusher plates replacing polyurethane pumps in later iterations [11]. They were *volume displacement pumps* that generated flow via unidirectional valves mimicking native heart pulsatility aimed at long-term support i.e., as a bridge-to-transplant (BTT). While the 1$^{st}$ Gen represent a significant leap in post-advanced-stage heart failure life expectancy, they were also accompanied by a substantial amount of unfavorable factors including but not limited to being bulky enough to compress patients' stomachs, having limited battery-life, proneness to mechanical malfunctioning, imposing a high risk of thrombosis, bleeding, and infection [12].

The next generation of LVADs was aimed at addressing the issues of their predecessors. Circulation in 2$^{nd}$ Gen LVADs was driven by single axial rotary motor pumps. Pulsatile flow generated by volume displacement was replaced by non-physiologic continuous flow which eliminated the need for valves or compliance chambers [13]. These alterations allowed for miniaturisation of the device, reducing

the risk of mechanical malfunction, boosting durability and patient quality of life [14]. However, a still-high number of mechanical surfaces made 2nd Gen LVADs more prone to clotting cascade activation thereby necessitating an excessive use of anticoagulants which posed an increased risk of bleeding [15].

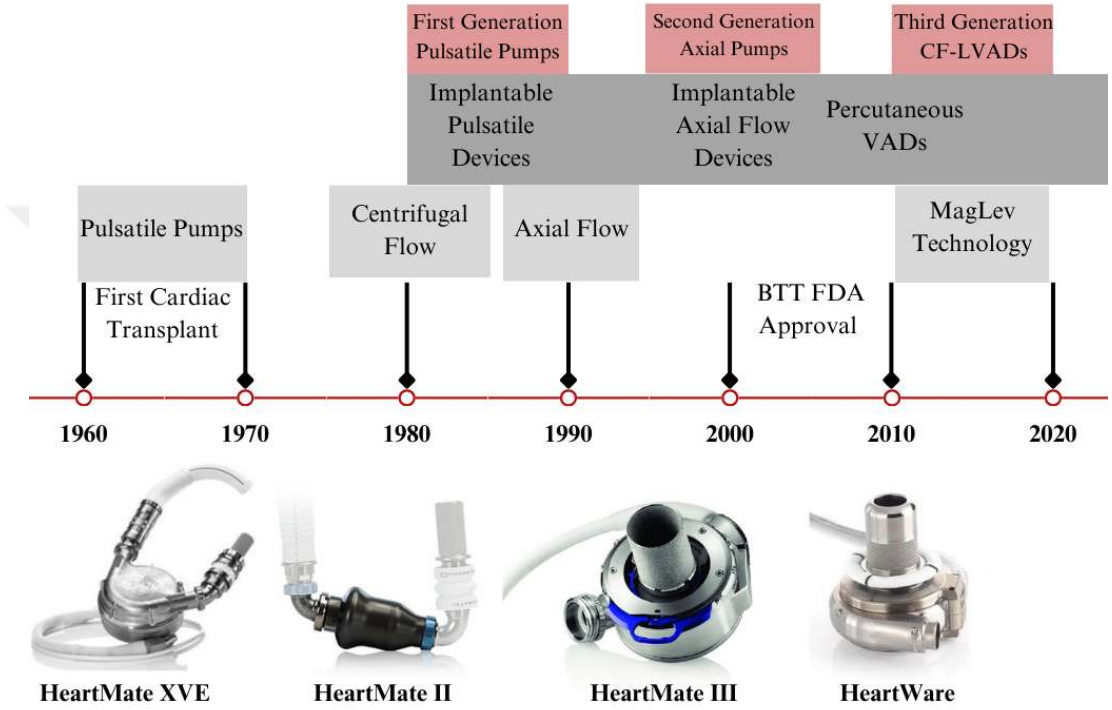


Figure 1.1: The evolution of LVADs across three generations [1].

The third or *current* generation of LVADs operate with continuous centrifugal flow featuring contact-less bearings harnessing the power of magnetic levitation (MagLev) technology [16]. Contemporary LVADs, with fewer moving components and minimum contact of blood with mechanical surfaces, aim to reduce thrombus incidents. Thrombosis in HeartMate III, a 3rd Gen LVAD with bearing-less MagLev design, is a rarity with no cases reported by 2018 [14], and one case requiring pump exchange reported in 2022 [17]. However, despite significant design modifications leading to further miniaturisation, shorter drivelines, wider flow passages

and programmatically activated pulsatile flow modes, LVADs are associated with a plethora of complications including bleeding, hemocompatibility related adverse events (HRAEs), stroke, ventricular arrhythmia, and aortic insufficiency to name a few [18].

Owing to the challenges associated with LVAD therapy, these devices have been the subject of extensive research for the last couple of decades with different research groups across the globe striving to optimize and subsidize the design of this life-saving marvel of biomedical engineering. The ultimate goal is to design a regulation-compliant life-saving device that is widely and readily accessible.

The design and development process involves virtual testing *in silico*, verification of the results *in vitro*, validation of performance in animals, i.e., *in vivo* and *ex vivo*, and ultimately, clinical trials. As we progress along its different phases, the development process becomes more complex, less controllable, and more costly. Under such circumstances, model-based design becomes imperative. An optimized approach entails adding detail to the earlier pre-clinical models in the design process to save time and minimize design changes at the more advanced ones. Thus, extensive *in silico* and *in vitro* simulations help optimize device parameters leading to accelerated development and less iterations following the physical prototype build.

## *1.2 Problem Statement*

The challenges to using LVADs in advanced-stage heart failure patients as a destination therapy, bridge-to-transplant, and in some fortuitous cases, bridge-to-recovery, require rigorous investigations into design optimization via modelling and simulation. The current work aims to develop an *in silico* model of the cardiovascular system (CVS) and an experimental prototype of the Istanbul Heart Ventricular Assist Device (iHeart VAD). The study is further extended to *in vitro* testing via a numerical-mechanical hybrid mock circulatory loop to assess the effectiveness of LVAD interventions in heart failure scenarios.

### *1.3 Aims and Objectives*

The primary aim of this study is to develop a comprehensive framework for the pre-clinical evaluation and testing of left ventricular assist devices in conformity with the model-based design concept, while specific objectives include:

- To develop detailed real-time executable object-oriented model of the CVS and the device under test.
- To model heart failure by identifying the most pertinent heart failure parameters and their realistic ranges for different degrees of disease severity.
- To develop a hardware-in-the-loop setup (HIL) using the cardiovascular model as the *software* and a prototype of the Istanbul Heart VAD as the *hardware*.

### *1.4 Scope and Limitations*

The presented work encompasses a comprehensive, real-time executable model of the CVS and an analytically derived LVAD model calibrated using characteristic data for the Istanbul Heart VAD prototype 1. Advanced-stage heart failure is simulated using realistic values of pertinent heart failure parameters obtained statistically from published patient data. A mock circulatory HIL setup is developed using object-oriented model to study LVAD behavior under different pathophysiological conditions. For real-time executability, a zero-dimensional lumped parameter model is developed in an acausal modelling environment.

In this research, all hemodynamic parameters apart from the atria and ventricles, have been assumed to be constant within the cardiac cycle. Real-time execution performance of the model is also subject to limitations due to its high numerical stiffness. Hence, the systemic venous resistance, short term arterial pressure control, drug intervention, compliance auto-regulation and cardiac auto-regulation are not included. Real-time executability necessitates the reduction of rapid changes and reducing system stiffness which is not only impracticable due to the transitory nature of the CVS but also precludes the possibility of incorporating auto-regulation.

Furthermore, the current setup has been developed to test the Istanbul Heart VAD prototypes, a continuous flow LVAD. Testing pulsatile VADs requires additional components outside the scope of the study. Lastly, echocardiographic assessments and clinical validation of the framework is beyond the scope of the current work and a statistical approach is instead adopted for validation.

## *1.5 Thesis Outline*

The thesis is organized as follows; a *Literature Review* chapter covering the significance of the study, modelling of the CVS and LVAD, etiology of the simulated heart failure condition, and mock circulatory loops, a *Materials and Methods* chapter describing the modelling and simulation approach, data curation and statistical compilation, applications of the model (*in silico* Hemodynamic Ramp Testing (HRT) and suction detection), and development of the mock circulatory HIL setup, followed by a *Results* chapter consisting of the results of different *in silico* and *in vitro* simulations, followed by a *Conclusion* chapter, a chapter containing the references cited throughout the thesis, and supplementary materials in the *Appendix*.

# Chapter 2

# LITERATURE REVIEW

Based on the findings delineated in a report conducted by the European Heart Network, the documented surge in heat failure incidence stands as a substantive and escalating health challenge in both the European Union (EU) and Europe at large. Despite the reported reduction in mortality rates attributed to cardiovascular disease (CVD), the statistics still indicated a mounting prevalence of heart failure, primarily propelled by demographic aging and an augmented occurrence of concurrent health conditions, such that at the time of reporting, CVD accounted for 37% of all deaths in the EU and 45% of all deaths in Europe [19].

The gold standard for advanced stage heart failure treatment is to carry out a transplantation, however, transplantation comes with its own set of complications including high donor rejection rates. 10-20% of complications in heart transplant arise from anti-body mediated rejection [20], while rejection rates are elevated due to donor alcoholism and chronic diseases [21]. Coupling the uncertainty of a successful heart transplant with a long backlog in the donor waiting list, it becomes imperative to have an interim solution that can serve either as a bridge to recovery (BTR), such that a CVD patient no longer needs a transplant or as a bridge to transplant (BTT), in order to afford enough time to find a suitable donor.

Currently, the most popular interim solution is the use of LVADs. However, as with all biomedical technologies, LVADs are both challenging to design and even more arduous to obtain the FDA approval for. A powerful mitigation strategy, under these circumstances, is the use of model-based design. This approach allows one to aptly understand the problem and rapidly troubleshoot and iterate through the design process using simulations.

While, model-based design allows one to test and reiterate designs without the need of physical prototypes earlier in the design process, once an optimal solution is reached, it is imperative to fabricate and test the working prototype. However, testing of prototype comes with its own set of ethical concerns regarding animal trials and very high costs of clinical trials. One mitigation strategy adopted by designers is to make use of mock circulatory loops, which can imitate the behavior of a human cardiovascular system by making use of a carefully designed hardware system.

Nonetheless, a complete emulation of the cardiovascular system can be cumbersome and have limited applications, hence, a versatile solution lies in hybrid mock circulatory loops (HMCL), which allow testing of a working prototype with a cardiovascular system model. HMCLs are, in effect, a hardware in the loop solution which allows the design and testing of an LVAD prototype under different pathophysiological scenarios.

## *2.1 Cardiovascular System Modelling*

Modellers develop mathematical representations of complex systems by methodically encoding our comprehension of their underlying structure and response to external as well as internal stimuli. Mathematical models in biomedical research are indispensable tools that allow researchers to study, document, control, and communicate the complex behaviour biomedical systems being studied[22]. Numerical models also enable medical students to study the operative relationships among different parameters of systems that govern human and animal physiology [3, 23, 4, 24]. Numerical modeling has contributed to cardiovascular research significantly by enabling researchers to simulate and predict cardiovascular events [25, 26, 27], evaluate the performance of cardiovascular devices [28, 29, 30], provide valuable perspectives for clinical research and treatment of CVDs [31, 32].

CVS models have evolved over the course of over a century. Some of the most significant cardiovascular models in the last century are depicted in Figure 2.1. The chronological and dimensional development of cardiovascular model starts from 1899 when German physiologist Otto Frank, expounding the ideas of Stephen Hales

(1733), published his pioneering work on the *Windkessel* model which marks one of the first attempts to describe arterial circulation mathematically [33]. This seminal work on cardiovascular modelling has influenced subsequent models that researchers proceeded to develop in the following decades.

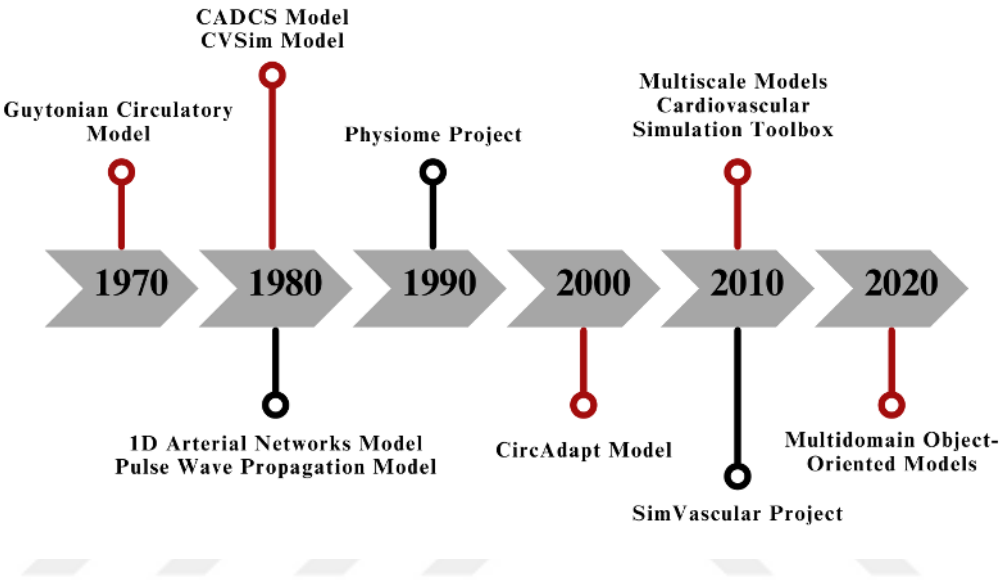


Figure 2.1: Cardiovascular system modelling over the years (zero-dimensional models in red).[2, 3, 4, 5, 6, 7]

Arthur C. Guyton began developing the Guytonian Circulatory Model in the 1950s the refinement of which extended into the following decades [8, 34]. Guyton lumps hemodynamic parameters on the basis of electrical analogue representations whereby pressure, flow, and volume in the circulatory circuit are analogous to voltage, current, and charge in an electrical circuit, respectively (Figure 2.2). The Guytonian model, with more than 359 variables, offers a holistic view of the cardiovascular system and its regulation [2]. It captures the interactions between venous circulation, blood volume, arterial pressure, and cardiac output, and also demonstrates the influence of renal balances on long-term pressure control [35]. From a dimensional viewpoint, the Guytonian model in its *lumped parameter* form is a zero dimensional (0-D) model.

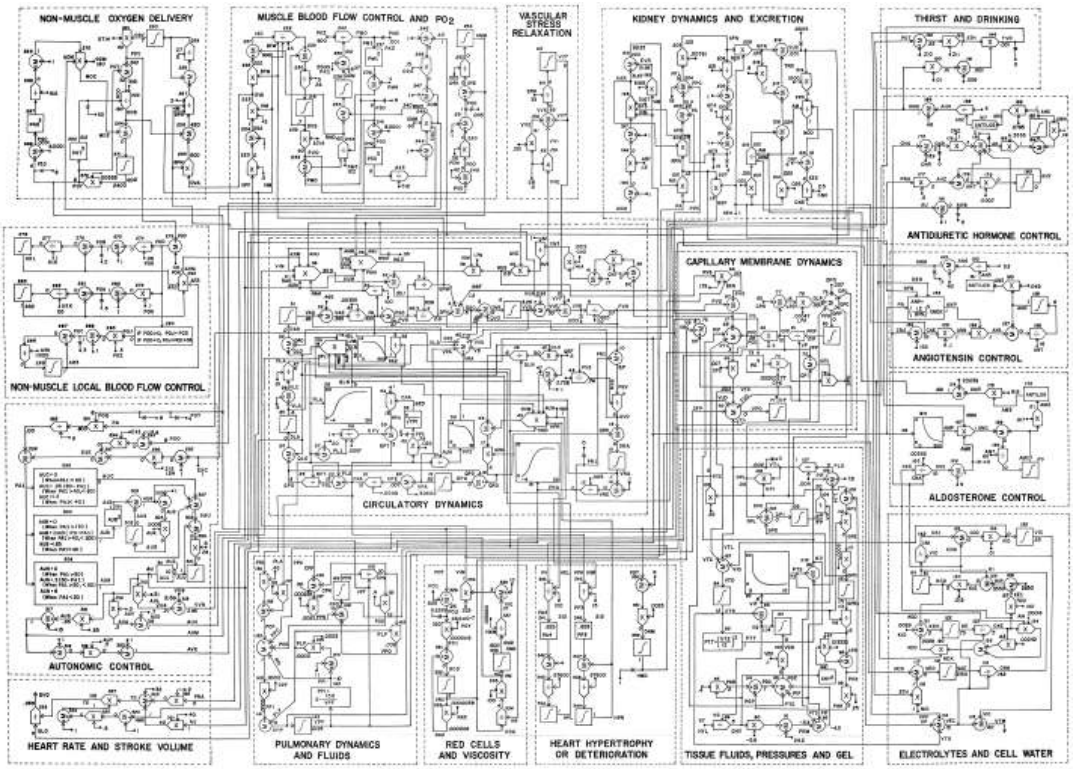


Figure 2.2: The Guytonian Circulation Model reprinted with permission from *Annual Review of Physiology* [8]

### *2.1.1 Zero Dimensional Modelling*

0-D or Lumped Parameter Models (LPM) are used when the temporal distribution of the fundamental variables of the CVS (i.e., pressure, volume, and volumetric flowrate) is adequate, and knowledge of their spatial distribution is superfluous. In essence, 0-D models serve as simplified abstractions of spatially and temporally distributed real-world artefacts, that capture system-level interactions. Therefore, 0-D models composed of ordinary differential equations with algebraic constraints (also referred to as *Differential-Algebraic Equations*) are used extensively in cardiovascular research to compute pressure-volume loops, cardiac output, stroke work, ejection fractions etc.. A widely used classical 0-D model (detailed description in Chapter 3.1) is the variable elastance model, which takes temporal distribution of ventricular and atrial elastance into account. Avanzolini et al. developed a flexi-

ble 0-D closed-loop model of the CVS in an interactive FORTRAN program called SIMNON, that simulates not only the basal steady-state hemodynamics but also the transient circulatory condition induced by an acute variation in peripheral resistance [36]. 0-D models find a wide array of applications including but not limited to arterial flow analysis [37], hemodynamic response under healthy and diseased conditions [38], surgical and therapeutic interventions [39], cardiac assist device support [40], as boundary conditions for higher dimensional cardiovascular simulations [41] etc.

0-D models have served as powerful didactic tools enabling real-time simulation of CVS dynamics under different physiological and pathophysiological scenarios. CircAdapt models the CVS as a series of modules emulating heart chambers, blood vessels, valves and the peripheral vasculature. A unique feature of this tool is that it can structurally adapt the vascular and myocardial tissues to the self-generated mechanical load [4]. Another CVS model developed and used for pedagogical purposes is MIT and Harvard Medical School's CVSim lumped parameter model that also makes use of electrical circuit analogy for the circulation circuit [3]. Different open-source versions of CVSim are available that feature six or more compartments and control models like arterial baroreflex or short-term pressure regulation depending upon the version. Applications of CVSim include system identification of regulatory mechanisms like baroreflex control, estimation of hemodynamic parameters, cardiac arrhythmia studies, investigation of hemodynamic implications of re-entry maneuvers into the Earth's atmosphere etc., to name a few.

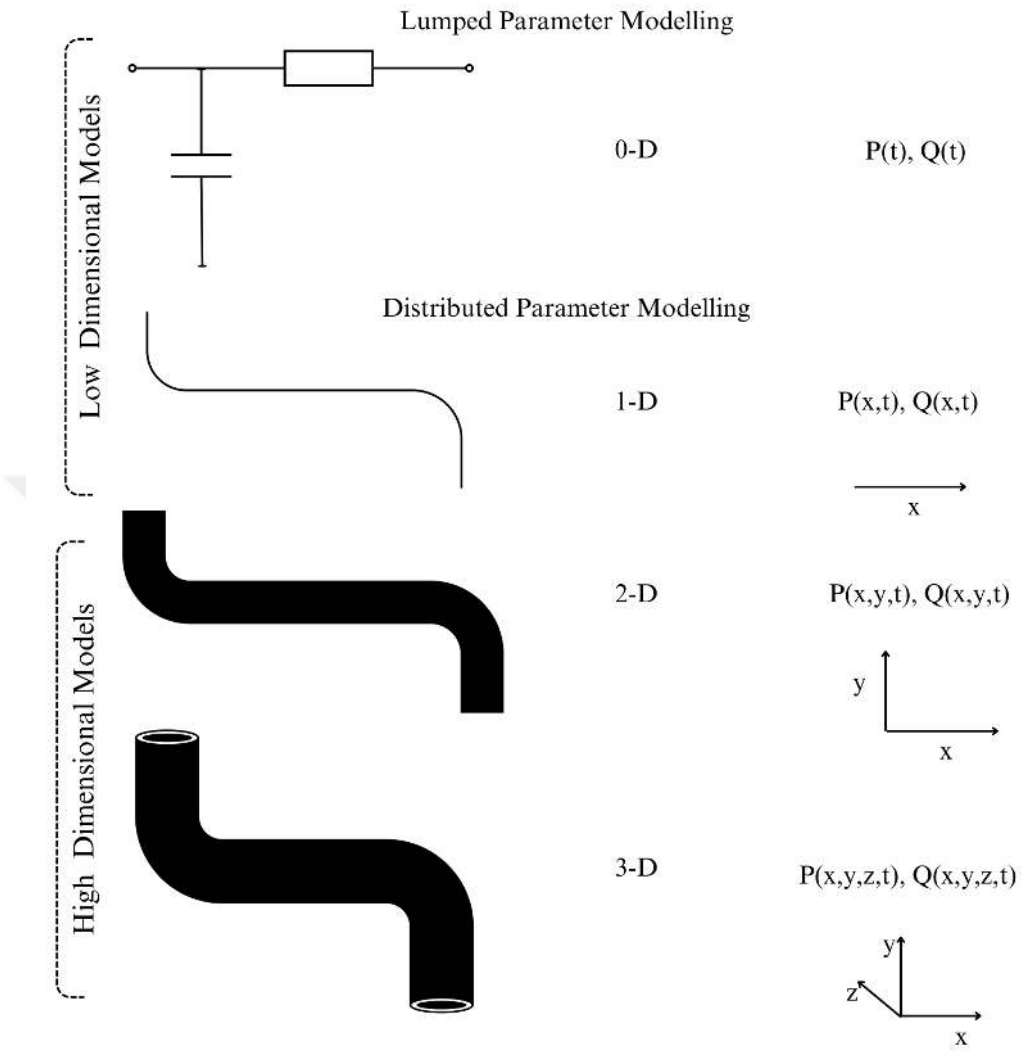


Figure 2.3: Modelling Dimensions.

### *2.1.2 Higher Dimensional Modelling*

0-D models are described by ordinary differential equations whereas higher order models are described by partial differential equations. Key circulation features like pressure-axial velocity relation along with their spatial and temporal derivatives [42], relationship between and effect of forward and backward travelling waves [43] can be captured and analyses like wave intensity analysis for left ventricle (LV), coronary vessels, and systemic and pulmonary arteries can be conducted by moving to one dimensional models (1-D) [7]. Governed by axisymmetric solutions to 3-D Navier-

Stokes equations, first order models regard blood vessels as tapered tubes with pressure and flow propagating through them as pulsating waves carrying information and are therefore called *Pulse Wave Propagation Models* or *1D Arterial Networks Models* [44]. Assuming a radial distribution of axial velocity, 1-D models can capture wave transmission in the CVS without the cost of 3-D representations [7]. Anliker at al. conducted a systematic study of the different components of the vasculature to synthesize a comprehensive description of the arterial system using the method of characteristics [45] in the 70s [46, 47]. 0-D models are in effect a special case of one dimensional (1-D) modes. Vessel network 0-D models can be considered as $1^{st}$ order discretisations of 1-D linear models which can be interpreted in terms of the 0-D model electrical analogues [48].

Moving to higher dimensions entails an increase in spatial complexity with 2-D models rendering cross-sectional views of vessels to represent blood flow patterns and interactions with vessel walls across a 2-D plane. 2-D models allow researchers to study localized phenomenon like blood flow patterns [49], vessel bifurcation [50] and to simulate echocardiograms [51]. 3-D models give the most complete representation of vascular anatomy by incorporating length, width, and depth to represent vessel geometry, branching patterns, and 3-D distribution of pressure and flow. Advances in clinical research have benefited heavily from open-source computational modelling software like SimVascular which is allows for patient-specific CVS modelling and simulation through an end-to-end pipeline from medical imaging data to 3-D model development and hemodynamic simulation [23].

### *2.1.3 Multiscale Modelling*

Multiscale modelling has been studied extensively in recent years in order to accurately represent both local and systemic features of the CVS using limited computational resources. Researchers have attempted to achieve this by incorporating multiple spatio-temporal scales in physiological models, which was first undertaken by Quateroni et al. [52]. Models pose different mathematical characteristics at different scales: ordinary differential equations govern 0-D models, hyperbolic par-

tial differential equations govern 1-D models, and highly nonlinear Navier-Stokes equations govern 2-D/3-D models. To create comprehensive cardiovascular system models, 0-D LPMs are integrated with 1-D, 2-D, and/or 3-D models whereby local hemodynamics is computed in a detailed 3-D organ model, with boundary conditions supplied by 0-D or 1-D models [53, 54]. A boundary condition must be set for all sides of each multi-scale model, since blood flow is often subcritical. Pressure or flowrate boundary conditions can be applied directly to 0-D models. The boundary conditions for 1-D, 2-D, or 3-D models can be specified by variables, their derivatives, or linear combinations of variables [7].

When discussing multiscale cardiovascular modelling this review would be remiss in not mentioning the Cardiac Physiome, a subset of the broader Physiome Project, that provides an open-source framework for the development of modelling standards, computational tools and databases. It calls for international for the development of mathematical models for interpreting experimental/clinical data and guiding new experiments, treatments, and interventions [55].

### *2.1.4 Object-Oriented Modelling*

0 or 1-D models based on analytical methods offer an optimal solution for hemodynamic simulations of sizeable sections of the CVS, to encapsulate the global properties of the CVS network without incurring high computational cost [56]. We have a range of programming tools to carry out low-dimensional modelling and simulation. Modelling approaches are further classified into two categories i.e., causal modelling and acausal modelling. Using causal models one explicitly codes system equations or their block diagrammatic renditions [57] with little reference to the underlying physiology that governs the system. Acausal modelling, on the contrary, offers an object-oriented solution. System components in acausal models are connected topologically, based on the intrinsic structure of the physical system [58]. The most significant advantage of acausal models is that it renders convoluted circuit analysis, formulation of DAEs, and explicit coding, trivial. A good instance of this can be found in the works of Peskin, whereby a single resistance element

connecting cardiac chambers was used to simulate congenital heart defects such as atrial or ventricular septal defects (ASD, VSD) (Figure 2.4) [9].

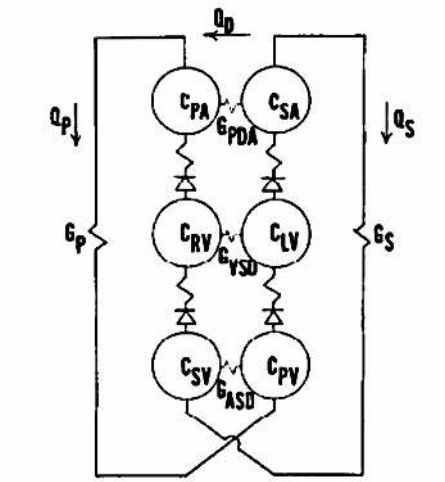


Figure 2.4: Peskin's heart model to simulate congenital heart diseases: patent ductus arteriosus, ventricular septal defect, or atrial septal defect [9]. Reprinted with permission from *Computers in Biology and Medicine*.

System equations can be formulated automatically using acausal modelling tools like Simscape$^{TM}$, making these models relatively more reusable, customizable and composable. Using acausal modelling, researchers can develop knowledge-based, readily interpretable, and and modifiable models, facilitating collaboration in multidisciplinary fields like biomedical engineering. Thus, acausal modeling, with its emphasis on modular design, multiphysics considerations, and efficient scaling of individual components into complete systems, offers significant advantages over causal modeling across a variety of domains [59], making it a preferred approach for CVS modelling and simulation.

Acausal CVS models offer valuable insights into the physiological and pathophysiological conditions of the cardiovascular system, contributing to advancements in cardiovascular research and treatment [60, 61]. Simscape$^{TM}$ has been used to

develop the 0-D CVS models in the electric [62] and the hydraulic domains [56]. Ortiz-León et al. developed the most recent version of the Cardiovascular Simulation Toolbox using SimPowerSystems (previous name for the electrical module of Simscape$^{TM}$) [5]. Simscape$^{TM}$ models have been used to model and simulate aortic stenosis (AS) [63], heart failure with preserved ejection fraction (HFpEF) [64], and multi-domain MCS simulations in axial flow pump-implanted HFpEF patients [6].

### *2.1.5 Pathophysiological Modelling*

The pathophysiology of heart failure is often the subject of oversimplification in cardiovascular simulations. Researchers often model heart failure by an arbitrary variation of their subjective choice of CVS model parameters [62]. Choi et al. modelled a change in preload by increasing the Pulmonary Vascular Resistance (PVR) from 0.02 mmHg s mL$^{-1}$ to 0.5 mmHg s mL$^{-1}$ [65]. Shi et al. simulated an impaired LV by reducing the value of the maximum elastance $E_{max}$ from the normal value of 2.5 mmHg mL$^{-1}$ to 0.5 mmHg mL$^{-1}$ [66]. Son et al. [67] also adopt the same approach from Faragallah et at. [68] by taking $E_{max} = 2$ mmHg mL$^{-1}$ as a threshold for *normal* cardiac function and $E_{max} < 2$ mmHg mL$^{-1}$ for the pathological case. Ghosh *et al.* adopt a similar approach in a multiscale CVS model whereby idiopathic dilated cardiomyopathy (DCM) is simulated by varying parameters at the protein (K4 binding affinity), cellular (extracellular calcium concentration), and organ (LV elastance) levels [69].

Cardiac failure pathophysiology involves accelerated changes in the heart function that attempt to sustain arterial blood pressure and cardiac output through compensatory processes but often aggravate the symptoms over time [70]. For pathophysiological modelling, we must first classify heart failure syndromes—an evolving area of research with the currently established cases being compared with the tip of an iceberg [71]. HFrEF has been a prevalent heart failure syndrome with HFpEF reported to have become even more prevalent in recent years [72]. Cardiomyopathies occupy a significant percentage of HFrEF cases with the most common being Dilated Cardiomyopathy (DCM) [73] and Eccentric Remodelling (ER) ailing a majority of

HFrEF left ventricular remodelling patients [74]. A comprehensive set of parameters that need to be be altered to pragmatically model HFrEF is not explicitly identified in heart failure simulation studies. Hence, a sound understanding of the pathophysiology of HFrEF may potentially allow for the identification of the most pertinent parameters and their realistic pathophysiological ranges.

Thus, the presented work focuses on developing a 0-D comprehensive real-time executable model of the cardiovascular system using the Simscape$^{TM}$ Electrical Library and simulates HFrEF as a pathological case. The detailed development methodology of the CVS model and HFrEF modelling is described in the next chapter.

## *2.2 Modelling Left Ventricular Assist Devices*

LVADs are modelled to study the interactions between these devices and the native heart. A 3-D anatomically detailed model of the CVS and LVAD would be highly computationally cumbersome, therefore researchers often opt for modelling parts of assisted circulation in detail and integrating it with low dimensional models in a multiscale configuration [75]. Zhang et al. coupled a model of the native heart to an axial flow LVAD to study the level of trauma incurred by the blood [76]. CVS-LVAD modelling has been used to study the outcomes of LVAD therapy for heart failure patients with anaemia and iron deficiency [77], aortic valve dynamics at different levels of activity and heart failure severity [68], to monitor heart contractility [78], to study the risk of neurological complications due to underperfusion and hyperperfusion [79], to guide therapeutic interventions and clinical decision-making [80]. Thus, the utility of CVS-LVAD modelling cannot be overstated as the benefits rendered by this approach are vast and varied.

LVADs are structurally less complicated as compared to the CVS. Contemporary LVADs are made up of an inflow cannula connected to the apex of the LV, an axial or centrifugal pump that impels the blood towards the aorta, and an outflow cannula connected to the aorta tasked with carrying the oxygenated blood back to the systemic vasculature. The input and output cannulae/grafts are modelled using

resistances serially connected to inductances, meanwhile a voltage source/pressure generator models the pump. Resistance in the cannula model simulates energy loss due to viscous effects, whereas an inductance models pulsatile blood flow generated as a result of the heart"s interaction with the varying pressure head [81]. Flowrate $Q$ of rotary blood pumps (RBP) depends upon the pressure head $H$, hence, RBPs are conventionally modelled via characteristic curves that relate $H$ and $Q$ at different constant speeds $\omega$. Researchers have proposed different polynomials to relate $H$, $Q$, and $\omega$ for modelling experimentally determined characteristic curves. For steady conditions, Euler's pressure head equation in its simplified form estimates $H$ by a linear relationship with $Q$ and a quadratic relationship with $\omega$ [82]. The quadratic term accounts for pressure generation:

$$H = aQ + b\omega^2 \tag{2.1}$$

where $a$ and $b$ are determined by fitting eq. 2.1 to the $H - Q$ curves of the impeller pump. In order to improve estimation accuracy, additional terms are added to eq. 2.1. Modellers have used a quadratic function of the flow to account for viscous losses and have added a linear term of the first derivative of flow to account for fluid inertia induced energy losses [83]:

$$H = [\alpha Q + \beta Q^2] + b\omega^2 + L\frac{dQ}{dt} \tag{2.2}$$

where $b$ is a pump speed constant, $\alpha$ and $\beta$ are hydraulic resistance parameters, and $L$ inductance is a fluid inertance parameter. An alternate model used for studying the role of backflow in a failing pump incorporates resistive and inertial terms to make the model valid for for pulsatile flow [84].

$$H = RQ \cdot Q^2 + b\omega^2 + L\frac{dQ}{dt} \tag{2.3}$$

where $R$ and $L$ depend upon cannulae dimension. For pulsating operation mode, the derivative of pump speed has been included [85]:

$$H = aQ + b\omega^2 + cQ\omega + d\frac{d\omega}{dt} + L\frac{dQ}{dt} \tag{2.4}$$

Additionally, including a motor model can help relate flow to pump motor variables i.e., current and speed:

$$J\frac{d\omega}{dt} = \frac{3}{2}K_b I + b\omega + c\omega^3 + dQ\omega^2 \tag{2.5}$$

where $K_b$ is the back EMF constant, $I$ is the amplitude of the phase currents. So far the models of the form $H = f(Q, \omega)$ have been presented. A model of the form $Q = f(H, \omega)$ for centrifugal pumps is as follows [86]:

$$Q = a + b\omega + cH + d\omega^2 + eH^2 + fH\omega \tag{2.6}$$

where $a$, $b$, $c$, $d$, $e$, $f$ are determined so as to optimally match pump characteristic curves. Hence, it can be seen that modellers have chosen different variants of the pump model-based on their requirements and application. Shi et al. address the shortcomings of this approach as the lack of consideration for the underlying physical laws that govern pump hydraulics [87]. They conducted analytical modelling of an impeller pump based on mass, momentum and energy conservation, and impeller geometry to provide a physics-based framework for not only selecting pump geomtry thereby aiding the design process, but also modelling pump characteristics. The final equations for axial pumps is:

$$H = (-\rho K_Q) \cdot Q^2 + (-\rho R\sigma \frac{\tan\beta}{A}) \cdot Q \cdot \omega + (\rho R^2 \sigma) \cdot \omega^2 \tag{2.7}$$

and that for centrifugal pumps is:

$$H = [-\rho(\frac{{A_i}^2 - {A_o}^2}{2{A_i}^2{A_o}^2} + K_Q)] \cdot Q^2 + [-\rho R_o \sigma \frac{\tan\beta}{A_o}] \cdot Q \cdot \omega + (\rho {R_o}^2 \sigma) \cdot \omega^2 \tag{2.8}$$

while both possess the same general form:

$$H = K_a \cdot Q^2 + K_b \cdot Q\omega + K_c \cdot \omega^2 \tag{2.9}$$

## *2.3 Applications of CVS-VAD Modelling*

Different applications of CVS-VAD modelling have been covered in the preceding sections of this chapter. The following sections discusses those applications in detail, that are the magnum opus of this work.

### *2.3.1 Clinical Decision-Making*

Modelling and simulation is a pre-clinical step that can not only supplement clinical studies but also enhance our understanding by generating synthetic clinical data. Researchers are exploring the role of 0-D models in supporting clinical studies, especially in the field of cardiovascular medicine, by providing insights into patient-specific conditions, surgical procedures, and physiological responses. Potential applicability of CVS LPMs in guiding treatment planning has been explored by a 0-D model employed to simulate the hemodynamics of a palliated congenital heart disease anomaly [88]. According to Keremati et al., the described process can be used to estimate the necessity and effectiveness of a heart operation to repair the septal defect pre-op. The study was conducted using a 0-D LPM of the cardiovascular system which was calibrated using a patient-specific multiscale CVS model. A similar application is found in the work of Zhao et al., using a multiscale model to investigate the most optimal anastomotic shape in cardiovascular shunt procedures [89]. Broome et al. develop a real-time capable, easily modifiable CVS model that can potentially facilitate not only medical pedagogy but also provide rapid feedback in a clinical decision support scenario for surgery and intensive care [90]. Feng et al. have used a 0-D CVS model to quickly, accurately, and more importantly, non-invasively diagnosis of myocardial ischemia [91]. CVS-VAD models have been used to study VAD-VAD interactions for bi-ventricular support on virtual patients [92] with commercially available LVAD models, to understand the implications of speed increments/decrements during intense activities like exercise, and for thrombogenicity evaluation of different anastomosis angles in LVAD surgeries [93].

Another potential application of CVS-VAD models is *in silico* hemodynamic ramp testing (HRT). HRT is an invasive post-implant clinical procedure whereby practicability of LVAD speed adjustments is investigated with the aim of patient hemodynamic profile optimization, patient management and treatment guidance, and post-implant life quality enhancement [94]. While promising results have been observed in clinical settings, HRT does not guarantee speed changes [95]. Furthermore, there is an absence of a standardized protocol across the board for HRT

procedures. Under these circumstances, HRT simulations can be advantageous for optimizing protocol, evaluation of efficacy and pre-clinical pedagogy whilst saving cost and time, the details of which are covered in the next chapter.

### *2.3.2 In vitro Testing*

In-vitro evaluations are also favoured over in-vivo when investigating certain controlled physiological parameters due to ethical concerns [96]. In-vitro testing involves mock circulatory loops (MCLs) that comprise abstractions of the native CVS's anatomy. Conventional MCLs were purely mechanical, with hydraulic pumps, fluid-filled tubes, and obstructions mimicking ventricles, compliances, and resistances [97]. Gehron et al., have developed a life-size fully mechanical MCL to study wave phenomena the large vessels [98]. Kado et al. developed a custom mechanical MCL to test BiVADs [99]. Such testing platforms are not readily modifiable to simulate different pathophysiological conditions or replicable to facilitate collaboration.

Hybrid MCLs, on the other hand, are based on the hardware-in-the-loop concept. They combine hardware and software components to simulate the CVS, where the VAD being tested is a commercial device or an experimental prototype, while the human circulation is completely simulated by real-time executable model. In the last decade, there has been an increase in the development of hybrid MCLs [100] as they offer more flexibility, reliability, and replicability compared to their predecessors, mechanical MCLs. HMCLs differ in complexity from detailed multi-chambered setups suitable for evaluating multiple cardiac assist devices [101], or suction studies [102], to dual-chambered designs for testing LVADs [103]. HMCLs also differ based on the implementation of the hydraulic-numerical interface. Designs can be found with piston actuators [104], pressurized air [103], and electro-mechanical voice coil actuators [105].

# Chapter 3

# MATERIALS AND METHODS

## *3.1 Acausal Modelling of the CVS and LVAD*

### *3.1.1 Cardiovascular System Model*

0-D lumped-parameter modelling involves the use of circuit analysis methods to model and simulate the dynamics of the CVS. Based on this method, hemodynamics in the CVS corresponds to electric conduction in a circuit. Similar to voltage difference pushing current to overcome electrical impedance in a circuit, pressure difference pushes the blood to overcome hydraulic impedance in the circulatory system. Frictional effects in the blood are described using resistance $R$, inertial effects using inductance $L$, and vessel elasticity using capacitance $C$, respectively.

Avanzolini and his colleagues developed a closed-loop model of the CVS in a FORTRAN-based interactive program [36]. Canete et al. replicated Avanzolini's model in Simulink and Simscape$^{TM}$ to model healthy and pathological conditions of the CVS [62]. The model in the current work is derived from the early works of Avanzolini, Shi, and Choi et al. [36, 66, 87, 65]. Inlet-outlet valves are linearly resistive and unidirectional in nature hence, ideal diode with a resistance in series are used to model them. The systemic and pulmonary systems are structurally similar. Two serially connected inverted L Windkessel elements are used to replicate the arterial system [7]. Avanzolini modelled veins using capacitors. In reality, the veins' blood collection and storage function is accompanied by viscous effects which the model incorporates using an additional L element (Figure 3.1). Ventricles are active components that accept and discharge blood by relaxation during diastole and contraction during systole. A non-linear elastance approximates the pulsating function of the ventricles. Varying systolic ventricular elastance is modeled using a

classical model that uses a normalized curve composed of the end-systole (or maximum) elastance $E_{es}$ and duration of systole $t_s$ to approximate systolic function. A mono-exponential model replaces the constant elastance approach for modelling diastolic function [106]. A resistance $R_M$ to represent myocardial viscosity is added in series to increase model accuracy [107]. The following pressure-volume (P-V) relation is obtained as a result:

$$P_v(t) = \begin{cases} E_{es}E_{n,v}(t)[V(t) - V_0] + ae^{b[V(t)-V_0]} + R_M\frac{dV}{dt} & 0 \leq t < t_s \\ ae^{b[V(t)-V_0]} & t_s \leq t \leq t_c \end{cases} \tag{3.1}$$

Descriptions of the parameters in the preceding and subsequent equations can be found in Table 3.3. $t_c$ is the length of one heart beat in seconds. $V_0$ is the initial ventricle volume before it accumulates a substantial amount of pressure. In the P-V relation for diastole, $a$ and $b$ are the a scaling factor and the chamber stiffness coefficient, respectively. $E_{n,v}(t)$ is an activation function that emulates systole and diastole [66].

$$E_{n,v}(t) = \begin{cases} 1 - \cos\left(\frac{t}{t_{s_1}}\pi\right) & 0 \leq t < t_{s_1} \\ 1 + \cos\left(\frac{t-t_{s_1}}{t_{s_2}-t_{s_1}}\pi\right) & t_{s_1} \leq t \leq t_{s_2} \\ 0 & t_{s_2} \leq< t_c \end{cases} \tag{3.2}$$

$t_{s_1}$ represents the time taken by the ventricle to reach peak systole and $t_{s_2}$ represents the duration of systole. Atria, in Avanzolini's model were simulated using a constant elastance element added to the venous compliance. In reality, however, atria are active components that take turns with the ventricles synchronously contracting and relaxing to carry out perfusion [36]. The model being developed for the current work describes atrial pressure using a linear function of volume and temporal function of elastance.

$$P_a(t) = E_a(t)[V_(t) - V_0] \tag{3.3}$$

The elastance function $E_a(t)$ is made up of minimum and maximum elastances ($E_{a,min}$ and $E_{a,max}$), respectively and, like ventricles, an activation function$E_{n,a}(t)$.

$$E_a(t) = E_{a,min} + \frac{E_{a,max} - E_{a,min}}{2}E_{n,a}(t) \tag{3.4}$$

The atrial activation function is obtained from CVS modelling literature [66].

$$E_{n,a}(t) = \begin{cases} 0 & 0 \leq t < t_{pwb} \\ 1 + \cos\left(\frac{t - t_{pwb}}{t_{pwb} - t_{pww}}\pi\right) & t_{pwb} \leq t \leq t_{pwb} + t_{pww} \\ 0 & t_{pwb} \leq t < t_c \end{cases} \tag{3.5}$$

$t_{pwb}$ and $t_{pww}$ are atrial depolarization parameters. $t_{pwb}$ marks the beginning of the wave and $t_{pww}$ quantifies the wave's duration.

*Acausal Modelling*

The complete Simscape$^{TM}$ CVS model can be seen in Figure 3.1. The Simscape$^{TM}$ Electrical Library provides R-L-C components for the model. The library contains current and voltage sensors which can be used to measure flowrates and pressures, respectively at any CVS location. Atria and ventrciles are modelled using controlled voltage sources that acts as pressure generators and produce the required amount of pressure at the output notwithstanding the fluid flow through them. Avanzolini's model uses initial conditions for solving the odes, these are provided to the Simscape$^{TM}$ model as *priority targets*. The model is composed of physical signal blocks (Simscape$^{TM}$ blocks) with Simulink blocks minimized. By doing so, algebraic loops that adversely impact simulation speeds are circumvented. The utility of this approach becomes evident when the simplicity of acausal modelling is juxtaposed with the complexity of the CVS.

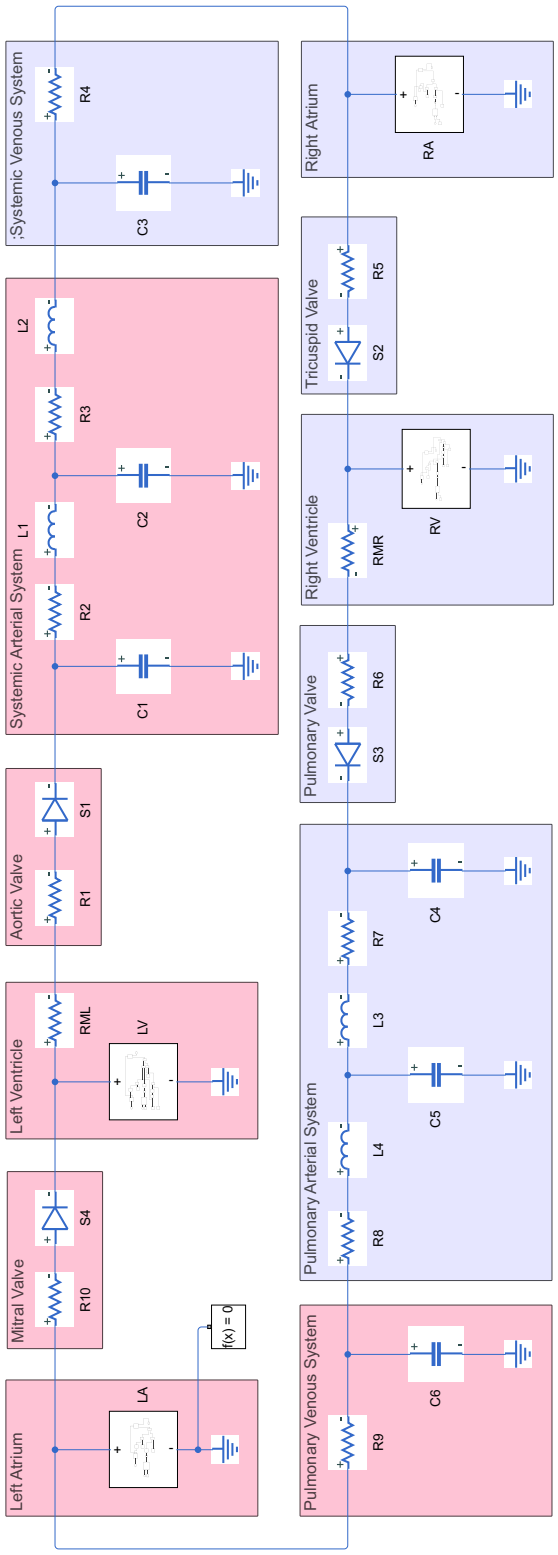


Figure 3.1: The complete lumped parameter model of the native heart in Simscape™

### *3.1.2 Left Ventricular Assist Device Model*

The iHeart VAD prototype 1 has been used evaluated *in vivo* in a porcine model [108]. In the current study, an acausal model of the iHeart VAD prototype 1 is developed to evaluate its performance under varying pathophysiological conditions. The input-output cannulae of the device are modelled using resistance elements serially connected to inductance elements. The pump acts as as an ideal voltage or pressure source. The cannulae are modelled to account for the In the cannulae models, $R_{i,o}$ simulate energy loss due to viscous effects, after that from pressure drop and $L_{i,o}$ model the pulsatile flow generated due to the exchanges between the heart and the dynamic pressure head [81]. To model suction, a variable resistance models is used which is a function of the left ventricle pressure $P_{lv}$ [109].

$$R_{suc} = \begin{cases} 0 & \text{if} P_{lv} > 1 \\ -3.5(P_{lv} - 1) & \text{if} P_{lv} < 1 \end{cases} \tag{3.6}$$

A polynomial relationship correlating the pump speed, flowrate, and pressure head in the form $H = f(\omega, Q)$ is used to model the pump. Many different of polynomials have been used by researchers to optimally match pump characteristic data in the form of $H - Q$ curves at different speeds. Unfortunately the choice of these polynomials is not well-founded in the governing physical laws but instead, the choice is driven based on the percentage of fit-to-estimation data. Yubing Shi and his colleagues attempt to remedy this by analytically deriving a mathematical model of the impeller pump based on the physical laws that account for pump hydraulic effects [87].

$$H = K_a \cdot Q^2 + K_b \cdot Q\omega + K_c \cdot \omega^2 \tag{3.7}$$

As described in section 2.2, $K_a$, $K_b$, and $K_c$ can take on different values depending upon the type of LVAD being modelled. In the current study, the Istanbul Heart VAD prototype 1 is modelled which is centrifugal flow CF-LVAD that operates with flowrates ranging from 1.5 to 7 L/min, and pump speeds of 1500 to 3200 (rpm) [108]. According to Shi et al., the values of $K_a$, $K_b$, and $K_c$ are:

$$K_a = -\rho \left( \frac{{A_i}^2 - {A_o}^2}{2{A_i}^2{A_o}^2} + K_Q \right) \tag{3.8}$$

$$K_b = -\rho R_o \sigma \frac{\tan \beta}{A_o} \tag{3.9}$$

$$K_c = \rho {R_o}^2 \sigma \tag{3.10}$$

To calculate $K_a$, $K_b$, and $K_c$ we utilize the published geometric data of the iHeart VAD prototype 1 [110].

Table 3.1: Geometric parameters of the Istanbul Heart VAD prototype 1.

| Parameter | Description | Value |
|---|---|---|
| $A_i$ | Inlet area | 201.6 mm$^2$ |
| $A_o$ | Outlet area | 63.62 mm$^2$ |
| $R_o$ | Impeller outer radius | 22.5 mm |
| $\beta$ | Blade angle | 36.5 deg |
| $Z$ | Number of blades | 5 |
| $\sigma$ | Slip factor | 0.75 |

iHeart VAD's characteristic $H-Q$ data is used to estimate the pump parameters $K_a$, $K_b$, and $K_c$ [108], for comparison. Instead of a tedious data-matching technique, an automated approach is adopted. Least-squares (LSQ) fitting is used, which also addresses the issue of sub-optimal matching reported for a model of the HeartMate III [87] (See Figure 3.2 for comparison). To this effect, problem 3.11 is solved for the nonlinear function (eq.3.7). Flowrate $Q$, in this equation, is the input, pressure head $H$ is the measured output, and $F(K_{a,b,c}, Q)$ is a vector-valued function with the same dimensions as $H$.

$$\min_{K_{a,b,c}} ||F(K_{a,b,c}, Q) - H||_2^2 = \min_{K_{a,b,c}} \sum_i (F(K_{a,b,c}, Q_i) - H_i)^2 \tag{3.11}$$

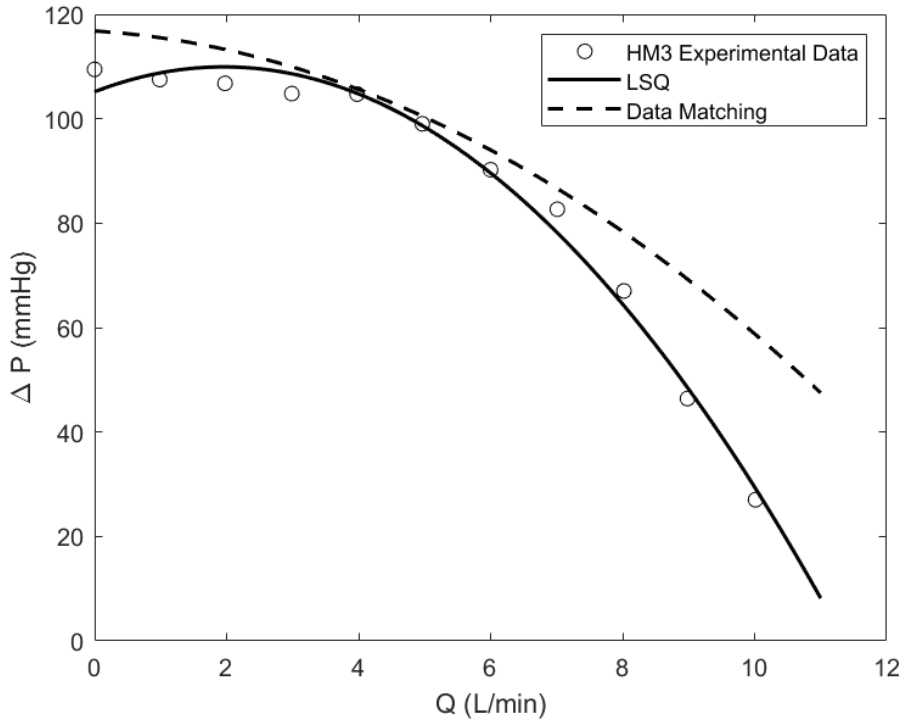


Figure 3.2: Data-matching vs. LSQ fitting for HeartMate III.

Values of $K_a$, $K_b$, and $K_c$ using eqs. 3.8, 3.9 - 3.10 and those determined using LSQ fitting for a range of pump speeds and subsequently averaging them are tabulated in Table 3.2.

Table 3.2: Pump parameters from eqs. 3.8 - 3.10 and LSQ fitting.

| Parameter (Unit) | Analytical | Curve-Fitted |
|---|---|---|
| $K_a$ $(mmHgmin^2L^{-2})$ | -0.2432 | -3.0503 |
| $K_b$ $(mmHgminL^{-1}\ rpm^{-1})$ | -0.0036 | $5.8481 \times 10^{-4}$ |
| $K_c$ $(mmHgrpm^{-2})$ | $3.1017 \times 10^{-5}$ | $2.2775 \times 10^{-5}$ |

A substantial difference is found difference between the analytically calculated and empirically estimated parameters (Table 3.2), indicating a potential need for revision of the parameters' definitions. Using the LSQ fitted values, ideal match-

ing is obtained over the complete operating range of the iHeart VAD; therefore, the model in eq.3.7 is calibrated with the LSQ parameters in Table 3.2 to conduct LVAD support simulations (Figure 3.3).

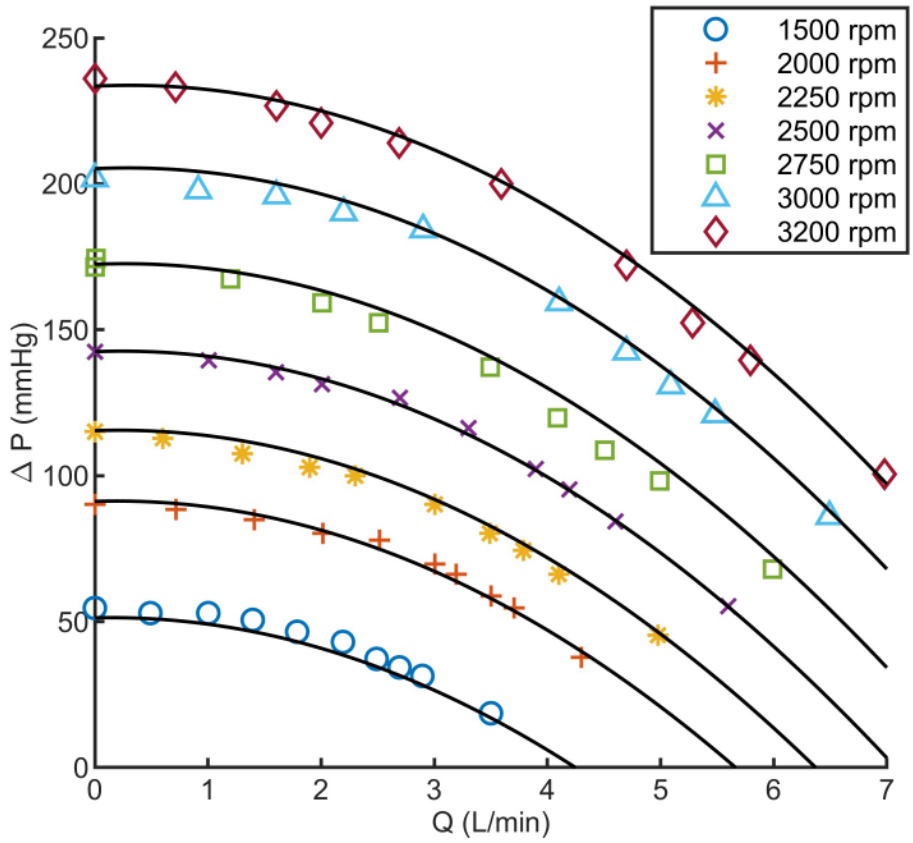


Figure 3.3: iHeart VAD characteristic $H - Q$ curves estimated using LSQ fitting.

*Acausal Modelling*

The iHeart VAD is surgically connected to the left ventricle (LV) apex directly obliterating the need for an inflow cannula. Downstream of the LVAD, an outflow graft is cannulated it to the ascending aorta (Figure 3.4). A resistance $R_o$ and inductance element $L_o$ needed to model the outflow cannula can be estimated in the laminar regime. Instead, an estimation made by Choi et al. reporting $R_{i,o}$ and $L_{i,o}$ as 0.0677 mmHg $s^2$ $ml^{-1}$ and 0.0127 mmHg s $ml^{-1}$, respectively, is used. Choi et al. determined $R_{i,o}$ and $L_{i,o}$ by applying an LSQ approach to HeartMate II data. The

HeartMate II values can be utilized with minimal error [65].

The acausal LVAD model shown in Figure 3.4 can be connected to the CVS model in Figure 3.1 to produce the complete acausal CVS-VAD model shown in Figure 3.5. The governing equations for the ventricle, atrium, suction resistance, and pressure head mask their respective subsystems in Figure 3.5. Detailed modelling of these components can be found in Figure 3.6.

Another advantageous feature of the acausal CVS-VAD model is that flowrate and pressure can be determined virtually at any CVS-VAD location by simply connecting current sensor in series or a grounded voltage sensor in parallel, respectively. The sensors can be found in Simscape$^{TM}$'s Electrical Library. $P_{lv}$ needed for suction resistance $R_{suc}$ calculation is measured at LV outlet using a voltage sensor, whereas LVAD flowrate $Q_{LVAD}$ needed for pressure head calculation is measured using a current sensor. To calculate volume, the flowrate signal must be integrated using a physical signal integration block. A custom-made signal using Simulink's Signal Builder and called *Stepped Ramp* is provided as an input to the model. All the components are connected to the Electrical Reference component which serves as a common ground (Figure 3.5). The solver settings upon which the model runs can be found in the solve configuration block. The solver type is a variable step solver (ode23t) and tolerances are set at a low value of 1e-9. It takes Simulink approximately 23 s to simulate 24 beats. The simulation time can be increased considerably by using a fixed-step solver instead of a variable-step solver. The models, due to their acausal nature are open-sourced by sharing their images, as researchers can reproduce the same by replicating the the structure shown.

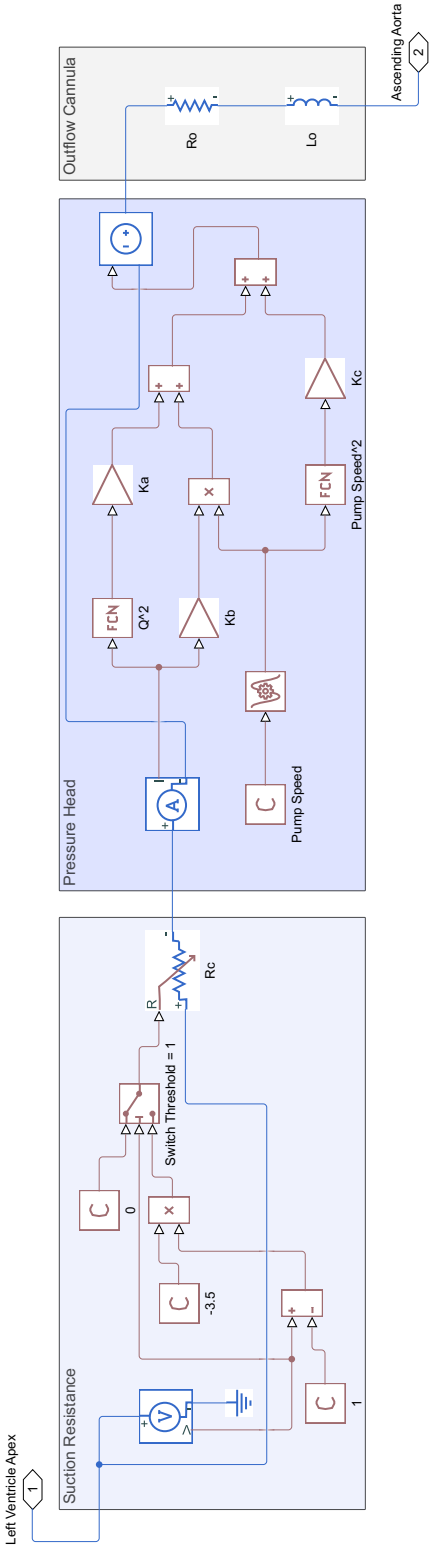


Figure 3.4: Simscape$^{TM}$ model of the LVAD.

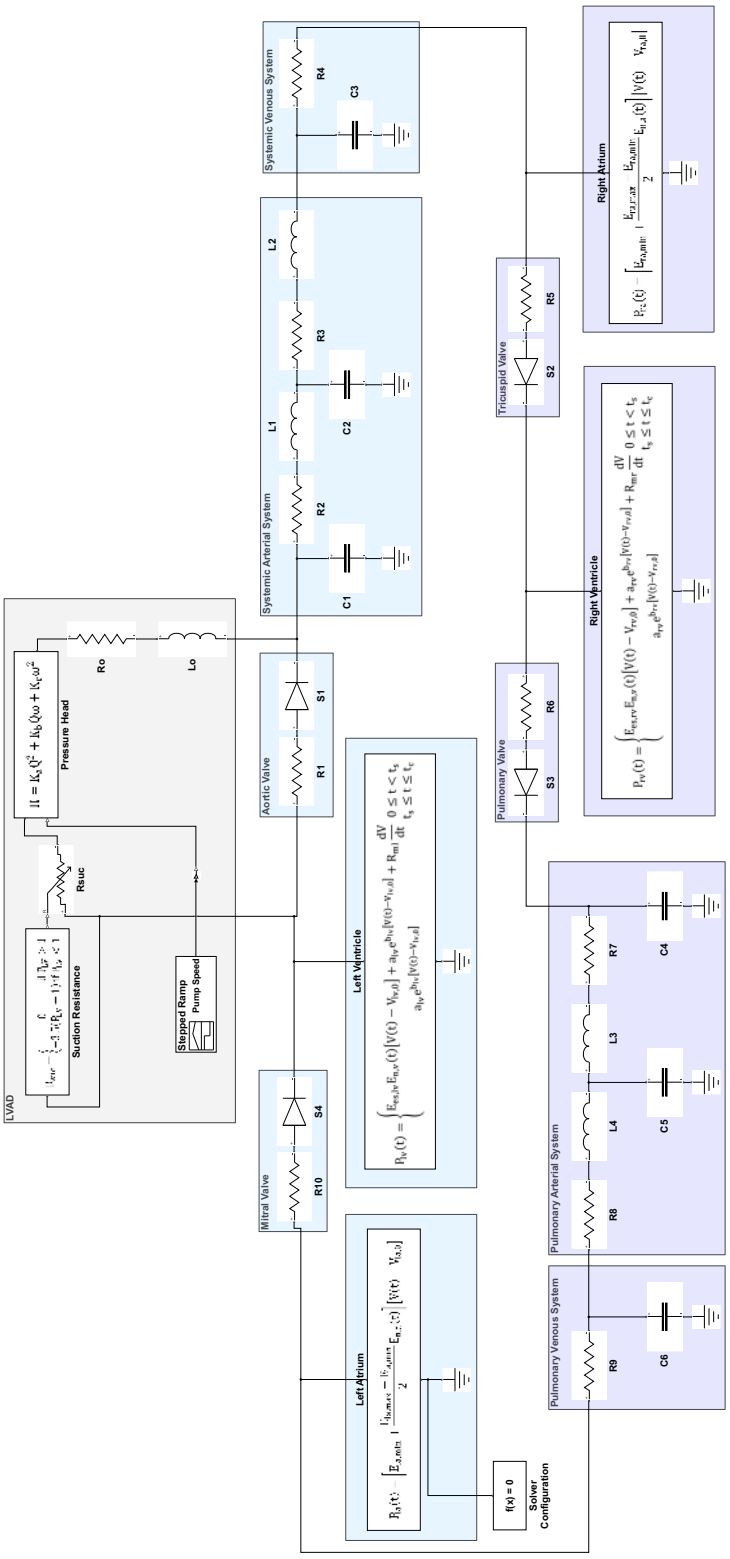


Figure 3.5: Simscape$^{TM}$ model of the CVS and LVAD.

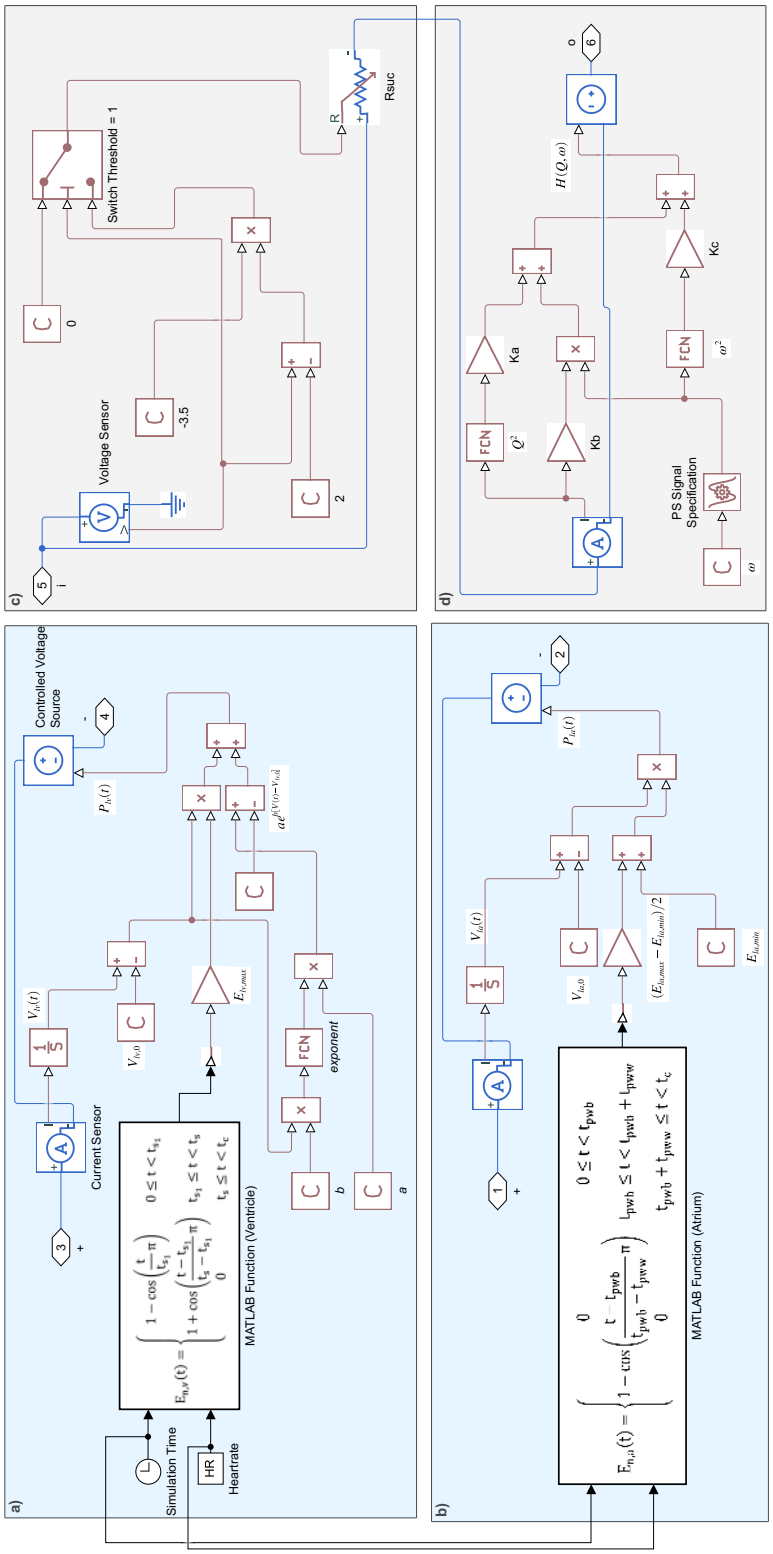


Figure 3.6: Subsystems of the acausal CVS-VAD model: (a) LV, (b) LA, (c) Suction Resistance, and (d) Pressure Head.

### *3.2 Healthy Heart Modelling*

The CVS model (Figure 3.1) is used to simulate a healthy unassisted heart. In order to do so, the model is calibrated with appropriate values of CVS parameters for a standard, healthy heart (Table 3.3). The pulmonary and systemic vascular resistances ($R_s$ and $R_p$) are made up of arterial resistances $R_{art}$, vascular bed resistances $R_{vb}$, and venous resistances$R_{ven}$, respectively, which are added in the following ratios [111]:

$$R_{s/p} = 0.05R_{art} + 0.92R_{vb} + 0.03R_{ven} \tag{3.12}$$

In the model just developed, systemic $R_{art}$ is denoted by $R_2$, $R_{vb}$ is denoted by $R_3$, and $R_{ven}$ is denoted by $R_8$. Pulmonary $R_{art}$ is denoted by $R_7$, $R_{vb}$ is denoted by $R_8$, and $R_{ven}$ is denoted by $R_9$. Healthy heart $R_s$ is 0.88 mmHg s ml and $R_p$ 0.05 mmHg s ml$^{-1}$ as reported in Washington Manual of Surgery [112].

Table 3.3: Healthy heart parameters to calibrate the CVS model.

| **Parameter** | **Description (units)** | **Value** | **Ref.** |
|---|---|---|---|
| $R_1$ | Aortic valve resistance (mmHg s ml$^{-1}$) | 0.003751 | [36] |
| $R_2$ | Systemic arterial resistance (mmHg s ml$^{-1}$) | 0.04 | [111] |
| $R_3$ | Systemic vascular bed resistance (mmHg s ml$^{-1}$) | 0.81 | |
| $R_4$ | Systemic venous resistance (mmHg s ml$^{-1}$) | 0.03 | |
| $R_5$ | Tricuspid valve resistance (mmHg s ml$^{-1}$) | 0.003751 | [36] |
| $R_6$ | Pulmonary valve resistance (mmHg s ml$^{-1}$) | 0.003751 | |
| $R_7$ | Pulmonary arterial resistance (mmHg s ml$^{-1}$) | 0.0025 | [111] |
| $R_8$ | Pulmonary vascular bed resistance (mmHg s ml$^{-1}$) | 0.046 | |
| $R_9$ | Pulmonary venous resistance (mmHg s ml$^{-1}$) | 0.0015 | |
| $R_{10}$ | Mitral valve resistance (mmHg s ml$^{-1}$) | 0.003751 | [36] |
| $R_{MR}$ | Right myocardial resistance (mmHg s ml$^{-1}$) | 0.0175 | |
| $R_{ML}$ | Left myocardial resistance (mmHg s ml$^{-1}$) | 0.08 | |
| $L_1$ | Aortic inductance (mmHg s$^2$ ml$^{-1}$) | 0.000825 | [36] |

| | | | |
|---|---|---|---|
| $L_2$ | Systemic inductance (mmHg $s^2$ $ml^{-1}$) | 0.0036 | |
| $L_3$ | Pulmonary artery inductance (mmHg $s^2$ $ml^{-1}$) | 0.00075 | |
| $L_4$ | Pulmonary inductance (mmHg $s^2$ $ml^{-1}$) | 0.003085 | |
| $C_1$ | Aortic compliance (ml $mmHg^{-1}$) | 0.08 | [66] |
| $C_2$ | Systemic arterial compliance (ml $mmHg^{-1}$) | 1.6 | |
| $C_3$ | Systemic venous compliance (ml $mmHg^{-1}$) | 20.5 | |
| $C_4$ | Pulmonary artery compliance (ml $mmHg^{-1}$) | 0.18 | |
| $C_5$ | Pulmonary arterial compliance (ml $mmHg^{-1}$) | 3.8 | |
| $C_6$ | Pulmonary venous compliance (ml $mmHg^{-1}$) | 20.5 | |
| $E_{es,LV}$ | Left ventricle end-systole elastance (mmHg $ml^{-1}$) | 2.5 | |
| $E_{es,RV}$ | Right ventricle end-systole elastance (mmHg $ml^{-1}$) | 1.15 | |
| $E_{LA,max}$ | Maximum left atrium elastance (mmHg $ml^{-1}$) | 0.3 | [66] |
| $E_{RA,max}$ | Maximum right atrium elastance (mmHg $ml^{-1}$) | 0.3 | |
| $E_{LA,min}$ | Minimum left atrium elastance (mmHg $ml^{-1}$) | 0.2 | |
| $E_{RA,min}$ | Minimum right atrium elastance (mmHg $ml^{-1}$) | 0.2 | |
| $a_{LV}$ | Diastole P-V relation scaling factor LV (mmHg) | 1 | [113] |
| $a_{RV}$ | Diastole P-V relation scaling factor RV (mmHg) | 1 | |
| $b_{LV}$ | Left ventricle stiffness coefficient ($ml^{-1}$) | 0.02 | |
| $b_{RV}$ | Right ventricle stiffness coefficient ($ml^{-1}$) | 0.02 | |
| $V_{LV,0}$ | LV unstressed volume (ml) | 15 | |
| $V_{RV,0}$ | RV unstressed volume (ml) | 50 | |
| $V_{LA,0}$ | LA unstressed volume (ml) | 4 | [66] |
| $V_{RA,0}$ | RA unstressed volume (ml) | 4 | |
| $HR$ | Heart rate (bpm) | 80 | [36] |
| $t_{pwb}$ | Beginning of P-wave (s) | 0.92 | [66] |
| $t_{pww}$ | Duration of P-wave (s) | 0.09 | |
| $t_{s,2}$ | Time to reach peak systole (s) | 0.33 | |
| $t_{s,2}$ | Systole duration (s) | 0.45 | |

### *3.3 Heart Failure Modelling*

Eccentric remodelling (ER) or eccentric hypertrophy accounts for a major portion of HFrEF left ventricular remodelling cases [74]. For this reason, ample amounts of patient data can be found in the literature which is why it is used as an demonstrative example for heart failure and assisted heart simulations. Dilation and impaired ventricular contractility is germane to ER. Therefore, it is usually modelled an arbitrary reduction in the LV end-systole elastance $E_{es,lv}$ or $E_{lv,max}$. Although following this approach allows makes it easy to distinguis the healthy case from the pathologial, other CVS parameters affected by this condition are either absent or ill-defined in modelling literature. In order to model ER realistically, we must understand the underlying pathophysiology of the condition.

In a patient afflicted by ER, neurohumoral responses working as compensatory mechanisms are triggered to increase afterload and preload. Increased afterload is characterized by an elevated aortic and pulmonary pressure, elevated vascular resistances, and diminished arterial compliances. Hence, simulating ER entails a reduction in left ventricular end-systole elastance $E_{es,lv}$, $C_2$, $C_5$, and an increase in $R_s$, $R_p$ and $V_{lv,0}$. Additionally, studies have also reported a reduction in the diastole P-V relation parameters $a$ and $b$ and the LV myocardial viscosity $R_{ML}$ [114]. Furthermore, a dilated LV results in reduced cardiac output (CO), ejection fraction (EF), and Stroke Volume (SV).

One of the essential points of this work is identifying realistic values of the pathophysiological parameters for simulating diseased hemodynamics which exhibits the utility of the model and the validity of its results. Therefore, published hemodynamic parameters observed for HFrEF patients are collected from the literature (Details of the collected data can be found in Appendix A). Table 3.4 summarizes the diseased heart data. The values reported here are calculated by pooling the means and standard deviations recursively using the statistical relationships given below [115]:.

$$\mu_{pooled} = \frac{1}{n_1 + n_2}[n_1\bar{x_1} + n_2\bar{x_2}] \tag{3.13}$$

$$s^2_{pooled} = \frac{1}{n_1 + n_2 - 1}[n_1 - 1)s_1^2 + (n_2 - 1)s_2^2 + \frac{n_1 n_2}{n_1 + n_2}(\bar{x_1} - \bar{x_2})^2] \tag{3.14}$$

Table 3.4: Pooled values of diseased heart parameters to calibrate the CVS from patient data. See Appendix A for detailed information.

| **Parameter (Unit)** | **Value** |
|---|---|
| $E_{es,lv}$ (mmHg ml$^{-1}$) | $0.71 \pm 0.33$ |
| $R_s$ (mmHg s ml$^{-1}$) | $1.65 \pm 0.85$ |
| $C_2$ (ml mmHg$^{-1}$) | $1.17 \pm 0.6$ |
| $R_p$ (mmHg s ml$^{-1}$) | $0.1238 \pm 0.0986$ |
| $C_5$ (ml mmHg$^{-1}$) | $3.1 \pm 1.9$ |
| $a$ (mmHg) | $0.02 \pm 0.03$ |
| $b$ (ml$^{-1}$) | $0.031 \pm 0.013$ |
| $R_{ML}$ (mmHg s ml$^{-1}$) | $0.0004 \pm 0.002$ |

P-V loops, pressure, flowrate, and volume are produced for the healthy, diseased, and LVAD-assisted cases (see Section 4.1). Healthy heart simulations are carried out by calibrating the model in Figure 3.1 with the values in Table 3.3. The requisite parameters are then replaced with those in Table 3.4 to simulate advanced-stage heart failure. Instead of the mean value for $E_{es,lv}$ reported in Table 3.4, 0.5 mmHg ml$^{-1}$ is used as this is a widely reported value [87, 67] and also lies within the observed pathological range (Table 3.4).

## *3.4 Applied CVS-LVAD Modelling*

### *3.4.1 Hemodynamic Ramp Testing*

A potential application of the acausal CVS-VAD model developed in the previous sections is *in silico* Hemodynamic Ramp Testing. HRT is a highly invasive procedure used by cardiologists to explore the possibilty of LVAD speed adjustments for patients' hemodynamic profile optimization, post-op. The aim of this procedure is to enhance life quality after VAD implantation and to guide symptom management which may entail increasing LVAD speed if support is found insufficient or decreasing it to avoid exacerbating heart failure. While the results of HRT may be promising, it does not always result in speed changes. Thus, there is a need for *a priori* assessment of the potential utility of conducting an invasive procedure. The current work uses the a CVS-VAD model with the HeartWare HVAD as the operating LVAD as this has been used in clinical studies aimed at HRT [116, 95].

*HVAD Acausal Model*

Like the iHeart VAD, the HVAD too comprises of an outflow graft cannulated to the ascending aorta, which returns the oxygenated blood to the systemic vasculature. The inflow cannula is absent as it is surgically connected directly to the LV apex. $R_o$ and $L_o$ estimated from HeartMate II experimental data are used as explained previously (Section 3.1.2). Calibrating eq.3.7 with HVAD $H - Q$ data [117] gives the following values for pump parameters:

Table 3.5: Pump equation calibrated with HVAD $H - Q$ data.

| Parameter (Unit) | Value |
|---|---|
| $K_a$ $(mmHgmin^2L^{-2})$ | 1.7619 |
| $K_b$ $(mmHgminL^{-1}\ rpm^{-1})$ | $1.8 \times 10^{-3}$ |
| $K_c$ $(mmHgrpm^{-2})$ | $1.3301 \times 10^{-5}$ |

Figure 3.7 shows the HVAD experimental data and the estimated $H-Q$ curves produced using the parameters in table 3.5. The HVAD model is connected to the CVS model in the same manner the iHeart VAD model was connected (Figure 3.5).

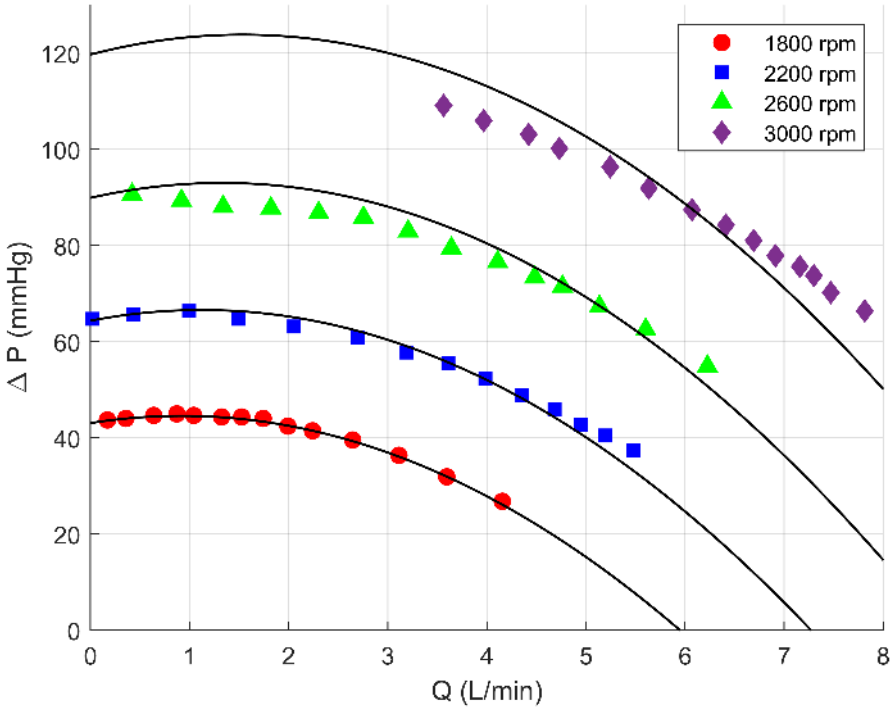


Figure 3.7: Estimated (dashed) and experimental HVAD H-Q curves at 3000 rpm (purple), 2600 rpm (green), 2200 rpm (blue), and 1800 rpm (red)

*Virtual Patients*

The pooled data used for simulating the heart failure case (Table 3.4) is used to create three virtual patients with severe, moderate, and mild degree of heart failure, respectively. For the severe case, the parameters that are detrimental when diminished ($E_{es,lv}$, $C_2$, $C_5$, $a$, $R_{ML}$) are set to their lowest values and those that are deleterious when elevated ($R_s$, $R_p$, and $b$) are to their highest. For the mild case, $E_{es,lv}$, $C_2$, $C_5$, $a$, and $R_{ML}$ are set to their highest values whereas $R_s$, $R_p$, and $b$ are set to their lowest. For the the moderate case mean values of all eight parameters are used.

Table 3.6: CVS model parameters for the three virtual heart failure patients.

| **Parameter (Unit)** | **Severe Case** | **Moderate Case** | **Mild Case** |
|---|---|---|---|
| $E_{es,lv}$ (mmHg ml$^{-1}$) | 0.37 | 0.71 | 1.05 |
| $R_s$ (mmHg s ml$^{-1}$) | 2.37 | 1.6 | 0.88 |
| $C_2$ (ml mmHg$^{-1}$) | 0.57 | 1.2 | 1.6 |
| $R_p$ (mmHg s ml$^{-1}$) | 0.2224 | 0.1238 | 0.05 |
| $C_5$ (ml mmHg$^{-1}$) | 1.2 | 2.5 | 3.8 |
| $a$ (mmHg) | 0.02 | 0.02 | 0.05 |
| $b$ (ml$^{-1}$) | 0.018 | 0.031 | 0.044 |
| $R_{ML}$ (mmHg s ml$^{-1}$) | 0.0004 | 0.0004 | 0.0024 |

*Ramp Test Protocol*

Uriel and his colleagues conducted a clinical HRT study using HVAD and HeartMate II patients [116]. For the current study, the same protocol is adopted with small adjustments to scale from the clinical setting to the *in silico* setting. Uriel et al. increased the speed of the HVAD from 2300 to 3200 rpm in steps of 100 rpm and holding it constant at every step for 2 min for hemodynamic stabilization and measurements. The researchers noted the arterial blood pressure (BP), pulmonary capillary wedge pressure (PCWP), central venous pressure (CVP), and cardiac output (CO) at every step to observe their trends. In the current simulation, the pump speed is maintained at every step for 30 s and readings are recorded at the 10 s mark to allow for the solution to stabilize. The speed is increased sequentially until either 3200 rpm is reached, or suction occurs. In the case of regurgitation, the simulation study is started beyond the pump speed where backflow ceases. LVAD speed is optimized based on hemodynamic normalization criteria for MAP, PCWP, CVP, and CO. Measurements of the hemodynamic variables are done as shown in Figure 3.8. Clinically, PCWP is used as an indirect measure of left atrial pressure (LAP), in current study LAP is measured directly. CO is taken the sum of the native LVCO

and $Q_{LVAD}$. MAP and CVP are measured at the aortic outlet and the vena cava, respectively.

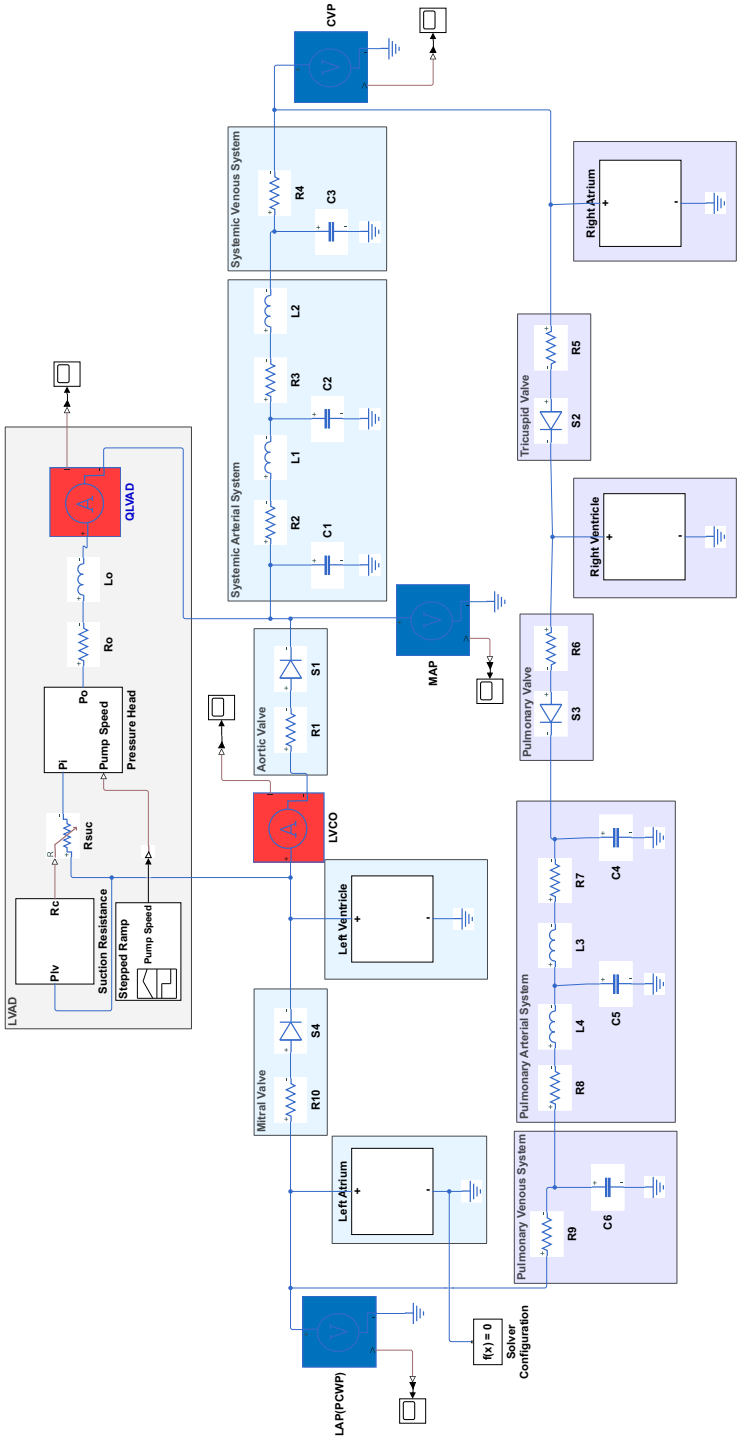


Figure 3.8: Measurement of hemodynamic variables in Simscape$^{TM}$.

### *3.4.2 Design of Experiments for Suction Detection*

0-D LPMs are used to test suction detection techniques [118, 119]. In this study, we explore a novel outlook towards a classical problem using a classical method. A structured and intuitive approach to data collection is adopted by following the Design of Experiments (DoE) method. DOE allows to study the functional relationships between multiple factors (heart failure parameters in Table 3.4) and key responses (suction speed) in an experiment systematically and efficiently. This approach is an efficient use of computational resources as it analyses responses at the edges of the design space. Suction prediction and detection techniques are usually tested on one type of patient or heart failure condition [118]. These studies fail to generalize over a wide range of inter-patient variabilities in the CVS. Hence, the physiological controllers developed based on these techniques cannot guarantee good performance across the entire clinical range of patients and heart failure conditions. An experimental design is conducted to identify and quantify the effect of hemodynamic variables pertinent to heart failure and their interactions on suction, or quantitatively, the pump speed at which suction occurs. DoE allows meticulous planning of experiments whilst maintaining objectivity and validity. Knowledge of the pathophysiology of heart failure is used to guide the DoE.

The aim is to screen the parameters in Table 3.4 based on their association with suction speed through analyses. A 2k full factorial design is chosen for this purposed whereby $k$ number of factors are explored at two levels each, high (+1) and low (-1). The two levels are readily obtained from patient data which is available in the forms of means and standard deviations. The experimental units are populated with all possible combinations of the factors for both levels allowing one to study the effect of every factor on the suction speed as well as their interactions. For an eight-factor experiment, there are $2^8 = 256$ different experimental units or *runs*. The design space is an 8-cube in this case which has 256 vertices. Each vertex represents a single run. With 256 experiments delineated, they are executed one-by-one. The pump speed is provided to the CVS-VAD model (Figure 3.5) as a ramp signal. Each run is 30 second long and pump speed ramp has the same slope $m_{ramp}$ across all

runs.

$$m_{ramp} = \frac{\text{iHeart Operational Range}}{30s} = \frac{(3200 - 1500)rpm}{30s} = 5.93rad/s^2$$

As the pump speed increases, the aortic flow successively decreases while the mean pump flow increases. For the present study, three different criteria are adopted from the literature to identify suction whereby a change in pump flow slope [118], a saddle on the rising arch of the flow peak (positive saddle), or a saddle on the falling arch (negative saddle) is classified as suction [120]. The pump speed corresponding to the suction cardiac cycle noted in each experiment.

*Factorial Design Analysis*

For individual hemodynamic variables, effects describe the predicted change in the mean suction speed as the variable goes from low to high. To understand how different hemodynamic variables are associated with the suction speed, we perform a multiple linear regression (MLR) analysis. In doing so, we investigate the association and directionality of the simulation data. For the present study, backward elimination is performed whereby, at the outset, all the factors are entered into the equation and then eliminated one-by-one based on a deletion criterion. Per the adopted deletion criterion, factors are removed if their p-values are higher than 0.1. In other words, if the risk of erroneously concluding the existence of an association (factor-to-response and factor-to-factor) falls at or below 10%, it is removed from the model. Therefore, all terms with a p-value greater than 0.1 indicate no statistically significant association between them and the suction speed. Factors and their interactions are collectively referred to as *terms*. *Effects* quantify and delineate the direction of the relationship between terms an the response. A main effect exists when different levels of the factors, or hemodynamic variables in our case, affect the response variable i.e., suction speed, differently. The magnitude of the slope represents the size of the effect, and the sign represents the relationship, positive or otherwise. Interaction plots demonstrate how the relationship between one factor and the suction speed depends upon the value of another factor. Analyses are

conducted using Minitab and MATLAB. The main effects and interaction effects are provided in Section 4.3. Interpreting main effects is trivial: the magnitude of the slope represents the strength of the relationship whereas the sign determines whether the association is positive or negative. Figure explains the interpretation of interaction plots.

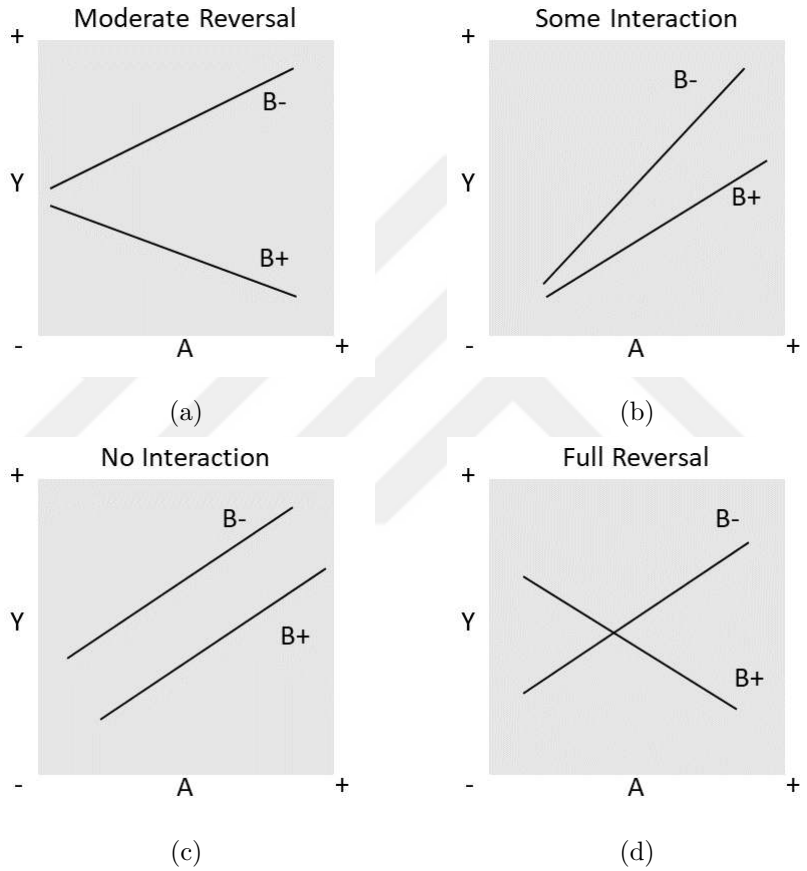


Figure 3.9: Types of interaction plots.

### *3.4.3 Developing a Hybrid Mock Circulatory Hardware-in-the-Loop Setup*

An air-actuated platform similar to that of Ochsner et al. [103] is developed to study the performance of the new Istanbul Heart LVAD. Previously researchers have adopted a similar approach but with a Simulink adaptation of a Dymola-based model and voice coil actuators for cardiac output estimation [**?**]. The design choices in this approach ensure easy replicability to facilitate VAD research and development. The

approach makes use of acausal modelling environment Simscape$^{TM}$ whereby different cardiovascular components are connected topologically without the need for writing complicated code for the plethora of differential equations that make up the system model. A snapshot of the model (Fig. 3, 4) serves as *code* that can be easily recreated from the image and calibrated using parameter values provided in this dissertation.

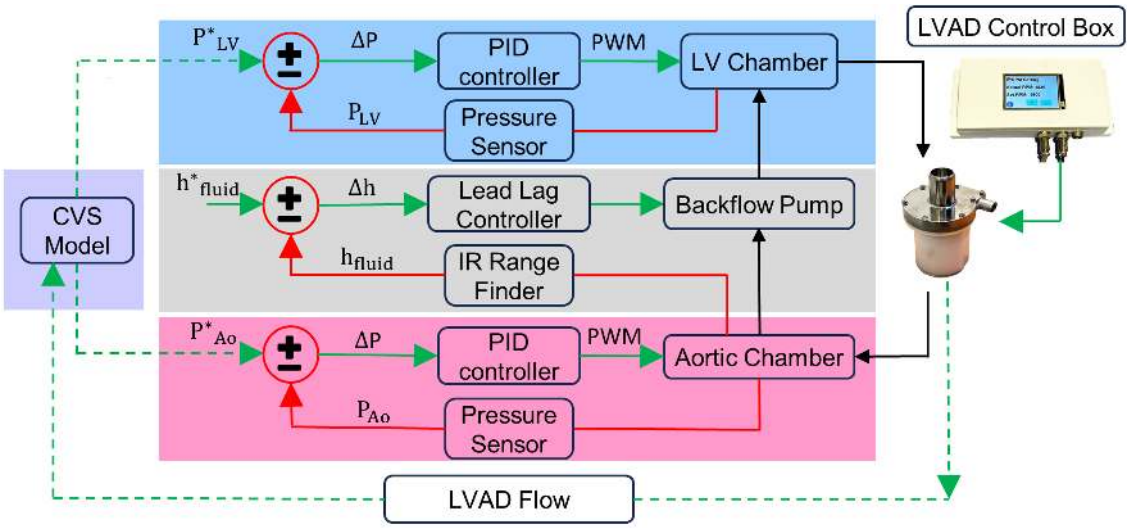


Figure 3.10: HMCL control diagram with physical (solid) and numerical (dashed) I/O signals.

In the hardware-in-the-loop simulations, a physiological environment is emulated using a left ventricle (LV) and aortic (Ao) chamber with the iHeart VAD prototype (hardware) connected between them. The flowrate of the VAD is fed back to the virtual heart to test its performance under different pathophysiological conditions. The CVS model, calibrated for a heart failure condition, generates the pressure waveforms that are tracked by solenoid valves fitted to the the aortic and LV chambers 3.10. The chambers are filled 70% with glycerin-water solution, and the remaining region acts as an air reservoir. Pressure sensors provide feedback and the air mass flowrate is varied via I/O solenoid valves to produce requisite pressures in the chambers. The LVAD alone would inevitably drain one chamber and overflow

the other hence a backflow pump supplanting systemic circulation is used to close the circuit and maintain fluid level. Thus, a controller is developed to ensure flow-matching between the two chambers via fluid level sensor measurements as feedback to vary the backflow pump speed. The controller output, i.e., input to all electromechanical components, is the pulse width modulation (PWM) duty cycle. This choice ensures easy replicability and uniformity throughout the approach. Real-time visualization is done using the ControlDesk application by dSpace GmbH.

Simultaneous utilization of in-silico and in-vitro approaches provides complementary information, allowing device behaviour and performance prediction and enhancing model accuracy.

*Hardware*

The chambers are modeled in Siemens NX to assess design feasibility, sensor placement, and assembly configuration. The pressure chamber's top and bottom Teflon casings are manufactured in-house using a 3-axis CNC. Each chamber is assembled using six 200 mm diameter rods, a $150 \times 150 \times 3$ mm plexiglass cylinder, and the machined casing with O-rings to ensure leak-proofing. The bottom casing of each chamber has a 12 mm diameter port for the pressure sensor, LVAD, and backflow pump. Similarly, the top casing of each chamber has three ports, one for the inlet and two for the outlet solenoid valves.

A pressure regulator installed on the air supply set to 3 bar feeds compressed air to the chambers. To create vacuum, the regulated air feed is supplied to the venturi pump (ZL112-K15LOUT-E26L-Q, SMC Pneumatics) and the input solenoid valves (PVQ33-5G-23-01F, SMC Pneumatics) installed on the top casing of chambers. The output valves (PVQ33-5G-40-01F, SMC Pneumatics) installed on the top casing are connected to the vacuum chambers connected with the venturi pump via 10 mm pipes. Peripheral circulation is provided by a backflow pump (FLOJET- R4105-501) connected downstream of the aortic chamber and upstream of the LV chamber. Flowrate is measured using an ultrasonic flowmeter (KEYENCE FD-Q10C), and pressure in both chambers is measured using industrial pressure sensors (PN2009,

IFM Electronic GmbH). Fluid level in the chambers quantifies flowrate mismatch between the two pumps. A short-range infrared transmitter (Tx) and phototransistor (Rx) pair is installed in the aortic chamber to monitor fluid level. The fluid level sensor provides more control over the level resolution compared to commercial distance sensors. The change in the fluid level is translated to the analogue voltage based on the magnitude of the reflected rays to the phototransistor.

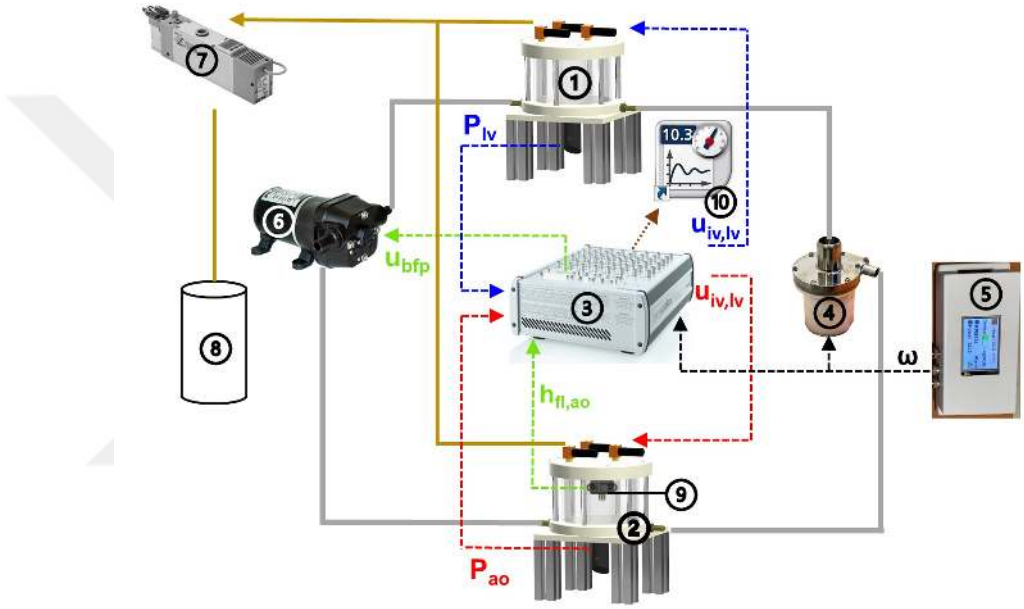


Figure 3.11: Connections between different components of the HMCL. 1) LV chamber, 2) Ao Chamber, 3) MLBX, 4) iHeart prototype, 5) iHeart control box, 6) Backflow pump, 7) Venturi pump, 8) Vacuum Chamber, 9)Fluid level sensor, 10) ControlDesk software

.

The backflow pump and the solenoid valves are controlled using power MOSFETs (IRL-540N). The PWM signals from the controllers are fed to the gate terminal of the MOSFETs to vary the voltage at the drain terminal, thus controlling the actuation of the electromechanical components.

The first prototype of the iHeart LVAD had an operational range of 1500-3200 rpm [108]. The new design features geometric updates for miniaturization and op-

timal hydraulic and hemolytic performance. With electromechanical upgrades the new iHeart LVAD has an operational range of up to 4500 rpm which is tested using the HMCL.

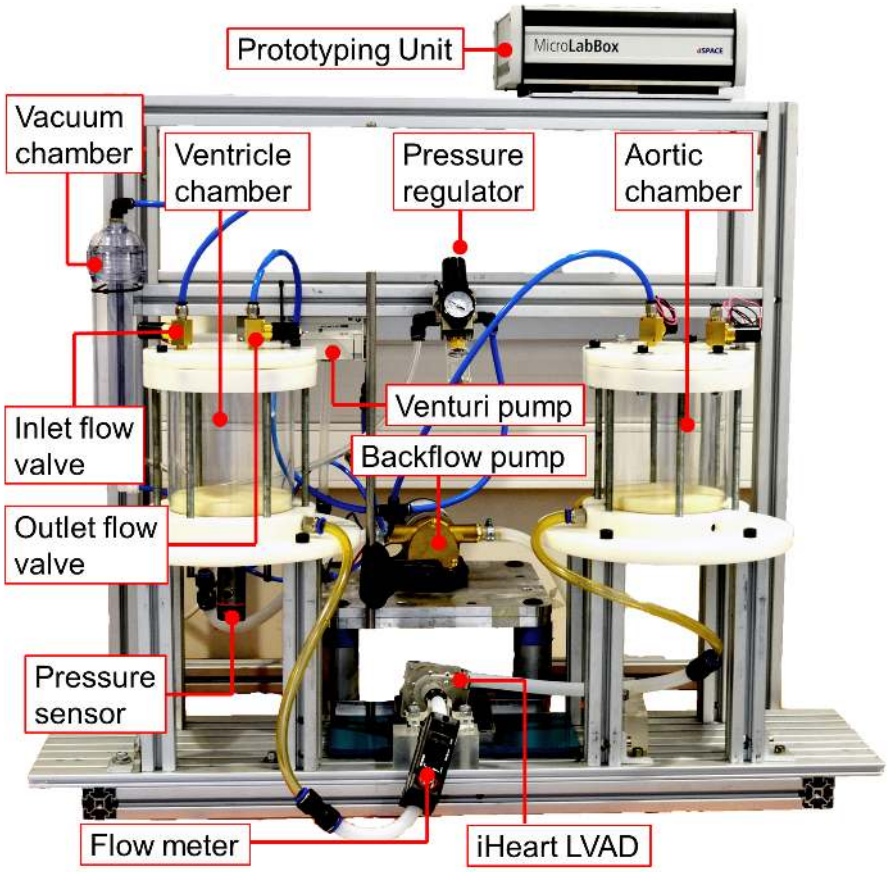


Figure 3.12: The complete hybrid mock circulatory loop

.

Figure 3.11 shows the complete connections between different components of the HMCL. Figure 3.2 shows the developed HMCL setup.

*Computation*

The real-time application requires quick measurements and execution of high-speed control loops making high computation power and low input-output latencies,

imperative. To achieve the desired performance, dSpace GmBH's prototyping unit MicroLabBox, is used. The simulation model interacts with the real world via I/O interfaces found in MicroLabBox's Real-Time Interface (RTI) software for Simulink (rtilib1202). The real-time application is accessed at run time using graphical instruments of the experiment software ControlDesk. MLBX's Field Programmable Graphic Array (FPGA) is used for analogue-to-digital (A/D) conversion and signal generation. Measurements from the flowmeter, pressure sensors, IR sensor, and LVAD motor controller are read using analog-to-digital (ADC) Class 1 converters configured for single conversion mode. The actuators, i.e., the input and output solenoid valves and the backflow pump, run on PWM signals. The PWM period is held constant at 1kHz, whereas the pressure and fluid level controllers command the duty cycle. The varying duty cycle is passed to the actuators at run time using the digital input/output (DIO) Class 1 PWM blocks (Figure 3.13).

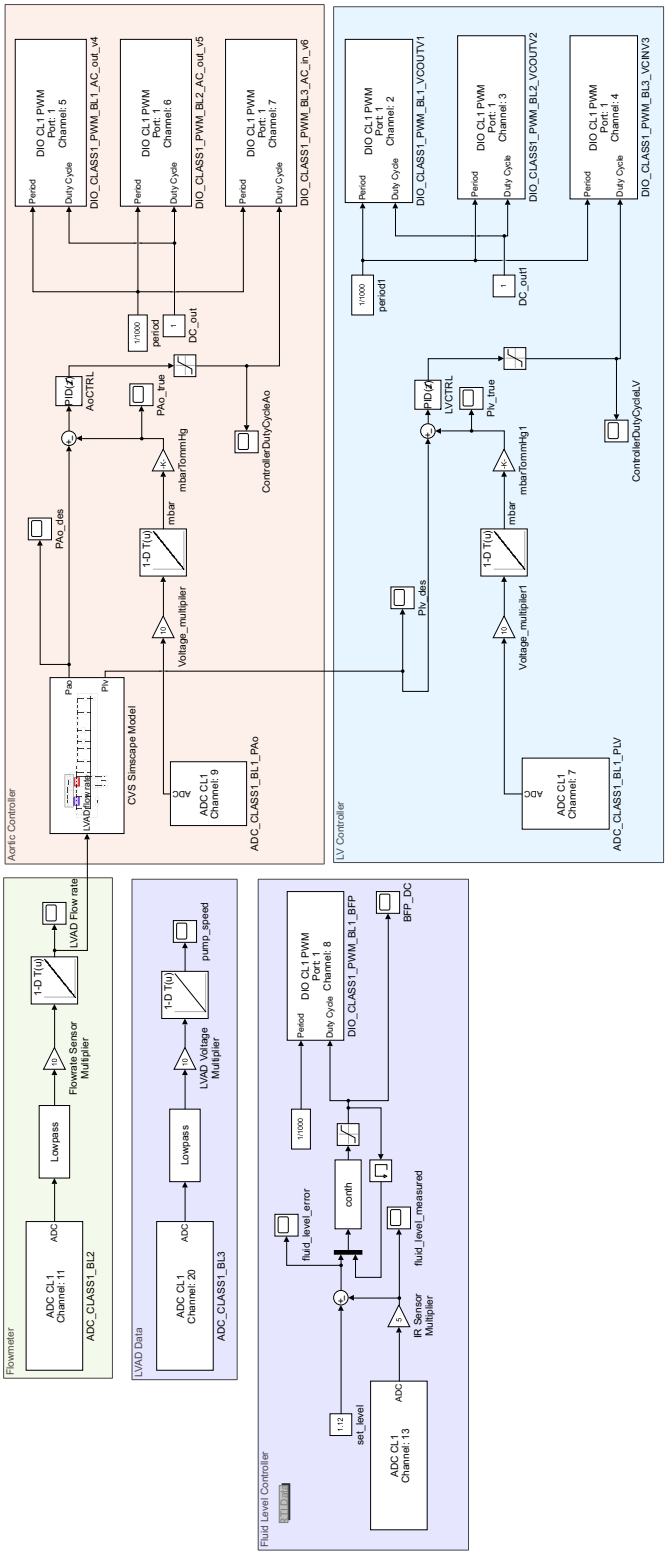


Figure 3.13: Simscape$^{TM}$ cardiovascular system model, pressure and fluid level controllers, sensor data acquisition and pulse signal generation RTI blocks.

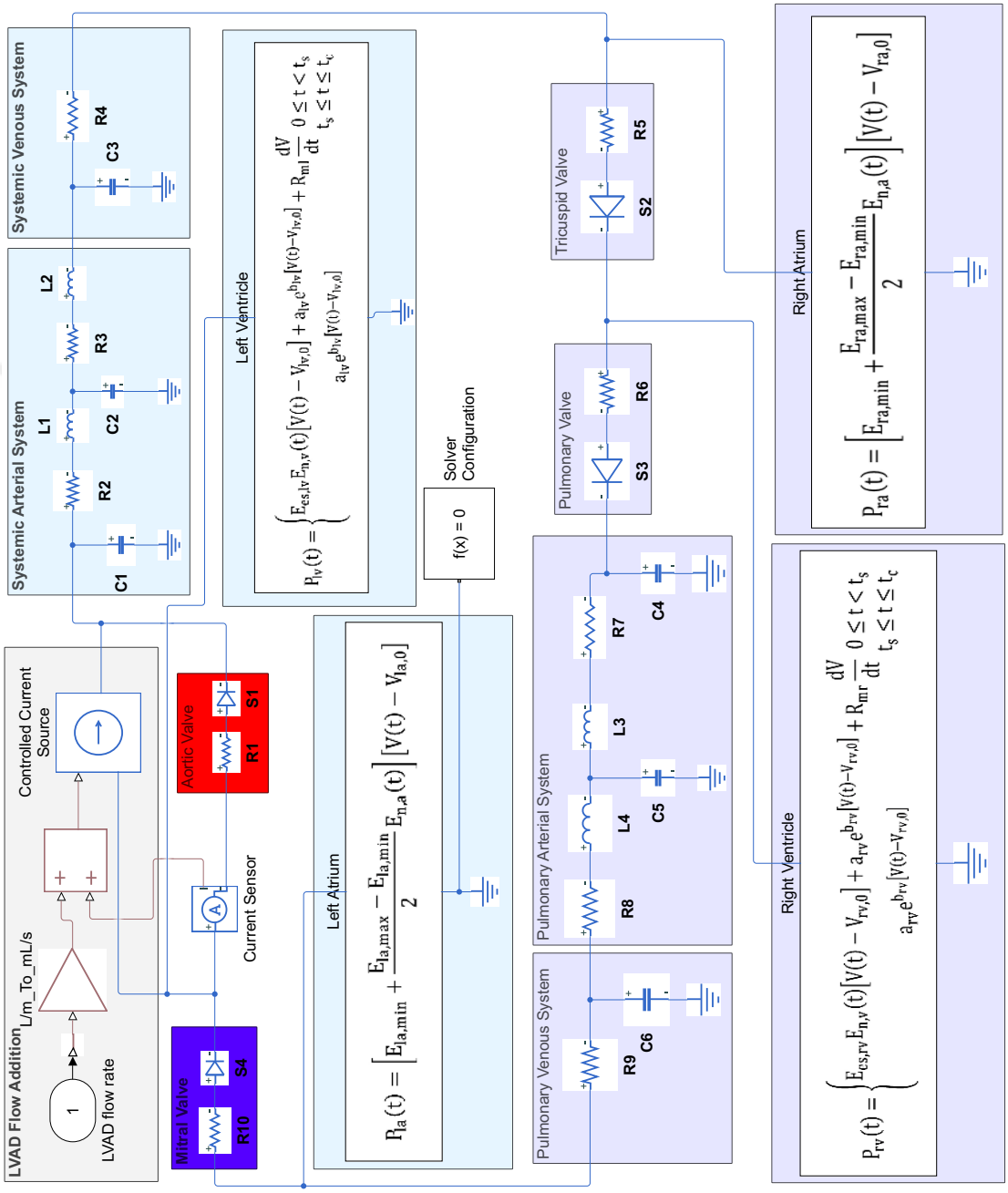


Figure 3.14: LVAD flowrate addition in the Simscape$^{TM}$ cardiovascular system model

*Pressure Controller*

LV pressure and aortic pressure are the upstream and downstream pressures for the LVAD, respectively, that are generated in the LV and aortic chambers (Figure 3.11). The CVS-VAD model generates reference pressure signals tracked by pressure controllers. A controller with low latency, minimal oscillations, overshoot, and steady-state error is required for real-time deployment of the system. A PID controller with anti-windup is chosen. Controller synthesis requires a realistic open-loop model. The valves are excited using pulse signals varying the air mass flowrate through them and, consequently, the pressure inside the chamber. If the outlet valves are excited with a 100% PWM signal, i.e., they remain fully open, the inlet valve alone can be used to control the pressure inside the chambers.

Thus, a single-input-single-output (SISO) model can be identified. System identification is done in MATLAB using the $u_{iv} - P_{lv/ao}$ data obtained for the constant air volume condition. A black-box model, the nonlinear Hammerstein-Wiener (NLHW) model, is identified and linearized for controller development. The NLHW model describes a dynamic system using input and output static nonlinear blocks connected serially with a dynamic linear block in the middle. A dead zone models the input nonlinearity because no pressure change occurs below an inlet valve PWM cycle of 52%. A piecewise linear function models the output nonlinearity. The linear block contains a discrete-time output error model estimated for the input-output data:

$$y(t) = \left[\frac{1 - z^{-1}}{1 - 2.926z^{-1} + 2.851z^{-2}0.9258z^{-3}}\right] u(t) + e(t)$$

The identified model has a 93.96% fit to estimation data. As the pressure chambers are identical, the same model is used for tuning the controllers for both. Owing to different pressure ranges, two PID controllers are tuned separately for the desired performance, i.e., rise time and settling time ¡ 1s, overshoot $< 5\%$ (Table 3.7). Integral clamping-based anti-windup is used to prevent the integral from growing unbounded.

Table 3.7: PID values for the aortic and left ventricle chamber pressure controllers.

| **Parameter** | **LV** | **Ao** |
|---|---|---|
| P | 0.63371 | 0.1949 |
| I | 16.25930 | 3.2394 |
| D | 0.00483 | 2.441e-3 |

*Fluid Level Controller*

Fluid level control prevents chamber drainage and fluid overflow due to LVAD-backflow pump flow mismatch. Furthermore, the pressure controllers are designed for the constant air volume condition, and a fluid level controller maintains air volume. While we can choose the LVAD flowrate as a reference, a simple and direct approach is to control the speed of the backflow pump based on the fluid level in the pressure chambers [103]. An in-house infrared sensor is placed in the aortic chamber to measure fluid height $h_{fl,ao}$ and a SISO model is identified by noting the variation in fluid height in response to changes in the backflow pump PWM cycle $u_{bfp}$. The $u_{bfp} - h_{fl,ao}$ model is identified using experimental data (eq.3.15) with a 73% accuracy. Despite the low the fit to estimation data, the model still sufficiently allows for controller tuning and achieving the desired performance.

$$\frac{Y(s)}{X(s)} = \frac{-0.02753s - 0.01026}{s - 0.004969} \tag{3.15}$$

The fluid level controller is a lead-lag compensator with anti-windup [121] (eq.3.16).

$$\frac{Y(s)}{U(s)} = -0.0685\frac{(s+100)^2}{(s+20)(s+0.01)} \tag{3.16}$$

Although the controller is designed for a constant LVAD pump speed, it readily generalizes for the entire operating range of the LVAD.

*Experimental Protocol*

The model in Figure 3.10 is converted to C-code to run on the MLBX. A system description file (.sdf) is generated, which ControlDesk$^{TM}$ uses to visualize and

log data in real-time. While variable step solvers are better suited for Simscape ™ models, C code mandates using a fixed step solver. An eighth-order Dormand-Prince (ode8) solver with 0.001 time-step is used.

Dilated Cardiomyopathy is simulated as done in Section 3.4.1. The LVAD starting speed is chosen such that regurgitation (backflow) does not occur. For the simulated case, backflow stops at 2500 rpm. The LVAD is operated from 2500 to 4000 rpm and its speed is held constant at each level for approximately 30 seconds.

# Chapter 4

# RESULTS AND DISCUSSION

## *4.1 Healthy and Diseased Heart Simulations*

### *4.1.1 Results*

Figure 4.1A-C and J depict normal hemodynamic behavior characteristics. Key parameters are the arterial pressure (112/70 mmHg), diastole LV volume (133 ml), systol LV volume (49 ml) and cardiac output (5.4 l $min^{-1}$). A comparison of simulated parameters against normal ranges published in prior literature is provided in Table 4.2.

Table 4.1: Comparison of healthy hemodynamic variable ranges in the literature with simulated healthy and heart failure variables. Case I: Simulation using pooled patient data, Case II: Simulation by $E_{es,LV}$.

| **Parameter (Unit)** | **Normal** | **Simulated Hemodynamics** | | |
|---|---|---|---|---|
| | | Simulated Normal | Case I | Case II |
| AoP (mmHg) | 90-140/60-90 | 112/70 | 93/57 | 51/32 |
| LVP $_{peak}$ (mmHg) | 100–140 | 115 | 94 | 52 |
| LAP (mmHg) | 6–12 | 10 | 12 | 18 |
| LVEDV (ml) | 67–171 | 133 | 205 | 143 |
| LVESV (ml) | 22–78 | 49 | 174 | 111 |
| SV (ml) | 50–100 | 73 | 31 | 32 |
| EF (%) | 50–70 | 55 | 15.1 | 22.4 |
| LVCO (L/min) | 4.0–8.0 | 5.4 | 2.5 | 2.6 |

This study presents two cases for the heart failure condition. With Case I representing simulation using pooled heart failure patient data and Case II representing simulation using $E_{es,LV}$ reduction. From Figure. 4.1D we can observe that LV diastolic and LA pressures increase, while LV arterial and systolic pressures decreased by about 20% for pooled heart failure patient data. In contrast Figure. 4.1G depicts a more exaggerated trend (approx. 50%) for $E_{es,LV}$ reduction case. A comparison of Figures 4.1F and 4.1I shows elevated volumes for LV and LA for Case I, while the stroke volume remains the same for each Case (31 ml and 32 ml for Case I and II respectively). Figure. 4.1E, H shows that the LVCO for both cases diminishes by 50% approximately. Figure. The P-V loops in 4.1J appear to be both thinner and shifted towards the left for both simulated heart failure cases when compared against healthy conditions.

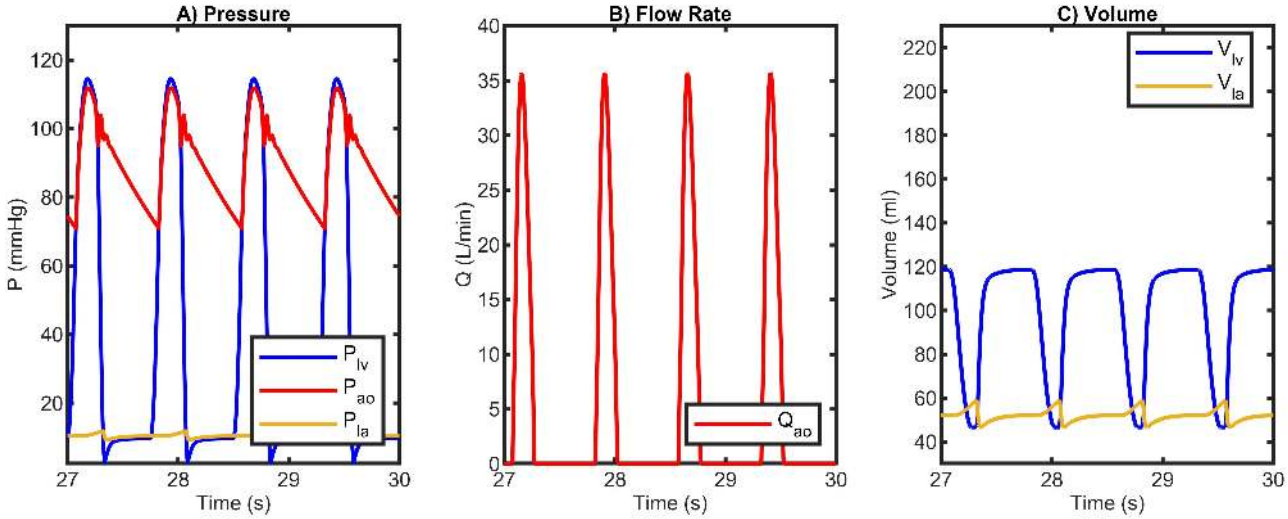

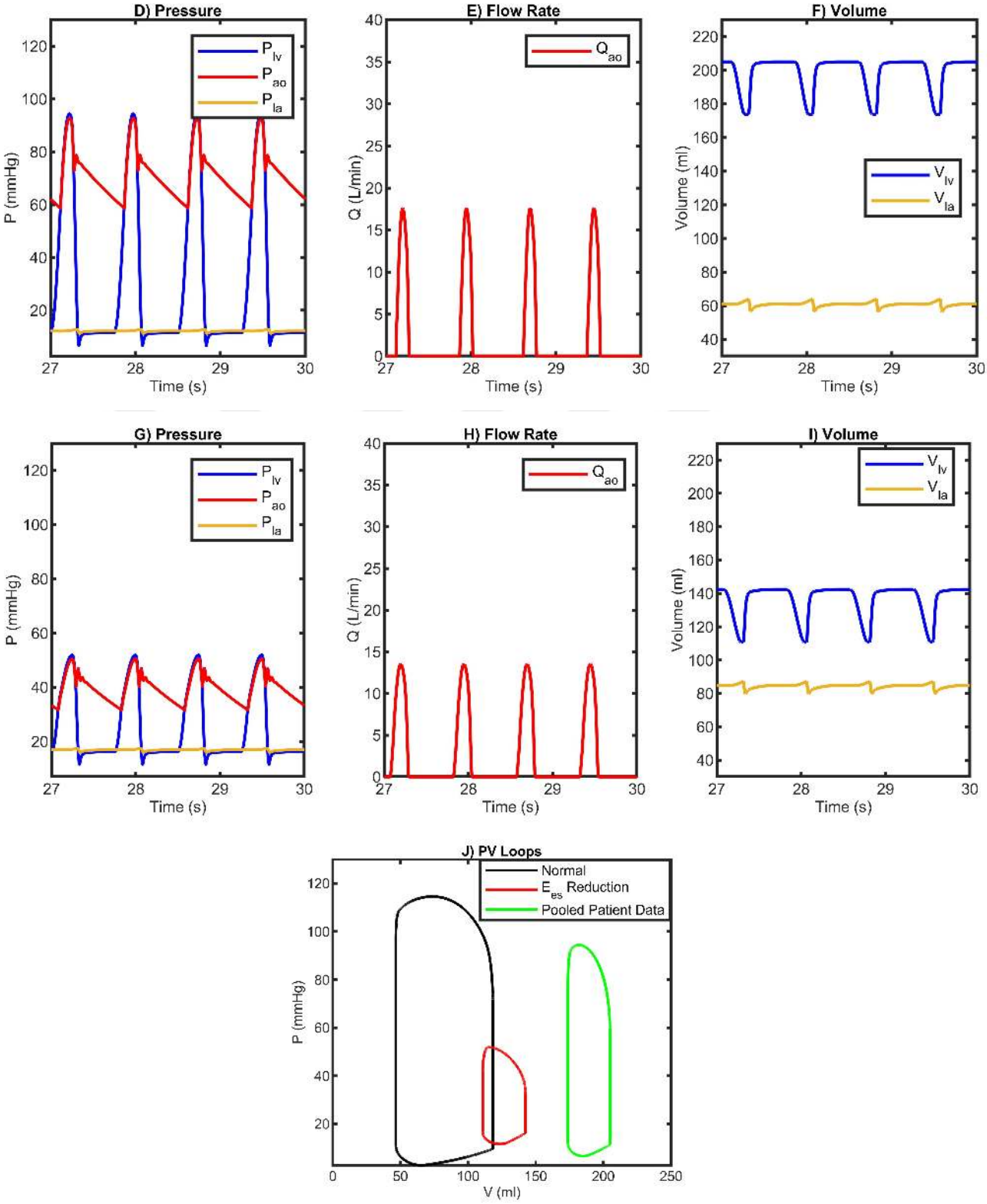


Figure 4.1: Waveforms of pressure, flowrate, and volume for the healthy case (A-C), heart failure modelled using pooled patient data (D-F), and heart failure simulated by a reduction in $E_{es,LV}$, only (G-I). J. P-V loops for healthy (black), heart failure modelled using patient data (green), and heart failure modelled by $E_{es,LV}$ reduction, only (red).

For validation, heart failure patient data from prior literature is compared against the simulated cases. To this end, data from 25 individual data and representative data from 79 patients were processed and layered to determine the P-V loop region for a patient with heart failure. As depicted in Figure. 4.3, Case I P-V loop lies within the layered region marked by collected patient data, while th P-V loop for Case II tends to fall within the outer edges of the region. This demonstrates that modelling heart failure using case II results in an incorrect representation of an actual patient with heart failure.

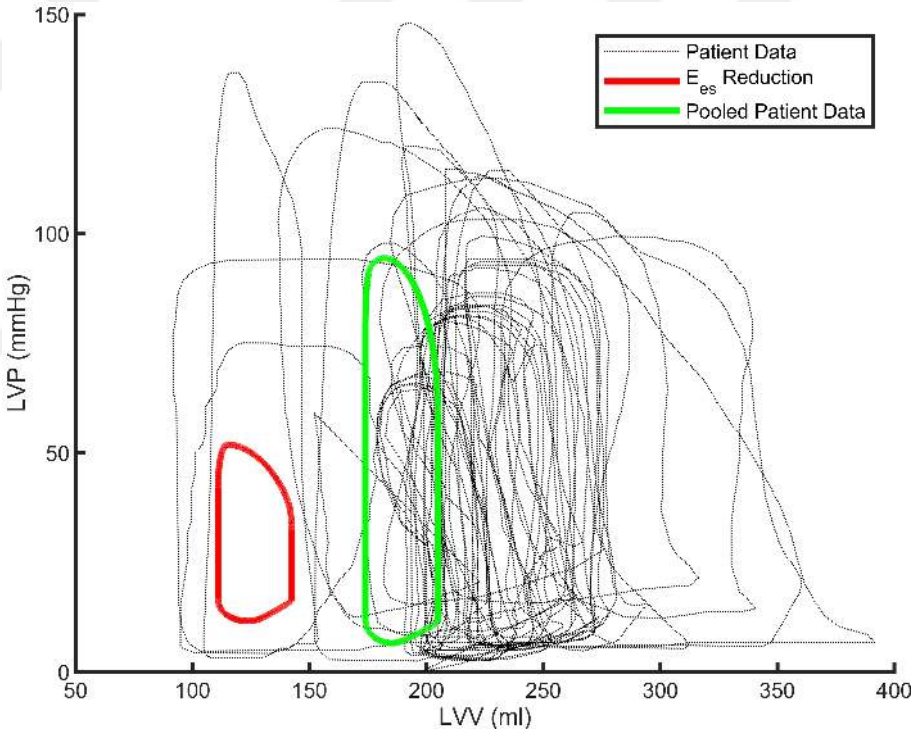


Figure 4.2: P-V loops for advanced-stage patients (published in literature) vs. model-generated P-V loops.

Details of the P-V data summarised in Table 4.2 can be found in Appendix A Table A.2 which have been visualized in the following figures:

Table 4.2: Pooled P-V Data for heart failure patients published in the literature. Case I: Simulation using pooled patient data, Case II: Simulation by $E_{es,LV}$ reduction.

| **Parameter** | **Patient Data** | **Case I** | **Case II** |
|---|---|---|---|
| EF (%) | $25.9 \pm 8.5$ | 15.1 | 22.4 |
| LVEDV (ml) | $214.9 \pm 71.8$ | 205 | 143 |
| LVESV (ml) | $150.2 \pm 63.4$ | 174 | 111 |
| $LVP_{peak}$ (mmHg) | $109 \pm 19.4$ | 94 | 52 |

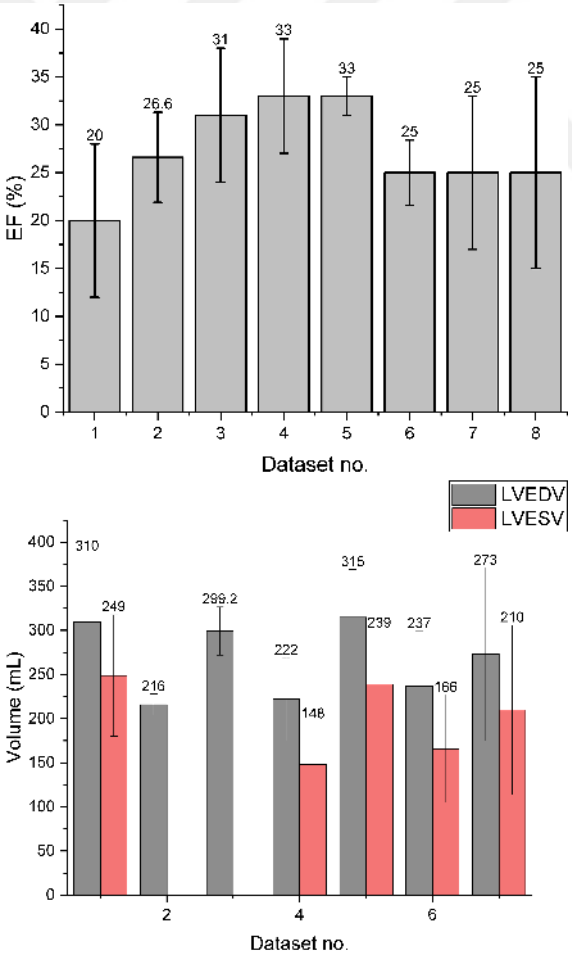

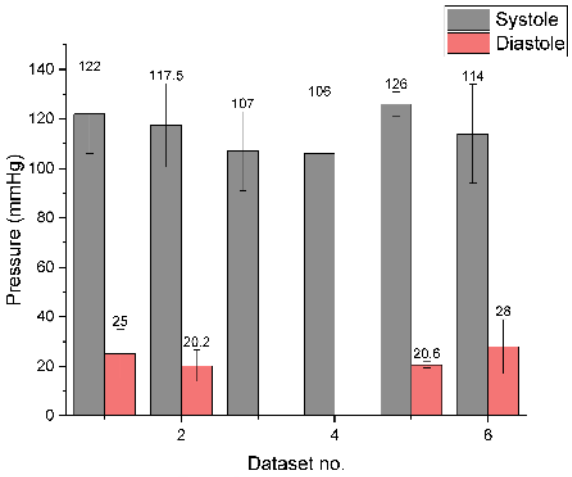


Figure 4.3: P-V loop data for heart failure patients published in literature.

The operational flow rate range of the iHeart VAD lies between 1.5 to 7 $lmin^{-1}$ at a respective rpm range of 1500 to 3200 [108]. Figure 4.4A shows a ramp input being provided to the LVAD, the figure also shows the pressure wave forms resulting from this input. As the rpm of the LVAD increases, the AoP values rise while LAP and LVP fall (Figure 4.4C). From Figure 4.4B, it can be deduced that at 2150 rpm the AoP starts to exceed the LVP, which in turn causes the aortic valve to close. The closing of aortic valve consequently causes the flowrate to become flat. While the pump flow is highly pulsatile and regurgitant in the beginning, eventually the pulsatility decreases with the increase in rpm until it reaches a minimum, after which it starts to gradually increase again. The slope observed for minimum pump flow tends to be positive when pulsatility is decreasing and negative when pulsatility is increasing. The change in sign alludes to a transient obstruction of the inflow graft,a phenomenon referred to as suction. The onset of suction describes the limiting pump speed (2980 rpm) while the critical pump speed (1750 rpm) is defined at the point where regurgitation or backflow stops.

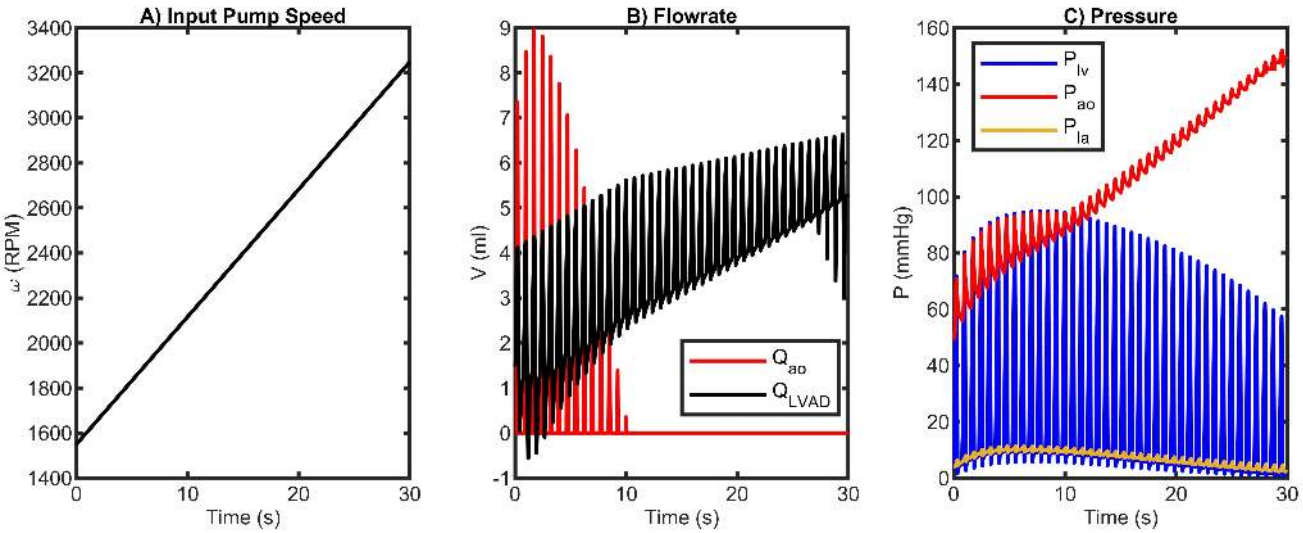


Figure 4.4: Flowrate and pressure waveforms resulting from a linearly increasing LVAD input.

In this study hemodynamic behavior for assisted condition is reproduced for intermediate, critical and limiting speeds (Figure 4.5). Figure 4.5D shows that at the intermediate speed of 2500 rpm, the pulse pressure drops significantly while LVP becomes less than AoP. Figure 4.5A shows the behavior at the critical speed of 1750 rpm, where systolic LVP becomes greater than AoP, while Figure 4.5B shows the aortic valve opening periodically. Figure 4.5G shows the characteristics at the limiting speed of 2980 rpm, where a vanishing pulse can be observed. The LVAD flowrate can be seen plummeting at the end of each cardiac cycle at this speed, which is a key indicator for suction (Figure 4.5H). Figures 4.5A, D, G show, that as LVAD speed increases LAP drops. In the no assist condition (Figure 4.5F) the LV volume drops from the dilated range (174-205 ml) to 115-145 ml at 2980 rpm (Figure 4.5I), and to 165-185 ml at 2500 rpm (Figure 4.5F). Atrial volume drops from an average value of 60 ml at the critical speed (Figure 4.5C) to 20 ml at the suction speed (Figure 4.5I). With increased pump speeds P-V loops shift towards the right (Figure 4.5J). The P-V loops change their shapes from trapezoidal in the no-assist condition to triangular in the assisted condition.

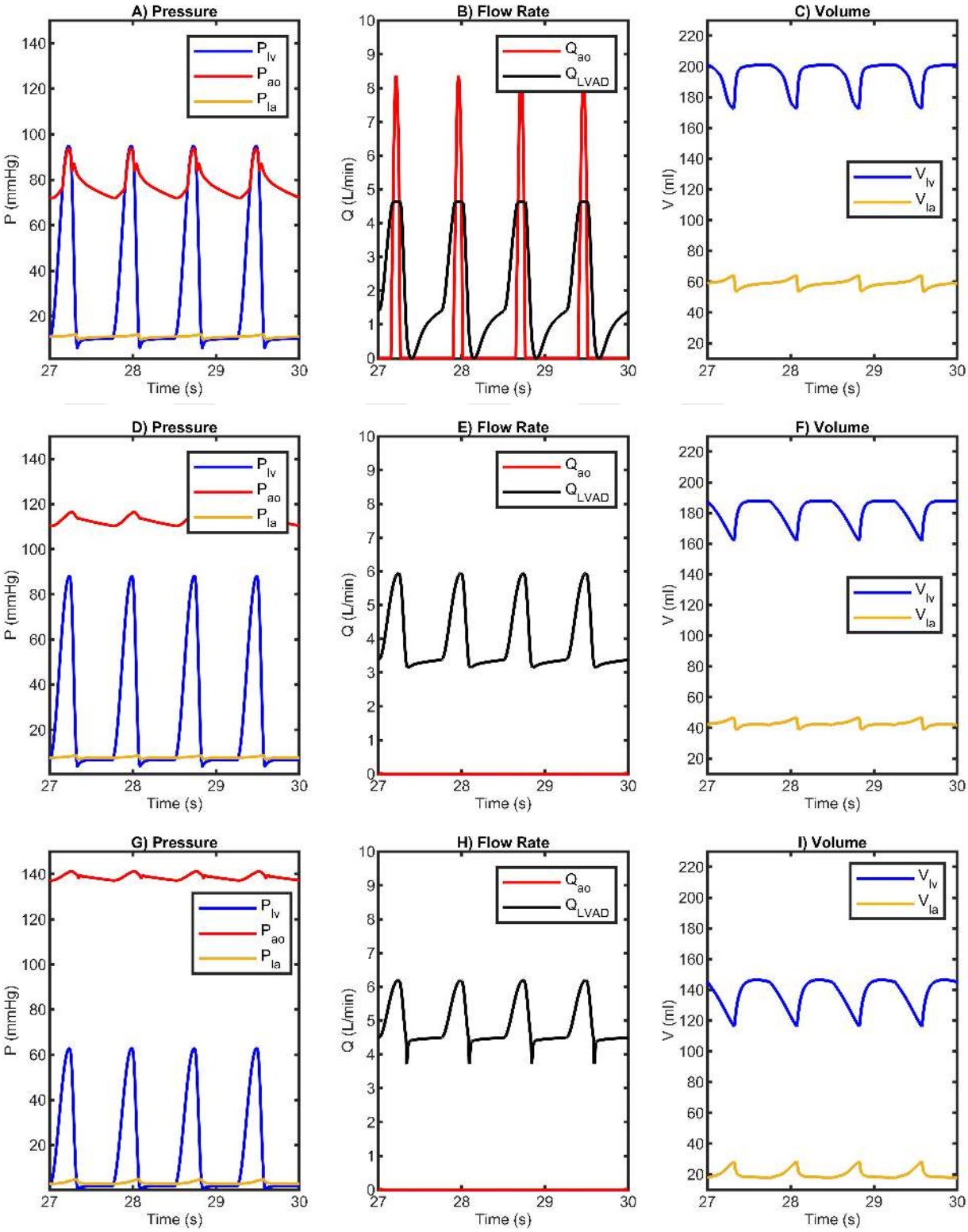
A) Pressure
P (mmHg)
Time (s)
$P_{lv}$
$P_{ao}$
$P_{la}$
B) Flow Rate
Q (L/min)
Time (s)
$Q_{ao}$
$Q_{LVAD}$
C) Volume
V (ml)
Time (s)
$V_{lv}$
$V_{la}$
D) Pressure
P (mmHg)
Time (s)
$P_{lv}$
$P_{ao}$
$P_{la}$
E) Flow Rate
Q (L/min)
Time (s)
$Q_{ao}$
$Q_{LVAD}$
F) Volume
V (ml)
Time (s)
$V_{lv}$
$V_{la}$
G) Pressure
P (mmHg)
Time (s)
$P_{lv}$
$P_{ao}$
$P_{la}$
H) Flow Rate
Q (L/min)
Time (s)
$Q_{ao}$
$Q_{LVAD}$
I) Volume
V (ml)
Time (s)
$V_{lv}$
$V_{la}$

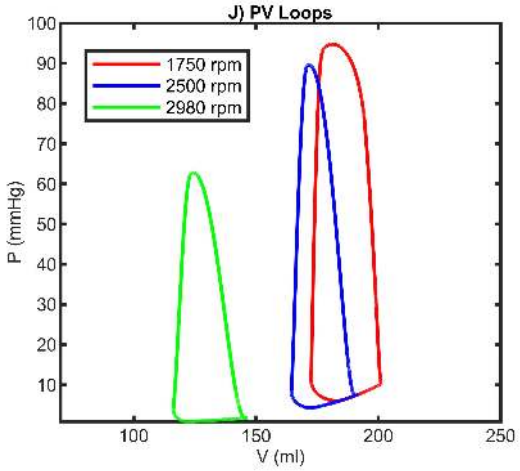


Figure 4.5: Waveforms of pressure, flowrate, volume, and P-V loops generated at critical (A-C), intermediate (D-F), and suction speed (G-I). J. P-V loops at critical (red), intermediate (blue), suction speed (green).

To understand behavior of hemodynamic variables, simulations are conducted at 100 rpm increments within the iHeart VAD's operating range (Figure 4.6). The sum of $Q_{LVAD}$ and LVCO is known as the practical cardiac output or CO. Figure 4.6A shows that CO tends to have a linear relationship with pump speed, however, LVCO becomes constant during the aortic valve closure region (which occurs at 2100 rpm approx.) before starting to increase again. The LVAD pressure head and consequently the MAP increases with LVAD rpm (Figure 4.6B). Figure 4.6C shows that there is a substantial reduction in LVEDV when compared against LVESV before aortic valve closure which occurs at 2150 rpm. This in turn leads to a decreased in their SV (Figure 4.6D). Even though preload continues to decrease after closure, a diminutive increase can be noted in the SV. The increase however, does not exceed pathological values i.e., remains $< 55$ ml.

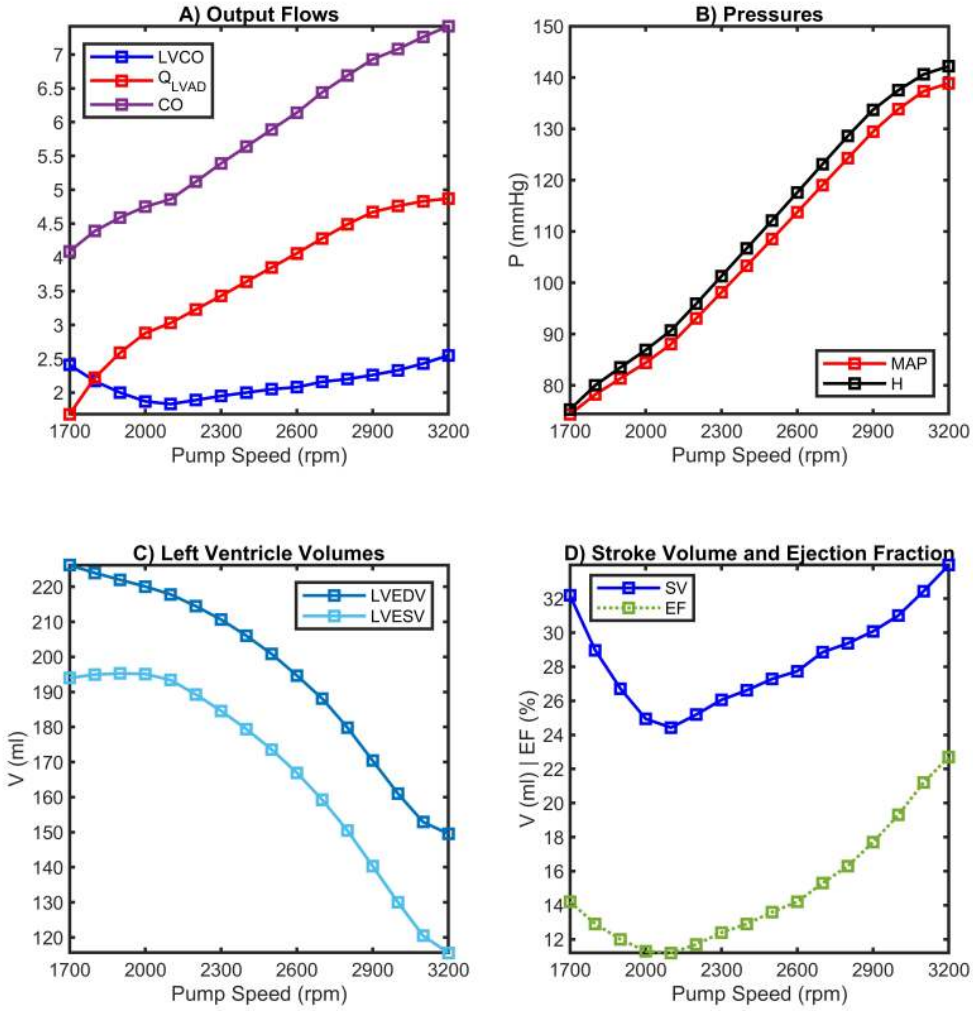


Figure 4.6: Variaton in (A) Output flows (LVCO, $Q_{LVAD}$, CO), (B) Pressures (MAP and H), (C) LV volumes (LVESV, LVEDV), (D) Stroke volume (SV), and ejection fraction (EF) with increasing LVAD speed.

Both the HeartWare and iHeart VAD are continuous flow centrifugal pumps that operate in approximately the same range. The operating range for the HVAD is 2300-3200 rpm and that for the iHeart VAD is 1500-3200 rpm. Table 4.3 compares hemodynamic parameters of iHeart VAD using simulated pathophysiological conditions with published HVAD parameters [95, 116].

Table 4.3: iHeart VAD vs. HVAD hemodynamic variables.

| **Parameter (Unit)** | **HVAD** | **iHeart VAD** |
|---|---|---|
| $\omega$ (rpm) | $2683 \pm 144$ | 2200 |
| EF (%) | $23 \pm 10$ | 11 |
| CO (L/min) | $4.5 \pm 1.4$ | 5.2 |
| $Q_{LVAD}$ (L/min) | $4.2 \pm 0.9$ | 3.3 |
| MAP (mmHg) | $88 \pm 13$ | 90 |
| LAP (mmHg) | $12.6 \pm 5.3$ | 8 |

### *4.1.2 Discussion*

The CVS model successfully reproduces healthy hemodynamics. Comparing the simulated healthy hemodynamics results to the ranges found in the literature corroborates the model's efficiency [112, 122, 123].

A dilated ventricle with diminished contractility, germane to ER, results in deteriorated perfusion conditions, higher intra-ventricular residual blood volume and rightwards shift of the heart failure P-V loops. An elevated afterload and preload can be observed from the rightwards shift of the P-V loops, whereas their thinning illustrates reduced CO. An increase in end-systolic volume (ESV) and hence, a decrease in SV is also caused by an increased afterload [70]. The CVS-VAD model adequately reproduces advanced-stage heart failure hemodynamics and this is substantiated by comparing the results with published data [114, 124, 125, 126, 127, 128, 129, 130, 131, 132, 133, 134, 135, 136, 137, 138, 139, 140]. All hemodynamic variables in Table 4.2 are within advanced-stage heart failure ranges found in the literature, except EF. This underestimation can be ascribed to statistical bias, since such diminished EFs have been observed (refer to collected hemodynamic data in Table A.2) for certain patients with severe heart failure. Further indicating the superiority of Case I, pressures are severely underestimated for simulations conducted with only a reduction in $E_{es,lv}$ (Case II).

At low pump speeds, some of perfusion takes place through the aortic valve while the remainder of the flow passes through the LVAD resulting in a partial-assist condition. At intermediate-to-high pump speeds, the aortic valve is completely closed throughout the cardiac cycle. A sustained closure of the aortic valve can potentially result in valve thrombus which can exacerbate to aortic stenosis [141]. High pump speeds reduce flow pulsatility. This reduction is a widespread consequence of using cf-LVADs that has been attributed to vascular dysfunction and remains a significant concern for cf-LVAD recipients [142]. At high speeds, the LVAD increasingly unloads the LV, i.e., LV unloading is higher at elevated pump speeds. Leftwards shift of the P-V loops also alludes to this unloading effect with increasing pump speed. As the LVAD continuously pumps blood to the aorta, bypassing the isovolumetric phase of the cardiac cycle's contraction and relaxation phases. This circumvention of the isovolumetric phase makes the P-V loops triangular. LV volumes: LVV, LVEDV, and LVESV are degraded with increasing pump speeds. LV dilation is ameliorated by the decrease in LVEDV as this reduces the ventricular volume range in a cardiac cycle, which can potentially lead to reverse ventricular remodelling. In this scenario, the LVAD acts as a bridge to recovery. Increasing afterload with increasing LVAD speed continually increases MAP. LVCO, on the other hand, does not vary significantly, conforming to the findings of clinical studies on HRT [116]. Since CO is defined as the product of the SV and HR, and HR is held at a constant value throughout the simulation; the trends in LVCO and EF can also be attributed to SV changes. With increasing pump speeds, SV decreases with increased afterload (a consequence of elevated MAP) independent of left ventricular ejection. A similar trend in CO has been reported for an HVAD-implanted patient [143]. Regardless of support levels, EF does not attain normal values. It is pertinent to note here that the LVAD's restorative effect on EF is not an acute phenomenon but rather studied over long durations of time clinically. Regardless, clinical LVAD studies report that EF only improves slightly and rarely reaches normal values. Hence, it is not just mechanical unloading which can be expected to lead LV recovery for advanced-stage heart failure patients, and it is imperative to investigate novel pharmacologic inter-

ventions [144].

Table 4.3 provides a comparison of the results of the iHeart VAD simulations with clinical studies conducted using the HVAD. It can be noted that the iHeart VAD prototype under test has comparable performance. The a CVS-VAD model's ability to replicate assisted hemodynamics is substantiated by the fact that similar trends in aortic pressure, LVAD flowrates, and flow pulsatility were reported in a clinical study conducted during cf-LVAD implantation [145].

Support simulations are conducted with 100-rpm increment to determine an optimal speed setting for the modelled heart failure condition. CO remains within the normal range (4-8 L/min) at all levels of support for the simulated pathophysiological condition. Specialists employ a CO-based method for LVAD selection while circumventing suction. According to this method, a CO increment. due to increased pump speed, of less than 0.25 L/min indicates a limiting condition and further increments in speed are not feasible [146]. The CO increment for the simulated case is below 0.25 L/min above 2800 rpm. The suction speed was identified previously as 2980 rpm based on the flowrate waveform. Hence, it is further reinforced that an increase in pump speed will result in suction. MAP is capped at 90 mmHg to optimize CO and minimize the risk of a cardiac stroke [147]. An LVAD operating pressure of 100 mmHg, however, has been reported to meet physiological needs [110]. Thus, under the pressure constraints, the pump speed is limited to 2200 rpm.

Owing to the modular design of the simulation platform, modifications can readily be made to study LVAD performance under a multitude of pathophysiological conditions. For this purpose, the hemodynamic parameters can be varied in their pathological ranges identified in Table 3.4, and their subsequent effect on hemodynamic variables, regurgitant, optimal, and limiting speeds can be studied. A study is conducted on the effect of changes in the pathophysiological parameters on suction speed in Section 4.3. The CVS-VAD model can also be adjusted to include patient-to-patient heterogeneity and could potentially assist clinicians in identifying optimal LVAD speed ranges prior to implantation. Furthermore, as is done for heart failure modelling, the LVAD modelling can be validated by calibrating

the pump equation 3.7 for a commercial LVAD and comparing the resulting hemodynamics with published data. The CVS model alone in itself is a valuable tool as it precludes the need to develop cumbersome fully mechanical mock circulatory loops. By developing pressure-generating numerical-hydraulic interfaces, an LVAD prototype can be tested by connecting it to the CVS model directly. The CVS-VAD model is utilized in a hybrid mock circulatory loop the details of which can be found in Section 4.4.

Certain limitation of this study include the absence of short-term arterial pressure regulation, autoregulation of CO, systemic venous resistance and compliance. Only the atria and ventricles are active components whereas the other hemodynamic parameters are maintained at constant values throughout the cardiac cycle. Heart rate, systemic vascular resistance and compliance, ventricles' end-systole elastances, etc., adapt through baroreflex control mechanisms, the implementation of which is necessary in order to model pathophysiological scenarios more reliably and comprehensively. Incorporating autoregulatory adaptive mechanisms in the model is limited due to the high numerical stiffness of the model, which, if included, would limit real-time executability. The model takes approx. 23s to simulate 24 beats (i.e., 30 s) using the ode23t solver. Implementation of autoregulation whilst retaining real-time executability requires the reduction of rapid changes in the system. Unfortunately this approach is unfeasible for the current study due to the mercurial nature of the CVS. Another mitigation strategy is to simplify the model; however, this is counter-productive as the goal of this study is develop a real-time capable all-encompassing model. Therefore, a sophisticated system with powerful computational resources becomes imperative for further improvements.

## *4.2 Hemodynamic Ramp Testing Simulations*

### *4.2.1 Results*

The hemodynamic variables undergo different changes with increasing pump speed (Figure 4.7). Increase in CVP is approximately 25% (Figure 4.7 a), decrease

in PCWP is approximately 26% (Figure 4.7 b), whereas MAP is approximately 27% (Figure 4.7d) elevated across all cases. Variation in CO is negligible i.e., approximately 5% (Figure 4.7c).

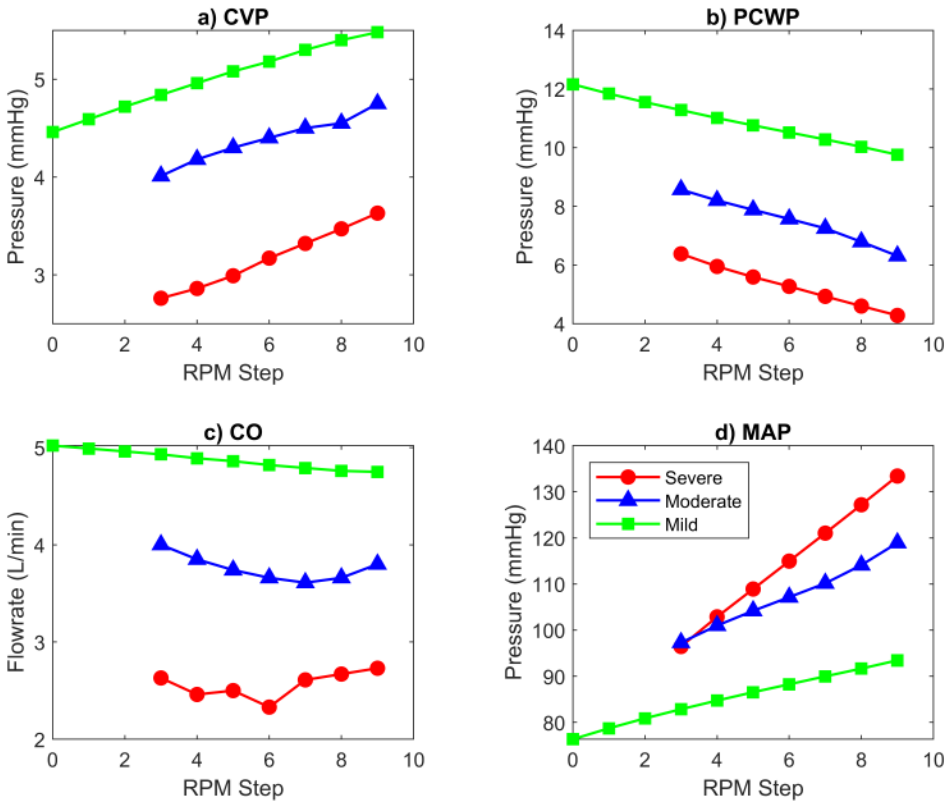


Figure 4.7: Trends in the hemodynamic variables for severe (red), moderate (blue), and mild (green) heart failure virtual patients. (A) CVP, (B) PCWP, (C) CO, and (D) MAP with increasing HVAD speed .

CVP-PCWP correlation plots are generated to observe hemodynamic trends for each patient. The CVP-PCWP is divided into five zones based on the normal ranges for CVP, PCWP and CVP/PCWP: normal, hypovolemic, LHF, RHF, and volume overload (Figure 4.8a). All three virtual patients fall in the southwest portion of the CVP-PCWP plot therefore an enlarged view of it is provided to better investigate the effect of speed changes (Figure 4.8b). The severe heart failure case lies in the

hypovolemic zone from 2600 rpm to 2800 rpm and enters the right heart failure zone after approximately 2950 rpm constraining the pump speed between 2800 and 2950 rpm. The moderate and mild heart failure cases occupy the normal portion for the entire speed range however the moderate case crosses the CVP/PCWP ratio line above 3000 rpm.

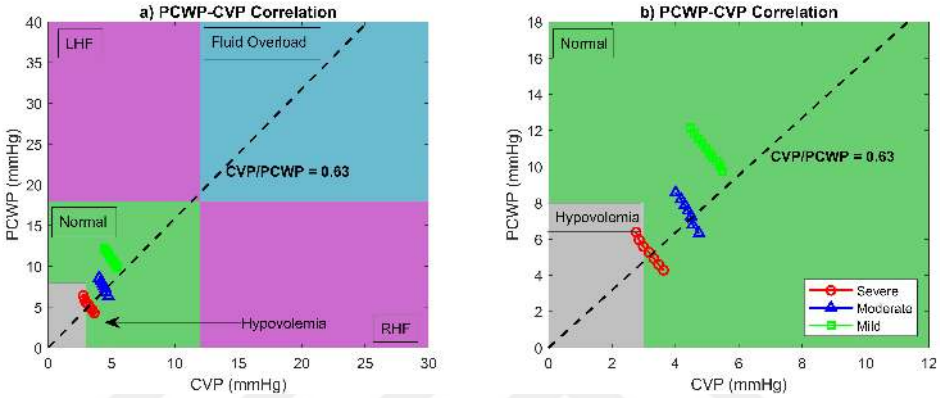


Figure 4.8: CVP-PCWP correlation for severe (red), moderate (blue), and mild (green) heart failure virtual patients. (A) CVP-PCWP plot with LHF, fluid overload, normal, hypovolemic, and RHF zones. (B) Enlarged CVP-PCWP plot with normal and hypovolemic zones.

Current sensors (Figure 3.8) are used to note regurgitation, aortic valve closure, and pulsatility variation resulting from pump speed increments (Figure 4.9). For the severe case, aortic valve closes at 2700 rpm and backflow stops at 2900 rpm (Figure 4.9c). For the moderate case, the aortic valve closes at 3100 rpm (Figure 4.9j), whereas regurgitation stops ahead of it at 2700 rpm (Figure 4.9g). Backflow is absent, and the aortic valve continues to open throughout the operating range of the LVAD for the mild case (Figure 4.9k-o). Flow pulsatility decreases with increasing speed.

Aortic pressure waveforms are recorded using voltage sensors at the same drive conditions (Figure 4.10). Increasing pump speed decreases the pulse pressure by approximately 25% whilst raising the MAP by approximately 27%. As Figure 4.6d

depicts, the severe and moderate cases are hypertensive from the outset whereas the mild case becomes hypertensive at 2500 rpm. Dicrotic notches disappear at elevated LVAD speeds i.e., at 2900 rpm for severe (Figure 4.10b) and 3100 rpm for moderate case (Figure 4.10j). Dicrotic notches persist for the mild case (Figure 4.10k-o). Peak LV pressure continues to fall with increasing LVAD speed with the most significant decrease in the severe case, followed by the moderate and mild cases respectively.

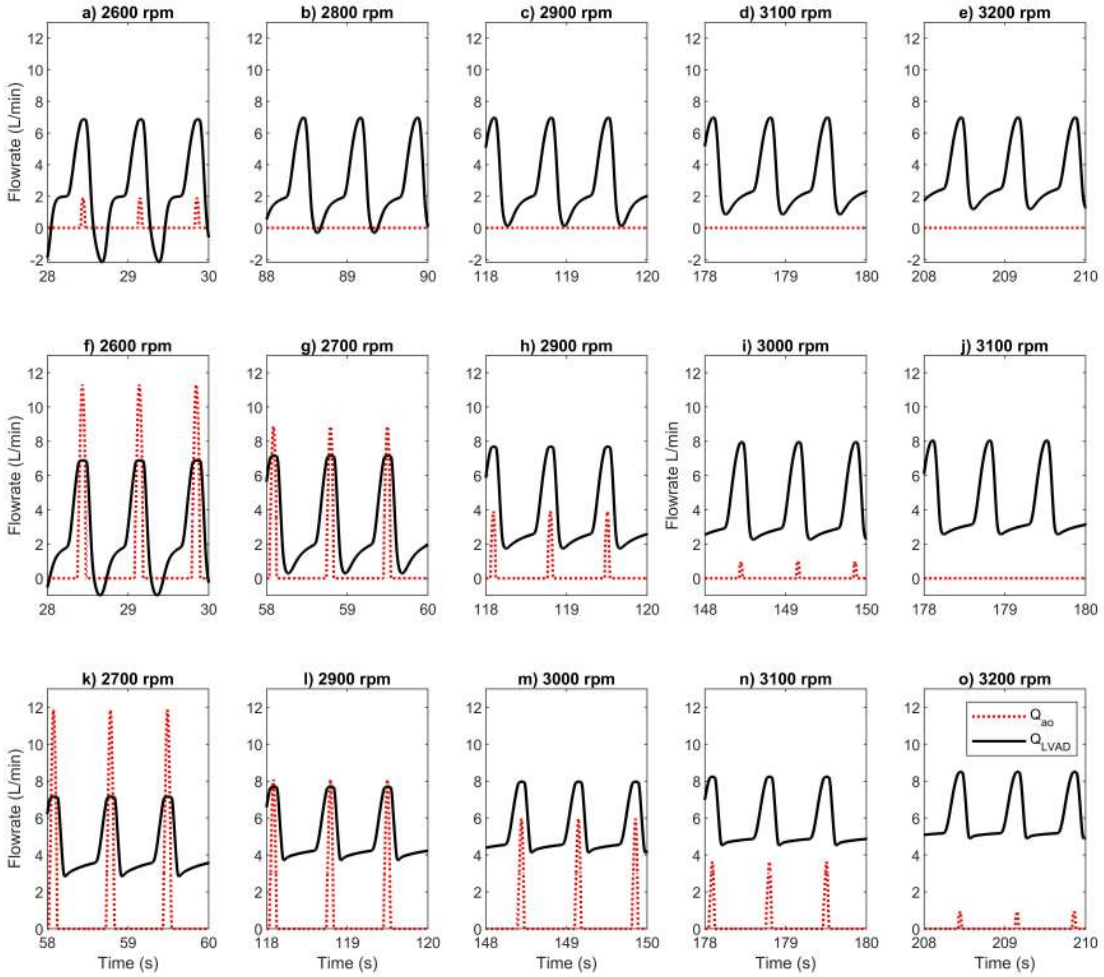


Figure 4.9: $Q_{Ao}$ and $Q_{LVAD}$ waveforms at different speeds in red and black, respectively, for the a-e) Severe, f-j) moderate, and k-o) mild heart failure patient.

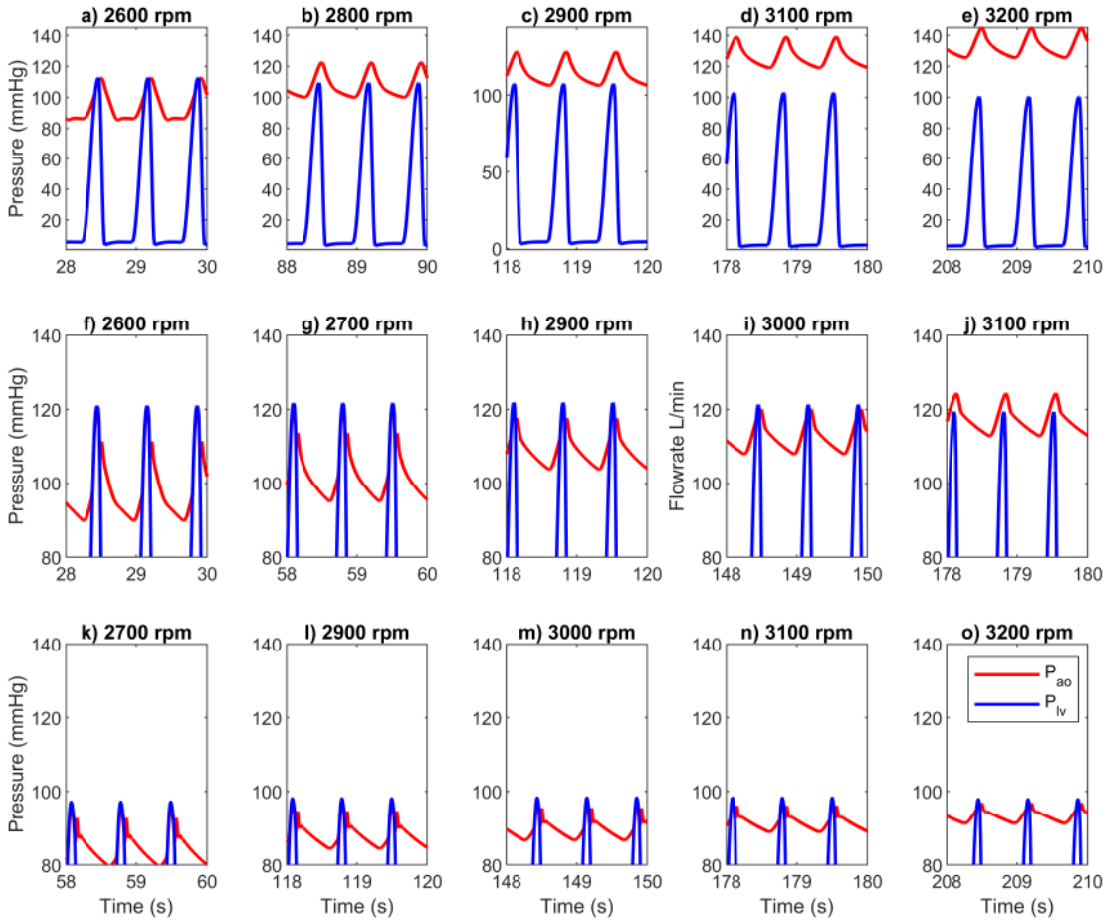


Figure 4.10: $P_ao$ and $P_{lv}$ waveforms at different speeds in red and blue, respectively, for the a-e) Severe, f-j) moderate, and k-o) mild heart failure patient.

### *4.2.2 Discussion*

Speed optimization requires a holistic view of the hemodynamic variables. Normal CVP lies between 3-12 mmHg, whereas normal PCWP lies between 8-18 mmHg [116]. CVP/emia and a low venous return substantiated by the low cardiac outputs. CVP for the moderate and mild cases is successively higher. A low PCWP is indicative of low compliance of the left ventricle. Thus, the severe case has the lowest PCWP, the mild case has the highest, and the moderate case lies midway between the two. Hypovolemia indicated by depreciated CVPs and COs is corroborated by the CVP-PCWP plot. The severe case is hypovolemic at low speeds, and the heart

failure condition worsens at high speeds whereby RHF is induced in both severe and moderate cases. The CVS-VAD model aptly demonstrates the exacerbating effect of LVADs. The mild case remains in the normal zone for the complete operating range.

With increasing LVAD speed, CO reaches a local minimum before increasing, which can be observed for severe and moderate virtual patients. The CO for the mild case would follow the same trend at higher speeds. However, CO does not vary significantly, in line with clinical findings [116]. The MAP increases with increasing LVAD speed due to increase in afterload. Trends observed in PCWP, CO, and MAP match those found in clinical studies [116, 95, 94]. In the case of CVP, a value of 8-10 mmHg is considered optimal for starting the HRT. For the simulated cases, CVP<8 mmHg, hence, an infusion of 250ml/h physiological solution must be administered [148]. True effect in CVP for the modeled cases requires simulating infusion over time which is beyond the scope of the current work.

Optimal speed considerations also include taking the flowrate and pressure waveforms into account. The recommended MAP is <80 mmHg thus all cases must be treated for hypertension by medication [149]. Aortic valve opening consideration limits the LVAD speed as persistent closure of the aortic valve can lead to valve thrombus which could cause aortic stenosis [141]. Optimal speed range are thus 2800 rpm $< \omega <$ 2900 rpm for the severe case, 2900 rpm $\leq \omega <$ 3000 rpm for the moderate case, and $\omega >$ 2900 rpm for the mild case.

Correlating the flowrate waveforms with pressure waveforms shows that a dicrotic notches coexist with AV opening. The secondary rise in pressure is due to the elastic recoil of the aortic wall due to closure of AV. Clinically, the appearance of the dicrotic notch is considered a good predictor of AV opening [150] which is corroborated by the model. Transaortic Gradient (TAG) is the difference between peak LV pressure and aortic pressure at systole. It is a measure of LVAD unloading and is found to linearly increase with pump speed, in clinical studies [151]. For the present case, as the aortic valve continues to open in the moderate and mild cases, TAG can be determined for the severe case only where it increases linearly. Lack of

TAG augmentation may be indicative of thrombosis.

The model is suited for a preclinical study by calibrating it for a specific patient. This requires the determination of the disease parameters; $E_{es,lv}$ , $C_2$, $C_5$, a, $R_{ml}$, $R_s$, $R_p$, and b, all of which can be determined non-invasively albeit indirectly by echocardiography and magnetic resonance imaging (MRI). The benefit of using an acausal approach and choosing Simscape to do so is that the model can be made dynamic. This can be done by generating the C-code of the model and deploying it to a real-time hardware platform whereby hemodynamic changes can be observed by changing parameter values in real-time.

While this in-silico approach allows us to assess hemodynamics and estimate optimal speeds, ramp studies also involve echocardiographic assessments that cannot be made using the current model. Other limitations include the lack of drug intervention effect and autoregulatory mechanisms' incorporation, however, these features can readily be added due to the modular nature of the modeling approach.

## *4.3 Design of Experiments for Suction Detection*

### *4.3.1 Results*

Main effects are presented in Figure 4.11, interaction plots in Figure 4.12 and 4.13. It can be seen that $E_{max,lv}$ and a undergo a similar variation i.e., direct proportionality across the operating range of the LVAD whereas $C_2$, $C_5$, a, $R_{ml}$, $R_s$, $R_p$, and b experience the opposite. The slopes of the curve show the strength of the direct and inverse effects with $R_{ml}$ having the largest slope followed by a, b, $C_5$, $R_p$, $E_{max,lv}$, $C_2$, and $R_s$. The parameters with the strongest effects are expected to have the most significant influence on suction speed. In the interaction effects, only 13 out of the total 28 are statistically significant while the others have a p-value of $<$ 0.1. Parameters with insignificant interaction effects are grey.

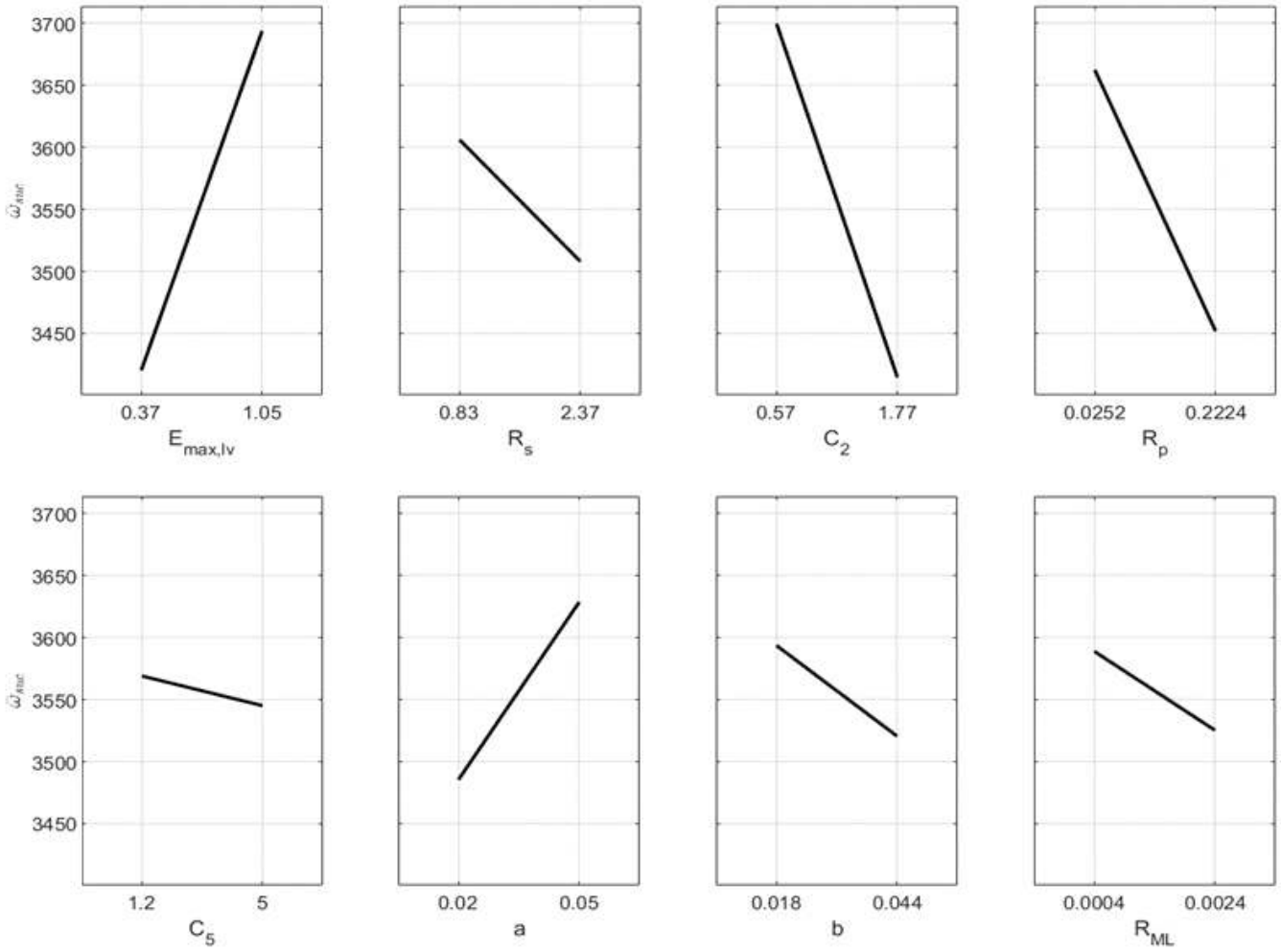


Figure 4.11: Main effect plots for suction speed

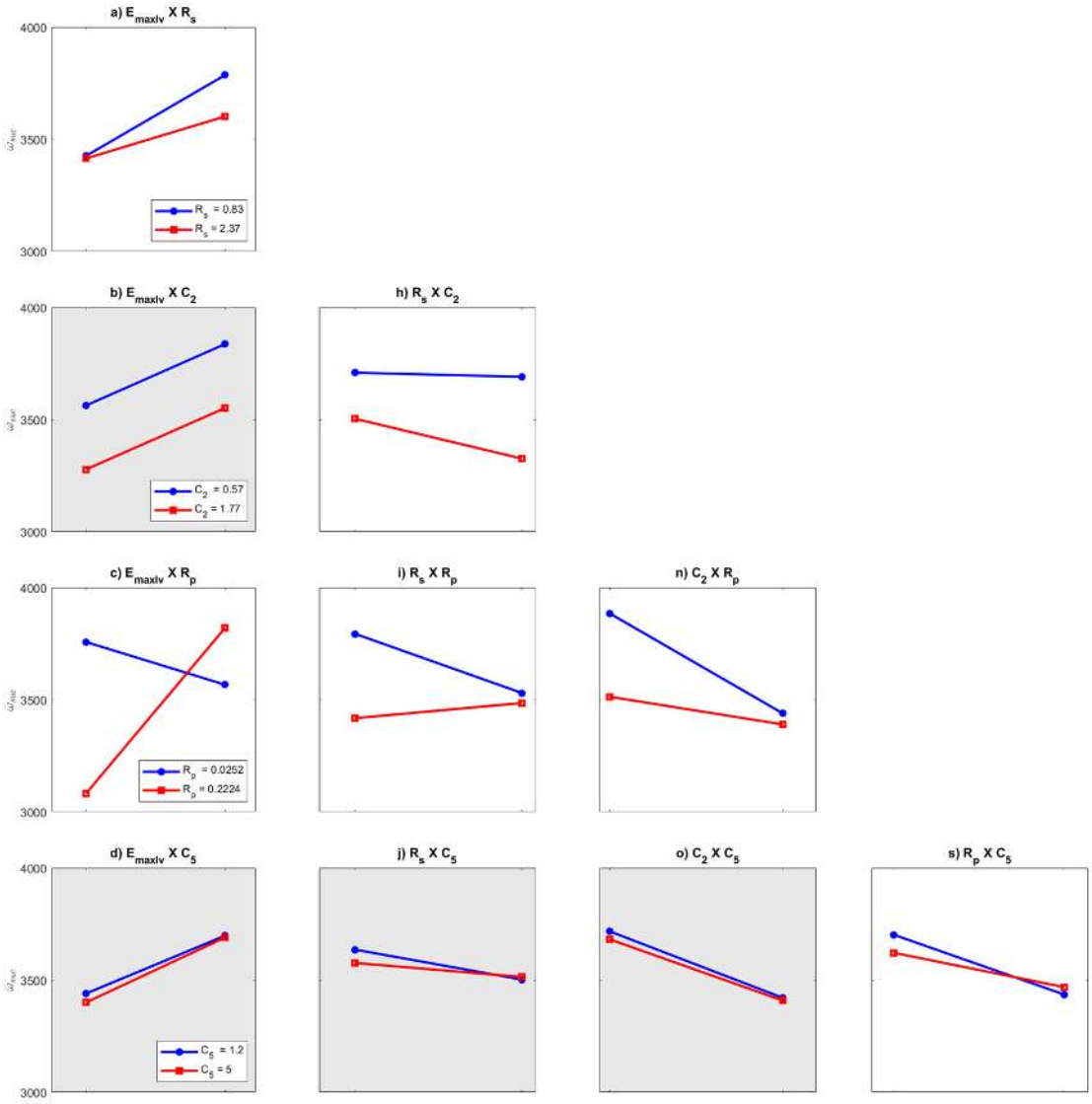


Figure 4.12: Interaction plots 1-10 of 28. Grey plots denote no statistically significant interactions ($p<0.1$)

.

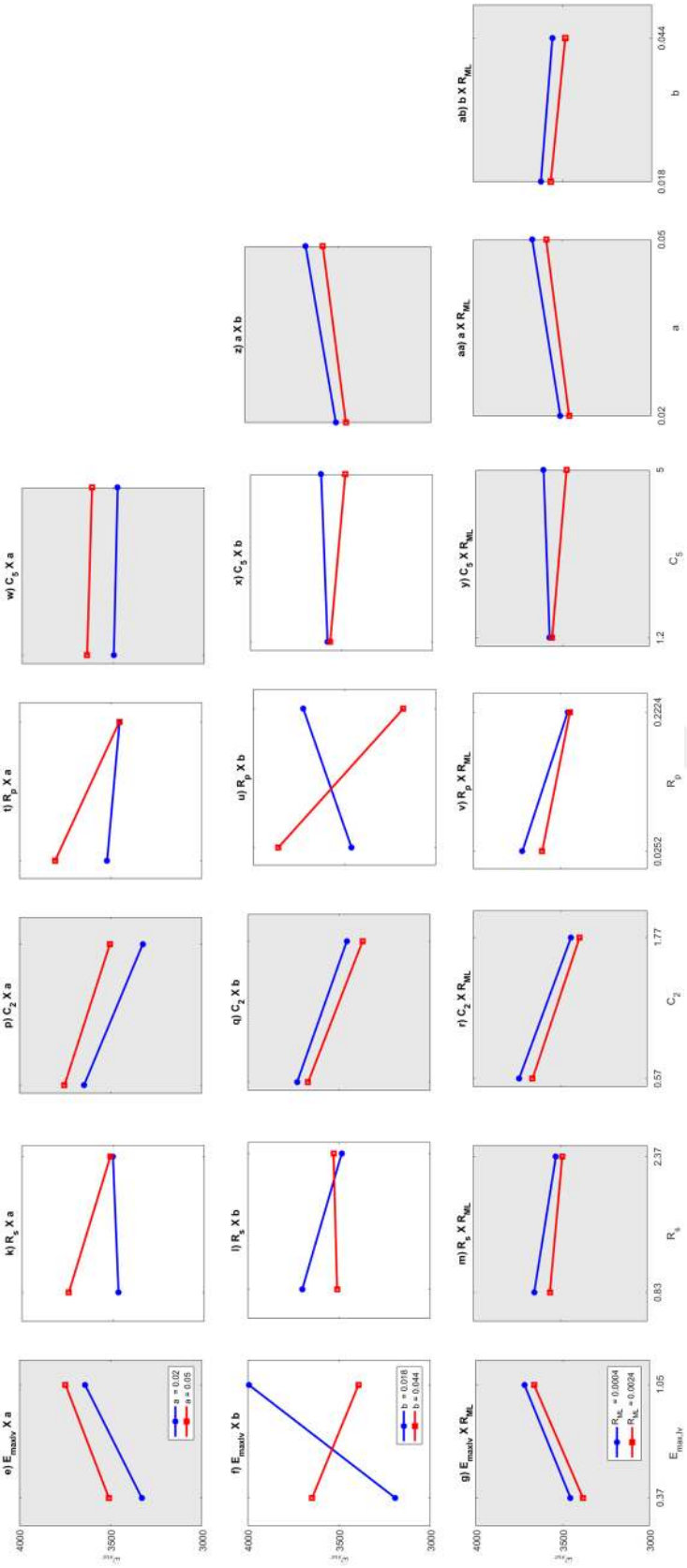


Figure 4.13: Interaction plots 11-28 of 28. Grey plots denote no statistically significant interactions ($p<0.1$)

.

### *4.3.2 Discussion*

Main effects are interpreted in conjunction with interaction effects. Main effect of $E_{max,lv}$ is positive and of a sizeable magnitude as seen from the slope (Figure 4.11). Increase in $E_{max,lv}$ i.e, a strong undilated ventricle has an ameliorating effect and results in delayed suction i.e., suction occurs at a higher pump speed. $E_{max,lv}$ has full reversals with $R_p$ and $b$ and insignificant interactions with the other parameters. Figure 4.12c shows that for a dilated ventricle with low pulmonary vascular resistance, suction occurs at a lower pump speed. In fact, studies have shown that reductions in $R_p$, such as those induced by the drug milrinone, can increase LVAD flow [152]. The left ventricle stiffness coefficient $b$ has a negative main effect and full reversal with $E_{max,lv}$ (Figure 4.13f) and $R_p$ (Figure 4.13u). A low value of $b$ indicates a weak ventricle which would lead to an early onset of suction. Ventricular stiffness affects the ventricle's ability to create sufficient volume and pressure to open the aortic valve and allow blood flow, which is vital for preventing suction events [68]. The earliest suction is noted for the high $b$ - high $R_p$ case. It has been found that pulmonary hypertension that is cause by increased $R_p$ impairs the diastolic compliance of the LV even in the absence of LV dysfunction [153].

A negative main effect is seen for $R_s$. Among the interaction plots, the $R_s \times R_p$ plot demonstrates a moderate reversal. Studies have shown that reductions in $R_s$ post-LVAD implant can impact pulmonary vascular resistance, which underscores the interplay between $R_s$ and $R_p$ [154].

A negative main effect is seen for $C_2$. Heart failure is associated with reduced arterial compliance, and one would expect suction at a low value of $C_2$. The main effects demonstrate a contrary phenomenon which may be explained based on ventricular-aortic coupling. High $C_2$ with a mean reduced value of $E_{max,lv}$ would cause a ventricular-aortic compliance mismatch resulting in greater workload on the ventricle [155] which may lead to early suction.$C_2$ has below-moderate interactions with other parameters (Figure 4.12 - 4.13n-r). The main and, consequently, interactions of $C_5$ are not statistically significant.

A positive effect is noted for $a$ in line with the pathophysiologic reasoning i.e.,

suction would be delayed for high $a$. There are neither any interactions between $a$ and $b$ nor with $R_{ML}$ (Figure 4.13z, aa, ab).

## *4.4 Hardware in the Loop Simulations*

### *4.4.1 Results*

Figure 4.14 shows the controller input, i.e., the backflow pump PWM cycle (a), and output, i.e., fluid level (b). The backflow pump adjusts its speed in response to fluid level variation, which can be seen in the duty cycle plot. The pump runs at full speed when the fluid level is above the set point value of 90 cm and nearly shuts down when the fluid level falls below the reference point.

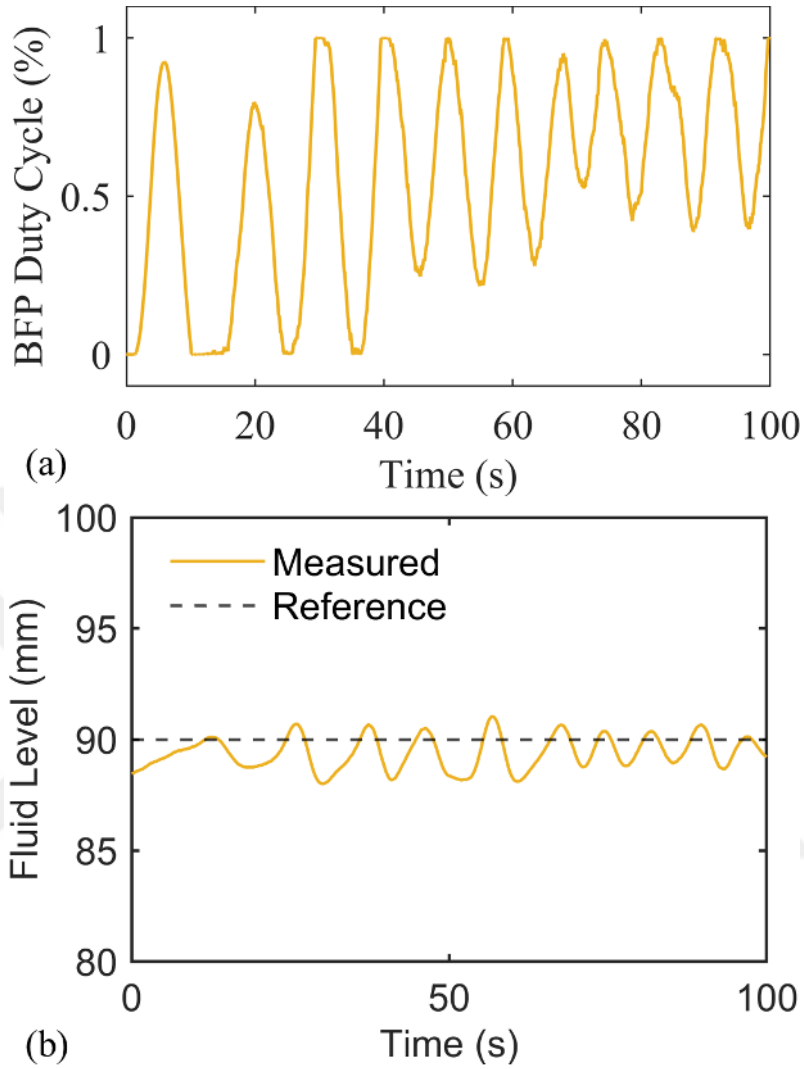


Figure 4.14: Fluid level controller performance: a) backflow pump PWM control signal, b) aortic chamber fluid level reference (dashed black) and measured (yellow)

Figure 4.15 shows the actuation of the LV and aortic inlet solenoid valves in terms of PWM cycles. This figure aptly demonstrates the compromise that must be made for reference pressure tracking. The aortic valve opens and closes almost three times more than the LV valve, and the reference tracking performance of the controllers is proportional to this effect (Figure 4.16). Excessive actuation of the valves leads to excessive wear and shorter lifespans.

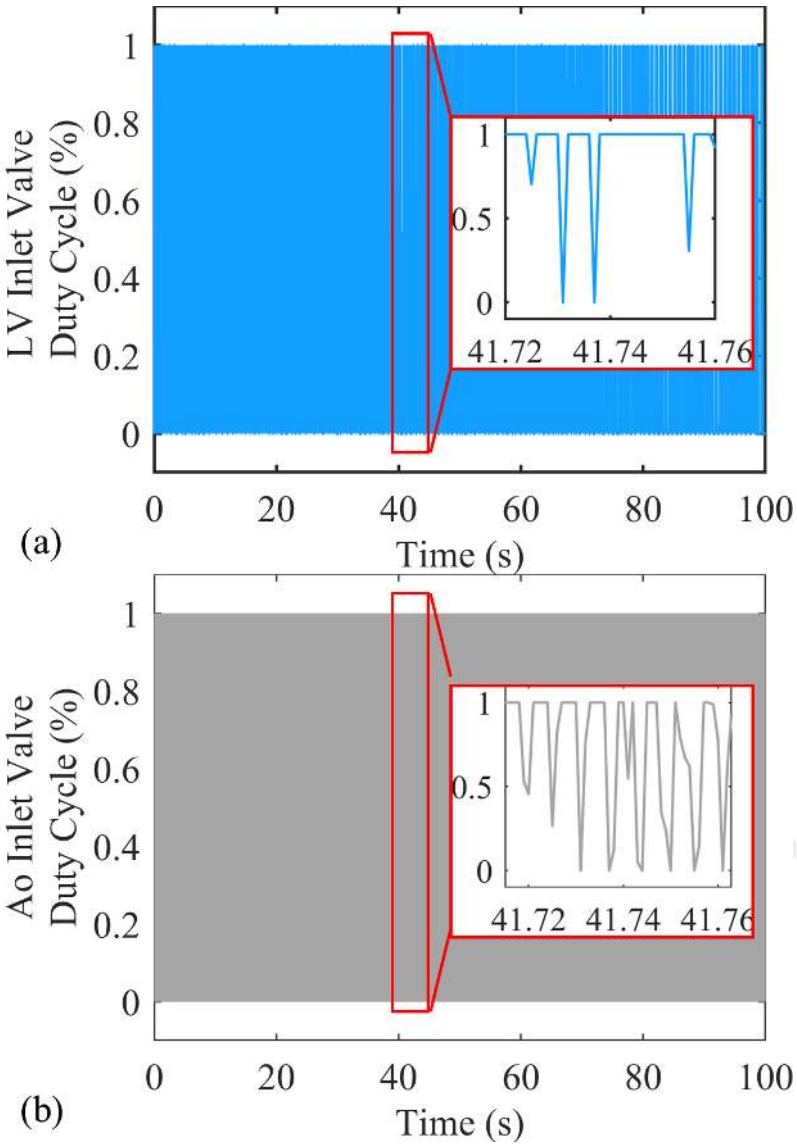


Figure 4.15: Fluid level controller performance: a) backflow pump PWM control signal, b) aortic chamber fluid level reference (dashed black) and measured (yellow)

Figure 4.16 shows the reference and tracked $P_{ao}$ and $P_{lv}$ at different LVAD speeds. The $P_{ao}$ controller achieves good reference tracking (4.16a). However, this is achieved at the cost of excessive actuation as the aortic chamber valve opens and closes multiple times during one decisecond (4.15a), which can be heard during the operation of the HMCL as a knocking sound. On the other hand, the LV chamber actuation rate is relatively lower (4.15b), leading to imperfect tracking in

the diastolic stage. The polarity of the two solutions, near-perfect tracking but high actuation rate with the $P_{ao}$ controller and low-speed actuation but moderate level tracking with the $P_{lv}$ controller, indicates that an optimal solution is needed whereby minimal damage is incurred by the solenoid valves while achieving good pressure tracking.

The aortic valve closes at 3500 rpm as $P_{ao}$ exceeds $P_{lv}$. The mean LVAD flow is taken as the cardiac output (CO). Flowrate increases from 2.3 L/min at 2500 rpm to 4.6 L/min at 4500 rpm. Mean Arterial Pressure (MAP) increases from a hypotensive 87 mmHg at 2500 rpm to a hypertensive 130 mmHg at 4000 rpm. Plv successively decreases, with increments in pump speed in line with clinical observations. Pulse pressure (PP) decreases from 15 mmHg at 2500 rpm to <10 mmHg at 4500 rpm.

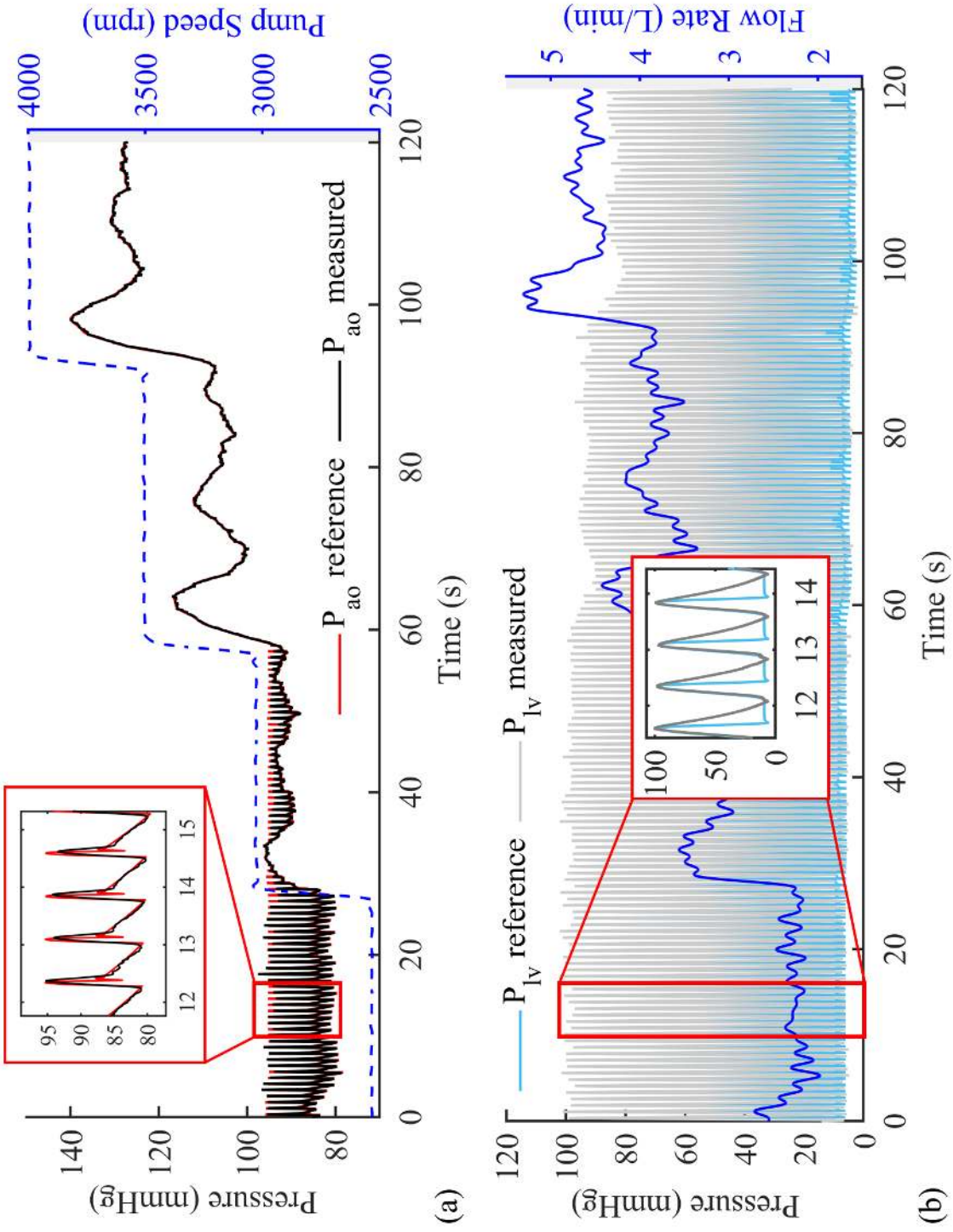


Figure 4.16: HMCL performance and hemodynamic trends in (a) Aortic pressure, (b) LV pressure, and cardiac output at LVAD speeds of 2500-4000 rpm.

### *4.4.2 Discussion*

With minimal mechanical components and simple control strategies, the current system offers comparable performance to a multi-compartment fully mechanical MCL [156]. Similar CO, $P_{ao}$, $P_{lv}$, and PP trends are observed, i.e., an increase in CO, minimum, maximum, and mean $P_{ao}$ and a decrease in $P_{lv}$ and PP. Unlike other HMCLs that preclude the LVAD model [103, 157], the iHeart model runs in parallel to the prototype and allows simultaneous in-silico and in-vitro evaluation. The performance of the developed system agrees with clinical observations with CF-LVADs [158, 159]. Complete offloading of the LV can be observed at around 3500 rpm, $P_{ao}$ is augmented, and LV is unloaded, thereby reducing peak systolic pressure. Due to a drop in the systolic contribution of the LV, the aortic valve remains shut, and flow becomes increasingly less pulsatile, which may lead to aortic insufficiency. The LVAD thereby replaces myocardial function and can replicate the full-support mechanism, which has been in clinical practice for over a decade. Since the LVAD continuously adds blood volume to the circulation, pressure decay in diastole decreases and PP is diminished to the extent that a perceptible pulse vanishes. Hemodynamic normalization for the simulated patient can be achieved between below 3500 rpm with 110 mmHg MAP and 4 L/min CO.

The presented work models a case of HFrEF using mean values of CVS model parameters from published patient data. The HMCL can be used to evaluate the performance of the LVAD for patients with different degrees of HF severity at varying levels of physical activity, such as rest, exercise, postural change etc., by simply modifying the requisite values of the CVS model parameters [160]. Due to its modular nature, the model can be easily modified to simulate other heart conditions like congenital heart diseases such as ventricular or atrial septal defects [161] and resulting LVAD performance can be evaluated in-vitro. Departing from model parameter variation, pressure waveforms from HF patients pre-VAD implant can also be supplied as reference signals that the pressure controllers can track for prognostication of LVAD performance. Personalized in-vitro evaluations of cardiac devices can be conducted using specialized control algorithms [162]. Effects like suction

can be emulated by physically occluding the inflow cannula, thereby facilitating the development and testing of suction detection and circumvention strategies [163] for LVAD physiological control [164].

The software and hardware sides have some limitations. Auto-regulatory mechanisms, provisions for modelling the effect of drug interventions necessitated for hypertensive cases, are not included in the current iteration of this work. Furthermore, the current setup has been developed to test a CF-LVAD. Testing pulsatile VADs will require additional components outside the scope of the current work.

# Chapter 5

# CONCLUSION

With an aging and growing population, the number of patients suffering from heart failure has also increased to unprecedented levels, as well as the number of LVADs implanted. It is becoming increasingly common for LVADs to be implanted as part of treatment for end-stage heart failure patients. However, a variety of complications can be associated with these procedures, including but not limited to atrial fibrillation, arrhythmia, tachycardia, aortic valve stenosis, and right heart failure, among others. Development of an LVAD involves a number of steps, including the virtual testing of the device in-silico, verification of the results in-vitro, validation of the device's performance in animals, i.e., in vivo, and finally going through clinical trials. It is important to realize that as we progress through the process of developing a product, the complexity, controllability, and cost of the process increase. As a result, it becomes critical that a reliable pre-clinical evaluation is conducted under such circumstances. As part of the current work, two preclinical models have been explored: in silico and in vitro models.

In-silico testing has been found to be the most simple, versatile, and cost-effective approach when it comes to modeling the cardiovascular system and studying the effect of the LVADs on the symptoms of advanced-stage heart failure. In this study, object-oriented simulations were conducted since they are flexible, easy to communicate, easy to replicate, and easy to interpret. I chose Simscape$^{TM}$ as the acausal modeling environment for this study in order to take advantage of its real-time capabilities as, to the best of my knowledge, it has never been harnessed for modeling and evaluating the performance of LVADs in real time. The cardiovascular model was developed based on the classical approaches of modellers like Avanzolini,

Shi, and Choi et al. [36, 66, 65] with the objective of maintaining the model's comprehensiveness whilst also ensuring it were real-time executable. A mathematical model of the impeller pump calculated by means of an analytical derivation was calibrated with characteristic data for the Istanbul Heart VAD by making use of its numerical model. The Istanbul Heart (iHeart) VAD, Turkiye's first indigenous experimental heart pump, was chosen as an illustrative example to apply the current approaches to as its hydraulic and geometric data was readily available. Lack of availability of LVAD patient data posed a significant challenge in achieving the objects of this work. To remedy this, a data-based approach was adopted whereby published patient data was collated and statistically pooled to model advanced-stage heart failure. In doing so, a utilitous corollary of this work was the collection of patient data which can be used by other modellers for research and development of heart failure treatment methods. In addition to this, pathophysiology-based identification of heart failure parameters allowed a more reliable modelling of the cardiovascular condition. The simulations conducted using pooled patient data were thus found to be significantly superior to those obtained by arbitrary reduction in LV end-systolic elastance, an approach often adopted for modelling heart failure.

Different degrees of heart failure severity were simulated by varying pathological parameters in realistic ranges identified from published studies. The model was used to study the effect of iHeart VAD speed changes on hemodynamics of patients with varying degrees of heart failure and to make LVAD support requirement predictions. Taking a novel route, the use of the in-silico model was extended to conduct Hemodynamic Ramp Testing, a clinical invasive procedure, on three virtual patients with mild, moderate, and severe heart failure. It was demonstrated that such applications of in-silico testing merit further research as pre-clinical evaluation tools since invasive procedures like HRT do not always result in hemodynamic amelioration for patients. An unconventional application of CVS-MCS modeling was thus presented which has the potential to support biomedical research and pedagogy as the versatile nature of the approach allows for the investigation of clinically

unobservable "edge cases" and invasively estimated or incomputable hemodynamic variables. The in-silico CVS-VAD model was also used to conduct a full-factorial design of experiments to study the functional relationships between hemodynamic parameters and LVAD suction speed which can be applied to the development of LVAD controllers.

Lastly, the in-silico model is used to conduct in-vitro testing by developing a hybrid mock circulatory loop with chambers emulating the left ventricle and aorta. The in-silico model served as a virtual heart in this case. An experimental prototype of the iHeart VAD was used as the hardware under test. Variations in hemodynamic parameters observed during the hardware-in-the-loop simulations demonstrated the same trends as clinical observations. While a case of HFrEF with moderate heart failure was used during the HIL simulations, the same approach can be applied to study the performance of the LVAD for patients with different levels of heart failure severity at varying degrees of physical activity strenuousness, from rest, to postural changes, and light exercise etc., by simply modifying the requisite values of the CVS model parameters.

The modular nature of the numerical part allows easy modification and implementation of different pathophysiological conditions like congenital heart diseases such as ventricular or atrial septal defects resulting LVAD performance can be studied in-vitro. Experimental software and real-time hardware enables us to create specific scenarios and observe LVAD performance in real-time. Instead of relying on parameter values, P-V waveforms from LVAD patients pre-implant can also be provided as reference signals that the LV and aortic pressure controllers can track for prediction of LVAD performance. This work represents a valuable step towards personalized medicine as customized in-vitro evaluations of mechanical circulatory support can be conducted using specialized control algorithms. Deleterious effects of phenomenon like suction can be replicated by occlusion of the inflow cannula, thereby facilitating the development and testing of suction detection and avoidance

strategies for physiological control of LVADs.

To facilitate collaborative efforts, the acausal numerical model and controllers developed to implement the hybrid mock circulation concept are presented in such a way that researchers can easily replicate them for designing LVADs and rapid prototyping of LVAD control strategies. This work, however, is not without its limitations, addressing which may serve as future work. Auto-regulatory mechanisms, provisions for modelling the effect of drug interventions imperative for hypertensive scenarios, are not included in the current iteration of this work. Furthermore, the current setup has been developed to test a continuous centrifugal flow LVAD. Testing pulsatile and axial flow VADs require modelling and fabrication of additional components which are although beyond the scope of the current work, they offer exciting opportunities for further research.

# BIBLIOGRAPHY

[1] M. Mazzei, S. Keshavamurthy, A. Kashem, and Y. Toyoda, *Heart transplantation in the era of the left ventricular assist devices*. IntechOpen, 2018.

[2] R. Moss, T. Grosse, I. Marchant, N. Lassau, F. Gueyffier, and S. R. Thomas, "Virtual patients and sensitivity analysis of the guyton model of blood pressure regulation: Towards individualized models of whole-body physiology," *PLOS Computational Biology*, vol. 8, pp. 1–16, 06 2012.

[3] T. Heldt, R. Mukkamala, G. B. Moody, and R. G. Mark, "Cvsim: an open-source cardiovascular simulator for teaching and research," *The open pacing, electrophysiology & therapy journal*, vol. 3, p. 45, 2010.

[4] T. Arts, T. Delhaas, P. Bovendeerd, X. Verbeek, and F. W. Prinzen, "Adaptation to mechanical load determines shape and properties of heart and circulation: the circadapt model," *American Journal of Physiology-Heart and Circulatory Physiology*, vol. 288, no. 4, pp. H1943–H1954, 2005. PMID: 15550528.

[5] G. Ortiz-Leon, M. Vilchez-Monge, and J. J. Montero-Rodriguez, "An updated cardiovascular simulation toolbox," in *2013 IEEE International Symposium on Circuits and Systems (ISCAS)*, pp. 1901–1904, IEEE, 2013.

[6] C. Ozturk, L. Rosalia, and E. T. Roche, "A multi-domain simulation study of a pulsatile-flow pump device for heart failure with preserved ejection fraction," *Frontiers in Physiology*, vol. 13, p. 815787, 2022.

[7] Y. Shi, P. Lawford, and R. Hose, "Review of zero-d and 1-d models of blood flow in the cardiovascular system," *Biomedical engineering online*, vol. 10, pp. 1–38, 2011.

[8] A. C. Guyton, T. G. Coleman, and H. J. Granger, "Circulation: overall regulation," *Annual review of physiology*, vol. 34, no. 1, pp. 13–44, 1972.

[9] C. S. Peskin and C. Tu, "Hemodynamics in congenital heart disease," *Computers in biology and medicine*, vol. 16, no. 5, pp. 331–359, 1986.

[10] A. McLarty, "Mechanical circulatory support and the role of lvads in heart failure therapy," *Clinical Medicine Insights: Cardiology*, vol. 9s2, p. CMC.S19694, 2015. PMID: 25983564.

[11] R. C. Robbins, M. H. Kown, P. M. Portner, and P. E. Oyer, "The totally implantable novacor left ventricular assist system," *The Annals of Thoracic Surgery*, vol. 71, no. 3, Supplement 1, pp. S162–S165, 2001.

[12] H. Martinez, N. R. Alberson, J. J. Guerra, and I. A. S. De Armas, "A historical review of mechanical circulatory support," in *Ventricular Assist Devices-Advances and Applications in Heart Failure*, IntechOpen, 2023.

[13] S. R. Wilson, M. M. Givertz, G. C. Stewart, and G. H. Mudge, "Ventricular assist devices: The challenges of outpatient management," *Journal of the American College of Cardiology*, vol. 54, no. 18, pp. 1647–1659, 2009.

[14] J. Fried, G. Sayer, Y. Naka, and N. Uriel, "State of the art review: Evolution and ongoing challenges of left ventricular assist device therapy," *Structural Heart*, vol. 2, no. 4, pp. 262–273, 2018.

[15] D. Kapuria, T. Khumri, S. Shamim, P. Surana, S. Khan, N. Calisi, S. Aggarwal, C. Koh, and R. Chhabra, "Characterization and timing of gastrointestinal bleeding in continuous flow left ventricular assist device recipients," *Heliyon*, vol. 6, 09 2020.

[16] S. Y. Chair, D. Yu, M. Ng, Q. Wang, H. Y. Cheng, E. Wong, and J. Sit, "Evolvement of left ventricular assist device: the implications on heart failure

management," *Journal of geriatric cardiology : JGC*, vol. 13, pp. 425–30, 07 2016.

[17] M. J. Pienta, K. Knott, A. Bitar, and J. W. Haft, "Late heartmate 3 thrombosis," *ASAIO Journal*, vol. 68, no. 5, pp. e87–e89, 2022.

[18] J. N. Heaton, S. Singh, M. Li, and S. Vallabhajosyula, "Adverse events with heartmate-3 left ventricular assist device: Results from the manufacturer and user facility device experience (maude) database," *Indian Heart Journal*, vol. 73, no. 6, pp. 765–767, 2021.

[19] W. K. B. P. L. J. L.-F. R. B. R. R. M. Wilkins E, Wilson L and T. N, "European cardiovascular disease statistics," 2017.

[20] J. A. Kobashigawa, M. G. Crespo-Leiro, S. Ensminger, H. Reichenspurner, A. Angelini, G. J. Berry, M. Burke, L. Czer, N. Hiemann, A. G. Kfoury, D. Mancini, P. Mohaçsi, J. Patel, N. L. Pereira, J. L. Platt, E. F. Reed, N. L. Reinsmoen, E. R. Rodríguez, M. L. Rose, S. D. Russell, R. Starling, N. Suciu-Foca, J. Tallaj, D. O. Taylor, A. V. Bakel, L. J. West, A. Zeevi, and A. Zuckermann, "Report from a consensus conference on antibody-mediated rejection in heart transplantation," *The Journal of Heart and Lung Transplantation*, 2011.

[21] J. Newman, M. Liebo, B. D. Lowes, H. I. Basha, Y. Peled, E. Cendrowski, R. Zolty, D. Douglas, J. Um, A. Heroux, and E. Raichlin, "The effect of donor alcohol abuse on outcomes following heart transplantation," *Clinical Transplantation*, 2019.

[22] M. Hakman and T. Groth, "Object-oriented biomedical system modeling—the rationale," *Computer methods and programs in biomedicine*, vol. 59, no. 1, pp. 1–17, 1999.

[23] S. Yogeswaran and F. Liu, "Vascular flow simulations using simvascular and openfoam," *medRxiv*, 2021.

[24] C. D. Lazzari, I. Genuini, D. M. Pisanelli, A. D'Ambrosi, and F. Fedele, "Interactive simulator for e-learning environments: A teaching software for health care professionals," *Biomedical Engineering Online*, 2014.

[25] T. Shen, D. Liú, Z. Lin, C. Ren, W. Zhao, and W. Gao, "A machine learning model to predict cardiovascular events during exercise evaluation in patients with coronary heart disease," *Journal of Clinical Medicine*, 2022.

[26] A. D. Molfetta, L. Santini, G. B. Forleo, V. Minni, K. Mafhouz, D. G. D. Rocca, L. Fresiello, F. Romeo, and G. Ferrari, "Towards a personalized and dynamic crt-d," *Methods of Information in Medicine*, 2012.

[27] M. Darowski, K. J. Pałko, M. Kozarski, K. Zieliński, K. Górczyńska, G. Ferrari, L. Fresiello, and A. D. Molfetta, "Heart and lung mechanical assist devices are comprehensively tested by the new hybrid simulators," *Engineering*, 2012.

[28] G. Ortiz-León, H. J. Barrantes-Vargas, M. Arguedas-Sandí, J. Pacheco-Chaverri, and M. Vílchez-Monge, "An approximation of heart failure using cardiovascular simulation toolbox," *Biomimetics*, 2019.

[29] A. L. Throckmorton, J. Carr, S. A. Tahir, R. Tate, E. A. Downs, S. S. Bhavsar, Y. Wu, J. D. Grizzard, and W. B. Moskowitz, "Mechanical cavopulmonary assistance of a patient-specific fontan physiology: Numerical simulations, lumped parameter modeling, and suction experiments," *Artificial Organs*, 2011.

[30] S. S. Schampaert, M. Veer, F. v. d. Vosse, N. N. Pijls, B. A. d. Mol, and M. M. Rutten, "In vitro comparison of support capabilities of intra-aortic balloon pump and impella 2.5 left percutaneous," *Artificial Organs*, 2011.

[31] J. Haniel, T. C. Lucas, and R. Huebner, "Evaluation of thrombogenic potential by partial differential equations in the blood flow dynamics with central venous catheter," *Journal of the Brazilian Society of Mechanical Sciences and Engineering*, 2019.

[32] R. A. Gray and P. Pathmanathan, "Patient-specific cardiovascular computational modeling: Diversity of personalization and challenges," *Journal of Cardiovascular Translational Research*, 2018.

[33] M. S. Olufsen and A. Nadim, "On deriving lumped models for blood flow and pressure in the systemic arteries," in *Computational Fluid and Solid Mechanics 2003*, pp. 1786–1789, Elsevier, 2003.

[34] A. C. Guyton, "Cardiac output and its regulation," *Circulatory physiology*, 1973.

[35] J.-P. Montani and B. N. Van Vliet, "Understanding the contribution of guyton's large circulatory model to long-term control of arterial pressure," *Experimental Physiology*, vol. 94, no. 4, pp. 382–388, 2009.

[36] G. Avanzolini, P. Barbini, A. Cappello, and G. Cevenini, "Cadcs simulation of the closed-loop cardiovascular system," *International Journal of Bio-Medical Computing*, vol. 22, no. 1, pp. 39–49, 1988.

[37] I. Kokalari, T. Karaja, and M. Guerrisi, "Review on lumped parameter method for modeling the blood flow in systemic arteries," *Journal of Biomedical Science and Engineering*, 2013.

[38] L. Garber, S. Khodaei, and Z. Keshavarz-Motamed, "The critical role of lumped parameter models in patient-specific cardiovascular simulations," *Archives of Computational Methods in Engineering*, vol. 29, no. 5, pp. 2977–3000, 2022.

[39] L. Civilla, A. Sbrollini, L. Burattini, and M. Morettini, "An integrated lumped-parameter model of the cardiovascular system for the simulation of acute ischemic stroke: description of instantaneous changes in hemodynamics," *Mathematical Biosciences and Engineering*, vol. 18, no. 4, pp. 3993–4010, 2021.

[40] F. Scardulla, V. Agnese, G. Romano, G. Di Gesaro, S. Sciacca, D. Bellavia, F. Clemenza, M. Pilato, and S. Pasta, "Modeling right ventricle failure after continuous flow left ventricular assist device: A biventricular finite-element and lumped-parameter analysis," *Cardiovascular Engineering and Technology*, vol. 9, pp. 427–437, 2018.

[41] F. Regazzoni, M. Salvador, P. C. Africa, M. Fedele, L. Dedè, and A. Quarteroni, "A cardiac electromechanical model coupled with a lumped-parameter model for closed-loop blood circulation," *Journal of Computational Physics*, vol. 457, p. 111083, 2022.

[42] F. Berntsson, A. Ghosh, V. Kozlov, and S. Nazarov, "A one dimensional model of blood flow through a curvilinear artery," *Applied Mathematical Modelling*, vol. 63, pp. 633–643, 2018.

[43] M. E. Casciaro, M. Alfonso, D. Craiem, J. Alsac, S. El-Batti, and R. L. Armentano, "Predicting the effect on pulse wave reflection of different endovascular repair techniques in abdominal aortic aneurysm using 1d patient-specific models," *Health and Technology*, vol. 6, pp. 173–179, 2016.

[44] F. N. van de Vosse and N. Stergiopulos, "Pulse wave propagation in the arterial tree," *Annual Review of Fluid Mechanics*, vol. 43, no. 1, pp. 467–499, 2011.

[45] C. R. Gómez, "Analysis of blood flow in one dimensional elastic artery using navier-stokes conservation laws," 2017.

[46] M. B. HISLAND and M. ANLIKER, "Influence of flow and pressure on wave propagation in the canine aorta," *Circulation Research*, vol. 32, no. 4, pp. 524–529, 1973.

[47] M. Anliker, R. L. Rockwell, and E. Ogden, "Nonlinear analysis of flow pulses and shock waves in arteries: part i: derivation and properties of mathematical model," *Zeitschrift für angewandte Mathematik und Physik ZAMP*, vol. 22, pp. 217–246, 1971.

[48] V. Milišić and A. Quarteroni, "Analysis of lumped parameter models for blood flow simulations and their relation with 1D models," *ESAIM: Mathematical Modelling and Numerical Analysis*, vol. 38, no. 4, pp. 613–632, 2004.

[49] A. R. Ghigo, J.-M. Fullana, and P.-Y. Lagrée, "A 2d nonlinear multiring model for blood flow in large elastic arteries," *Journal of Computational Physics*, vol. 350, pp. 136–165, 2017.

[50] J. J. R. Fojas and R. L. De Leon, "Carotid artery modeling using the navier-stokes equations for an incompressible, newtonian and axisymmetric flow," *APCBEE Procedia*, vol. 7, pp. 86–92, 2013. The 3rd International Conference on Biomedical Engineering and Technology - ICBET 2013.

[51] M. Balakrishnan, S. Chakravarthy, and S. Guhathakurta, "A simple 2d whole heart model for simulating electrocardiograms," in *Computing in Cardiology 2014*, pp. 517–520, IEEE, 2014.

[52] A. Quarteroni, "Modeling the cardiovascular system— a mathematical adventure: Part ii," *SIAM News*, vol. 34, 01 2001.

[53] R. Piersanti, F. Regazzoni, M. Salvador, A. F. Corno, C. Vergara, A. Quarteroni, *et al.*, "3d–0d closed-loop model for the simulation of cardiac biventricular electromechanics," *Computer Methods in Applied Mechanics and Engineering*, vol. 391, p. 114607, 2022.

[54] H. J. Kim, I. E. Vignon-Clementel, C. A. Figueroa, J. F. LaDisa, K. E. Jansen, J. A. Feinstein, and C. A. Taylor, "On coupling a lumped parameter heart model and a three-dimensional finite element aorta model," *Annals of Biomedical Engineering*, 2009.

[55] P. J. Hunter and N. P. Smith, "The cardiac physiome project," *The Journal of Physiology*, vol. 594, no. 23, pp. 6815–6816, 2016.

[56] L. Rosalia, C. Ozturk, D. V. Story, M. A. Horvath, and E. T. Roche, "Object-oriented lumped-parameter modeling of the cardiovascular system for physiological and pathophysiological conditions," *Advanced Theory and Simulations*, 2021.

[57] H. Nilsson, J. Peterson, and P. Hudak, "Functional hybrid modeling," in *Practical Aspects of Declarative Languages* (V. Dahl and P. Wadler, eds.), (Berlin, Heidelberg), pp. 376–390, Springer Berlin Heidelberg, 2003.

[58] J. Kofránek, M. Mateják, P. Privitzer, and M. Tribula, "Causal or acausal modeling: labour for humans or labour for machines," *Technical computing prague*, pp. 1–16, 2008.

[59] G. Schweiger, H. Nilsson, J.-P. Schoeggl, W. Birk, and A. Posch, "Modeling and simulation of large-scale systems: A systematic comparison of modeling paradigms," *Applied Mathematics and Computation*, 2020.

[60] S. Bozkurt and S. Bozkurt, "In-silico evaluation of left ventricular unloading under varying speed continuous flow left ventricular assist device support," *Biocybernetics and Biomedical Engineering*, vol. 37, no. 3, pp. 373–387, 2017.

[61] Y. Feng, R. Fu, B. Li, N. Li, H. Yang, J. Liu, and Y. Liu, "Prediction of fractional flow reserve based on reduced-order cardiovascular model," *Computer Methods in Applied Mechanics and Engineering*, vol. 400, p. 115473, 2022.

[62] J. F. de Canete, P. del Saz-Orozco, D. Moreno-Boza, and E. Duran-Venegas, "Object-oriented modeling and simulation of the closed loop cardiovascular system by using simscape," *Computers in Biology and Medicine*, vol. 43, no. 4, pp. 323–333, 2013.

[63] L. Rosalia, C. Ozturk, J. Coll-Font, Y. Fan, Y. Nagata, M. Singh, D. Goswami, A. Mauskapf, S. Chen, R. A. Eder, *et al.*, "A soft robotic sleeve mimicking the haemodynamics and biomechanics of left ventricular pressure overload and aortic stenosis," *Nature biomedical engineering*, vol. 6, no. 10, pp. 1134–1147, 2022.

[64] L. Rosalia, C. Ozturk, and E. T. Roche, "Lumped-parameter and finite element modeling of heart failure with preserved ejection fraction," *JoVE (Journal of Visualized Experiments)*, no. 168, p. e62167, 2021.

[65] S. Choi, *Modeling and control of left ventricular assist system.* PhD thesis, University of Pittsburgh, 1998.

[66] Y. Shi and T. Korakianitis, "Numerical simulation of cardiovascular dynamics with left heart failure and in-series pulsatile ventricular assist device," *Artificial organs*, vol. 30, no. 12, pp. 929–948, 2006.

[67] J. Son, D. Du, and Y. Du, "Stochastic modeling and dynamic analysis of the cardiovascular system with rotary left ventricular assist devices," *Mathematical Problems in Engineering*, vol. 2019, pp. 1–18, 2019.

[68] G. Faragallah, M. A. Simaan, *et al.*, "An engineering analysis of the aortic valve dynamics in patients with rotary left ventricular assist devices," *Journal of healthcare engineering*, vol. 4, pp. 307–327, 2013.

[69] B. Bhattacharya-Ghosh, S. Bozkurt, M. C. Rutten, F. N. Van de Vosse, and V. Díaz-Zuccarini, "An in silico case study of idiopathic dilated cardiomy-

opathy via a multi-scale model of the cardiovascular system," *Computers in Biology and Medicine*, vol. 53, pp. 141–153, 2014.

[70] R. Klabunde, *Cardiovascular Physiology Concepts*. Wolters Kluwer Health/Lippincott Williams & Wilkins, 2011.

[71] E. E. van Riet, A. W. Hoes, K. P. Wagenaar, A. Limburg, M. A. Landman, and F. H. Rutten, "Epidemiology of heart failure: the prevalence of heart failure and ventricular dysfunction in older adults over time. a systematic review," *European Journal of Heart Failure*, vol. 18, no. 3, pp. 242–252, 2016.

[72] S. J. Shah, D. W. Kitzman, B. A. Borlaug, L. v. Heerebeek, M. R. Zile, D. A. Kass, and W. J. Paulus, "Phenotype-specific treatment of heart failure with preserved ejection fraction," *Circulation*, 2016.

[73] U. Tayal, S. Prasad, and S. A. Cook, "Genetics and genomics of dilated cardiomyopathy and systolic heart failure," *Genome medicine*, vol. 9, no. 1, pp. 1–14, 2017.

[74] J. F. Nauta, Y. M. Hummel, J. Tromp, W. Ouwerkerk, P. van der Meer, X. Jin, C. S. Lam, J. J. Bax, M. Metra, N. J. Samani, *et al.*, "Concentric vs. eccentric remodelling in heart failure with reduced ejection fraction: clinical characteristics, pathophysiology and response to treatment," *European journal of heart failure*, vol. 22, no. 7, pp. 1147–1155, 2020.

[75] A. K. Heikhmakhtiar, A. J. Ryu, E. B. Shim, K. Song, N. A. Trayanova, and K. M. Lim, "Influence of lvad function on mechanical unloading and electromechanical delay: A simulation study," *Medical & Biological Engineering & Computing*, 2017.

[76] Y. Zhang, X. Wu, Y. Wang, H. Liu, and G.-M. Liu, "The hemodynamics and blood trauma in axial blood pump under different operating models," *Artificial Organs*, 2022.

[77] S. Bozkurt, "Computational evaluation of heart failure and continuous flow left ventricular assist device support in anaemia," *International Journal for Numerical Methods in Biomedical Engineering*, 10 2023.

[78] M. A. Simaan, V. S. Vasudevan, T. Maul, and P. D. Wearden, "Aortic valve ejection fraction for monitoring heart contractility in patients supported with a continuous flow left ventricular assist device," *American Journal of Cardiovascular and Thoracic Surgery*, 2019.

[79] S. Bozkurt, "Effect of cerebral flow autoregulation function on cerebral flow rate under continuous flow left ventricular assist device support," *Artificial Organs*, 2018.

[80] M. Capoccia, S. Marconi, S. A. Singh, D. M. Pisanelli, and C. De Lazzari, "Simulation as a preoperative planning approach in advanced heart failure patients. a retrospective clinical analysis," *Biomedical engineering online*, vol. 17, pp. 1–21, 2018.

[81] M. Capoccia, "Review of mathematical modelling of the interactions between left ventricular assist devices and the cardiovascular system with a simulation based approach as a tool for training and preoperative planning," in *Cardiovascular and Pulmonary Artificial Organs: Educational Training Simulators*, CNR Edizioni, 2017.

[82] A. Stepanoff, *Centrifugal and Axial Flow Pumps: Theory, Design, and Application.* J. Wiley, 1948.

[83] F. Moscato, G. A. Danieli, and H. Schima, "Dynamic modeling and identification of an axial flow ventricular assist device," *The International Journal of Artificial Organs*, vol. 32, no. 6, pp. 336–343, 2009.

[84] S. Vandenberghe, P. Segers, B. Meyns, and P. R. Verdonck, "Effect of rotary

blood pump failure on left ventricular energetics assessed by mathematical modeling," *Artificial organs*, vol. 26, no. 12, pp. 1032–1039, 2002.

[85] K.-W. Gwak, M. Ricci, S. Snyder, B. Paden, J. Boston, M. Simaan, and J. Antaki, "In-vitro evaluation of multi-objective hemodynamic control of heart-assist pump," in *2004 43rd IEEE Conference on Decision and Control (CDC) (IEEE Cat. No.04CH37601)*, vol. 1, pp. 1069–1074 Vol.1, 2004.

[86] F. Casas, N. Ahmed, and A. Reeves, "Minimal sensor count approach to fuzzy logic rotary blood pump flow control," *Asaio Journal*, vol. 53, no. 2, pp. 140–146, 2007.

[87] Y. Shi and T. Korakianitis, "Impeller-pump model derived from conservation laws applied to the simulation of the cardiovascular system coupled to heart-assist pumps," *Computers in Biology and Medicine*, vol. 93, pp. 127–138, 2018.

[88] H. Keramati, L. van Houts, C. K. Chen, F. van de Vosse, M. Nakao, S. Kim, and H. L. Leo, "Multiscale modeling of a modified blalock-taussig surgery in a patient-specific tetralogy of fallot," *International Journal for Numerical Methods in Biomedical Engineering*, vol. 37, no. 4, p. e3436, 2021.

[89] X. Zhao, Y. Liu, J. Ding, R. Xue-ping, F. Bai, M. Zhang, L. Ma, W. Wang, J. Xie, and A. Qiao, "Hemodynamic effects of the anastomoses in the modified blalock–taussig shunt: A numerical study using a 0d/3d coupling method," *Journal of Mechanics in Medicine and Biology*, 2015.

[90] M. Broomé, E. Maksuti, A. Bjällmark, B. Frenckner, and B. Janerot-Sjöberg, "Closed-loop real-time simulation model of hemodynamics and oxygen transport in the cardiovascular system," *Biomedical engineering online*, vol. 12, no. 1, pp. 1–20, 2013.

[91] Y. Feng, R. Fu, B. Li, N. Li, H. Yang, J. Liu, and Y. Liu, "Prediction of frac-

tional flow reserve based on reduced-order cardiovascular model," *Computer Methods in Applied Mechanics and Engineering*, vol. 400, p. 115473, 2022.

[92] T. Kuroda, T. Miyamoto, D. W. Horvath, C. Miyagi, D. J. Horvath, A. R. Polakowski, K. Fukamachi, and J. H. Karimov, "Evaluation of centrifugal blood pump performances for biventricular support in the virtual simulation model," *Artificial Organs*, vol. 46, no. 8, pp. 1544–1554, 2022.

[93] A. Aliseda, V. K. Chivukula, P. M. McGah, A. R. Prisco, J. Beckman, G. J. M. Garcia, N. A. Mokadam, and C. Mahr, "Lvad outflow graft angle and thrombosis risk," *Asaio Journal*, 2017.

[94] N. Uriel, S. Adatya, J. Malỳ, E. Kruse, D. Rodgers, G. Heatley, A. Herman, P. Sood, D. Berliner, J. Bauersachs, *et al.*, "Clinical hemodynamic evaluation of patients implanted with a fully magnetically levitated left ventricular assist device (heartmate 3)," *The Journal of Heart and Lung Transplantation*, vol. 36, no. 1, pp. 28–35, 2017.

[95] N. Uriel, D. Burkhoff, J. D. Rich, S. G. Drakos, J. J. Teuteberg, T. Imamura, D. Rodgers, J. Raikhelkar, E. E. Vorovich, C. H. Selzman, *et al.*, "Impact of hemodynamic ramp test-guided hvad speed and medication adjustments on clinical outcomes: the ramp-it-up multicenter study," *Circulation: Heart Failure*, vol. 12, no. 4, p. e006067, 2019.

[96] X. Wu, L. Xu, E. Li, and G. Dong, "Application of molecular dynamics simulation in biomedicine," *Chemical Biology & Drug Design*, 2022.

[97] D. L. Timms, S. D. Gregory, N. A. Greatrex, M. J. Pearcy, J. F. Fraser, and U. Steinseifer, "A compact mock circulation loop for the in vitro testing of cardiovascular devices," *Artificial organs*, vol. 35, no. 4, pp. 384–391, 2011.

[98] J. Gehron, J. Zirbes, M. Bongert, S. Schäfer, M. Fiebich, G. A. Krombach, A. Böning, and P. Grieshaber, "Development and validation of a life-sized

mock circulatory loop of the human circulation for fluid-mechanical studies," *Asaio Journal*, 2019.

[99] Y. Kado, T. Miyamoto, D. J. Horvath, S. Gao, and K. Fukamachi, "Development of a circulatory mock loop for biventricular device testing with various heart conditions," *The International Journal of Artificial Organs*, 2020.

[100] F. Cappon, T. Wu, T. Papaioannou, X. Du, P.-L. Hsu, and A. W. Khir, "Mock circulatory loops used for testing cardiac assist devices: A review of computational and experimental models," *The International Journal of Artificial Organs*, vol. 44, no. 11, pp. 793–806, 2021.

[101] A. Petrou, M. Granegger, M. Meboldt, and M. S. Daners, "A versatile hybrid mock circulation for hydraulic investigations of active and passive cardiovascular implants," *Asaio Journal*, vol. 65, no. 5, p. 495, 2019.

[102] M. Rocchi, L. Fresiello, B. Meyns, S. Jacobs, C. Gross, J. P. Pauls, R. Graefe, A. Stecka, M. Kozarski, and K. Zieliński, "A compliant model of the ventricular apex to study suction in ventricular assist devices," *Asaio Journal*, vol. 67, no. 10, pp. 1125–1133, 2021.

[103] G. Ochsner, R. Amacher, A. Amstutz, A. Plass, M. S. Daners, H. Tevaearai, S. Vandenberghe, M. J. Wilhelm, and L. Guzzella, "A novel interface for hybrid mock circulations to evaluate ventricular assist devices," *IEEE transactions on biomedical engineering*, vol. 60, no. 2, pp. 507–516, 2012.

[104] S. Schampaert, K. Pennings, M. Van De Molengraft, N. Pijls, F. Van De Vosse, and M. Rutten, "A mock circulation model for cardiovascular device evaluation," *Physiological measurement*, vol. 35, no. 4, p. 687, 2014.

[105] E. S. Rapp, S. R. Pawar, and R. G. Longoria, "Hybrid mock circulatory loop simulation of extreme cardiac events," *IEEE Transactions on Biomedical Engineering*, vol. 69, no. 9, pp. 2883–2892, 2022.

[106] K. Sagawa, *Cardiac contraction and the pressure-volume relationship*. Oxford University Press, USA, 1988.

[107] K. B. Campbell, J. A. Ringo, Y. Wakao, P. A. Klavano, and J. E. Alexander, "Internal capacitance and resistance allow prediction of right ventricle outflow," *American Journal of Physiology-Heart and Circulatory Physiology*, vol. 243, no. 1, pp. H99–H112, 1982.

[108] I. Lazoglu, D. S. Kucukaksu, C. Ozturk, I. B. Aka, V. Bakuy, N. Arat, O. Yalcin, E. Ugurel, E. Aksoy, S. Ruacan, *et al.*, "A short-term in vivo evaluation of the istanbul heart left ventricular assist device in a pig model.," *Experimental and Clinical Transplantation: Official Journal of the Middle East Society for Organ Transplantation*, 2019.

[109] H. Schima, J. Honigschnabel, W. Trubel, and H. Thoma, "Computer simulation of the circulatory system during support with a rotary blood pump.," *ASAIO transactions*, vol. 36, no. 3, pp. M252–4, 1990.

[110] C. Ozturk, I. B. Aka, and I. Lazoglu, "Effect of blade curvature on the hemolytic and hydraulic characteristics of a centrifugal blood pump," *The International journal of artificial organs*, vol. 41, no. 11, pp. 730–737, 2018.

[111] G. Comunale, P. Peruzzo, B. Castaldi, R. Razzolini, G. Di Salvo, M. A. Padalino, and F. M. Susin, "Understanding and recognition of the right ventricular function and dysfunction via a numerical study," *Scientific Reports*, vol. 11, no. 1, p. 3709, 2021.

[112] M. E. Klingensmith *et al.*, *The Washington manual of surgery*. Lippincott Williams & Wilkins, 2008.

[113] O. Barnea and N. Sheffer, "A computer model for analysis of fluid resuscitation," *Computers in Biology and Medicine*, vol. 23, no. 6, pp. 443–454, 1993.

[114] P. H. Pak, W. L. Maughan, K. L. Baughman, and D. A. Kass, "Marked discordance between dynamic and passive diastolic pressure-volume relations in idiopathic hypertrophic cardiomyopathy," *Circulation*, vol. 94, no. 1, pp. 52–60, 1996.

[115] B. O'Neill, "Some useful moment results in sampling problems," *The American Statistician*, vol. 68, no. 4, pp. 282–296, 2014.

[116] N. Uriel, G. Sayer, K. Addetia, S. Fedson, G. H. Kim, D. Rodgers, E. Kruse, K. Collins, S. Adatya, N. Sarswat, *et al.*, "Hemodynamic ramp tests in patients with left ventricular assist devices," *JACC: Heart Failure*, vol. 4, no. 3, pp. 208–217, 2016.

[117] M. R. Noor, C. H. Ho, K. H. Parker, A. R. Simon, N. R. Banner, and C. T. Bowles, "Investigation of the characteristics of h eart w are hvad and t horatec h eart m ate ii under steady and pulsatile flow conditions," *Artificial Organs*, vol. 40, no. 6, pp. 549–560, 2016.

[118] J. Son, D. Du, and Y. Du, "Modelling and control of a failing heart managed by a left ventricular assist device," *Biocybernetics and Biomedical Engineering*, vol. 40, no. 1, pp. 559–573, 2020.

[119] L. Liang, M. Meki, W. Wang, P. Sethu, A. El-Baz, G. A. Giridharan, and Y. Wang, "A suction index based control system for rotary blood pumps," *Biomedical Signal Processing and Control*, vol. 62, p. 102057, 2020.

[120] M. Vollkron, H. Schima, L. Huber, R. Benkowski, G. Morello, and G. Wieselthaler, "Advanced suction detection for an axial flow pump," *Artificial Organs*, vol. 30, no. 9, pp. 665–670, 2006.

[121] R. Hanus, M. Kinnaert, and J.-L. Henrotte, "Conditioning technique, a general anti-windup and bumpless transfer method," *Automatica*, vol. 23, no. 6, pp. 729–739, 1987.

[122] J. E. Hall and M. E. Hall, *Guyton and Hall textbook of medical physiology e-Book*. Elsevier Health Sciences, 2020.

[123] E. Aune, M. Bækkevar, O. Rødevand, and J. E. Otterstad, "Reference values for left ventricular volumes with real-time 3-dimensional echocardiography," *Scandinavian Cardiovascular Journal*, vol. 44, no. 1, pp. 24–30, 2010.

[124] H. Ishihara, M. Yokota, T. Sobue, and H. Saito, "Relation between ventriculoarterial coupling and myocardial energetics in patients with idiopathic dilated cardiomyopathy," *Journal of the American College of Cardiology*, vol. 23, no. 2, pp. 406–416, 1994.

[125] H. Senzaki, B. Fetics, C.-H. Chen, and D. A. Kass, "Comparison of ventricular pressure relaxation assessments in human heart failure: quantitative influence on load and drug sensitivity analysis," *Journal of the American College of Cardiology*, vol. 34, no. 5, pp. 1529–1536, 1999.

[126] D. R. Warriner, A. G. Brown, S. Varma, P. J. Sheridan, P. Lawford, D. R. Hose, A. Al-Mohammad, and Y. Shi, "Closing the loop: modelling of heart failure progression from health to end-stage using a meta-analysis of left ventricular pressure-volume loops," *PLoS One*, vol. 9, no. 12, p. e114153, 2014.

[127] H. S. Ribner, D. A. Plucinski, A.-M. Hsieh, D. Bresnahan, A. Molteni, J. Askenazi, and M. Lesch, "Acute effects of digoxin on total systemic vascular resistance in congestive heart failure due to dilated cardiomyopathy: a hemodynamic-hormonal study," *The American journal of cardiology*, vol. 56, no. 13, pp. 896–904, 1985.

[128] T. Bombardini, M. F. Costantino, R. Sicari, Q. Ciampi, L. Pratali, E. Picano, *et al.*, "End-systolic elastance and ventricular-arterial coupling reserve predict cardiac events in patients with negative stress echocardiography," *BioMed research international*, vol. 2013, 2013.

[129] W. K. Laskey, H. G. Parker, V. A. Ferrari, W. G. Kussmaul, and A. Noordergraaf, "Estimation of total systemic arterial compliance in humans," *Journal of Applied Physiology*, vol. 69, no. 1, pp. 112–119, 1990.

[130] P. Pellegrini, A. Rossi, M. Pasotti, C. Raineri, M. Cicoira, S. Bonapace, F. L. Dini, P. L. Temporelli, C. Vassanelli, R. Vanderpool, *et al.*, "Prognostic relevance of pulmonary arterial compliance in patients with chronic heart failure," *Chest*, vol. 145, no. 5, pp. 1064–1070, 2014.

[131] J. Schreuder, F. Van der Veen, E. Van der Velde, F. Delahaye, O. Alfieri, O. Jegaden, R. Lorusso, J. Jansen, S. Hoeksel, G. Finet, *et al.*, "Left ventricular pressure-volume relationships before and after cardiomyoplasty in patients with heart failure," *Circulation*, vol. 96, no. 9, pp. 2978–2986, 1997.

[132] F. Berk, S. Isgoren, H. Demir, G. Kozdag, D. Ural, and B. Komsuoglu, "Evaluation of left ventricular function and volume in patients with dilated cardiomyopathy: gated myocardial single-photon emission tomography (spect) versus echocardiography," *Annals of Saudi Medicine*, vol. 25, no. 3, pp. 198–204, 2005.

[133] J.-i. Suzuki, G. R. Caputo, T. Masui, J.-M. Chang, M. O'Sullivan, and C. B. Higgins, "Assessment of right ventricular diastolic and systolic function in patients with dilated cardiomyopathy using cine magnetic resonance imaging," *American heart journal*, vol. 122, no. 4, pp. 1035–1040, 1991.

[134] A. Bielecka-Dabrowa, S. von Haehling, W. S. Aronow, M. I. Ahmed, J. Rysz, and M. Banach, "Heart failure biomarkers in patients with dilated cardiomyopathy," *International journal of cardiology*, vol. 168, no. 3, pp. 2404–2410, 2013.

[135] A. D'andrea, G. Salerno, R. Scarafile, L. Riegler, R. Gravino, F. Castaldo, R. Cocchia, G. Limongelli, M. Romano, P. Calabro, *et al.*, "Right ventricular myocardial function in patients with either idiopathic or ischemic dilated

cardiomyopathy without clinical sign of right heart failure: effects of cardiac resynchronization therapy," *Pacing and clinical electrophysiology*, vol. 32, no. 8, pp. 1017–1029, 2009.

[136] M. Tachi, Y. Amano, K. Inui, M. Takeda, F. Yamada, K. Asai, and S. Kumita, "Relationship of postcontrast myocardial t1 value and delayed enhancement to reduced cardiac function and serious arrhythmia in dilated cardiomyopathy with left ventricular ejection fraction less than 35%," *Acta Radiologica*, vol. 57, no. 4, pp. 430–436, 2016.

[137] E. J. Birks, S. G. Drakos, S. R. Patel, B. D. Lowes, C. H. Selzman, R. C. Starling, J. Trivedi, M. S. Slaughter, P. Alturi, D. Goldstein, *et al.*, "Prospective multicenter study of myocardial recovery using left ventricular assist devices (restage-hf [remission from stage d heart failure]) medium-term and primary end point results," *Circulation*, vol. 142, no. 21, pp. 2016–2028, 2020.

[138] F. Streitner, T. Herrmann, J. Kuschyk, S. Lang, C. Doesch, T. Papavassiliu, I. Streitner, C. Veltmann, D. Haghi, and M. Borggrefe, "Impact of shocks on mortality in patients with ischemic or dilated cardiomyopathy and defibrillators implanted for primary prevention," *PLoS One*, vol. 8, no. 5, p. e63911, 2013.

[139] A. Ortega, E. Tarazon, C. Gil-Cayuela, M. Garcia-Manzanares, L. Martinez-Dolz, F. Lago, J. R. González-Juanatey, J. Cinca, E. Jorge, M. Portoles, *et al.*, "Intercalated disc in failing hearts from patients with dilated cardiomyopathy: Its role in the depressed left ventricular function," *PLoS One*, vol. 12, no. 9, p. e0185062, 2017.

[140] H. Sato, M. Hori, H. Ozaki, H. Yokoyama, K. Imai, M.-a. Morikawa, H. Takeda, M. Inoue, and T. Kamada, "Exercise-induced upward shift of diastolic left ventricular pressure-volume relation in patients with dilated car-

diomyopathy. effects of beta-adrenoceptor blockade.," *Circulation*, vol. 88, no. 5, pp. 2215–2223, 1993.

[141] J. Goodman and S. Lerakis, "The aortic valve: the gatekeeper of the lvad," *CASE: Cardiovascular Imaging Case Reports*, vol. 4, no. 5, p. 341, 2020.

[142] J. R. Hydren, J. R. Gifford, C. L. Jarrett, S. H. Park, K. L. Shields, R. M. Broxterman, A. C. Kithas, A. V. Bisconti, T. S. Thurston, S. M. Ratchford, *et al.*, "Vascular function in continuous-flow left ventricular assist device recipients: effect of a single pulsatility treatment session," *American Journal of Physiology-Regulatory, Integrative and Comparative Physiology*, vol. 320, no. 4, pp. R425–R437, 2021.

[143] Y. Sujino, K. Kuroda, K. Yoshitake, N. Yagi, E. Anegawa, H. Mochizuki, K. Iwasaki, S. Nakajima, T. Watanabe, M. Yanase, *et al.*, "Clinical potential of hemodynamic ramp test by simultaneous echocardiography and right heart catheterization for aortic insufficiency in a patient with continuous-flow left ventricular assist device," *Journal of Artificial Organs*, vol. 24, pp. 265–268, 2021.

[144] S. Dunlay, S. Park, K. Chandrasekaran, J.-O. Choi, N. Pereira, L. Joyce, R. Daly, J. Stulak, and S. Kushwaha, "Changes in left ventricular ejection fraction following implantation of left ventricular assist device as destination therapy," *The Journal of Heart and Lung Transplantation*, vol. 32, no. 4, p. S116, 2013.

[145] A. R. Travis, G. A. Giridharan, G. M. Pantalos, R. D. Dowling, S. D. Prabhu, M. S. Slaughter, M. Sobieski, A. Undar, D. J. Farrar, and S. C. Koenig, "Vascular pulsatility in patients with a pulsatile-or continuous-flow ventricular assist device," *The Journal of thoracic and cardiovascular surgery*, vol. 133, no. 2, pp. 517–524, 2007.

[146] A. T. Tzallas, N. S. Katertsidis, E. C. Karvounis, M. G. Tsipouras, G. Rigas, Y. Goletsis, K. Zielinski, L. Fresiello, A. Di Molfetta, G. Ferrari, *et al.*, "Modeling and simulation of speed selection on left ventricular assist devices," *Computers in biology and medicine*, vol. 51, pp. 128–139, 2014.

[147] D. W. Markham and M. H. Drazner, "Measuring nonpulsatile blood pressure: say goodbye to the doppler?," 2013.

[148] A. Montalto, C. Amarelli, V. Piazza, K. Hopkins, M. Comisso, R. Pantanella, and F. Musumeci, "A new hemodynamic index to predict late right failure in patients implanted with last generation centrifugal pump," *Journal of Cardiac Surgery*, vol. 36, no. 7, pp. 2355–2364, 2021.

[149] H. J. Eisen, J. M. Flack, P. Atluri, N. Bansal, K. Breathett, A. L. Brown, S. R. Hankins, P. Khazanie, C. Masri, P. Pirlamarla, *et al.*, "Management of hypertension in patients with ventricular assist devices: a scientific statement from the american heart association," *Circulation: Heart Failure*, vol. 15, no. 5, p. e000074, 2022.

[150] J. R. Martina, B. E. Westerhof, N. de Jonge, J. van Goudoever, P. Westers, S. Chamuleau, D. van Dijk, B. F. Rodermans, B. A. de Mol, and J. R. Lahpor, "Noninvasive arterial blood pressure waveforms in patients with continuous-flow left ventricular assist devices," *Asaio Journal*, vol. 60, no. 2, pp. 154–161, 2014.

[151] A. N. Rosenbaum, R. P. Frantz, S. S. Kushwaha, J. M. Stulak, S. Maltais, and A. Behfar, "Novel left heart catheterization ramp protocol to guide hemodynamic optimization in patients supported with left ventricular assist device therapy," *Journal of the American Heart Association*, vol. 8, no. 4, p. e010232, 2019.

[152] N. C. Dang, V. Topkara, M. L. Mercando, J. Kay, K. Kruger, M. S. Aboodi, M. C. Öz, and Y. Naka, "Right heart failure after left ventricular assist device

implantation in patients with chronic congestive heart failure," *The Journal of Heart and Lung Transplantation*, 2006.

[153] M. Kasner, D. Westermann, P. Steendijk, S. Dröse, W. Poller, H.-P. Schultheiss, and C. Tschöpe, "Left ventricular dysfunction induced by non-severe idiopathic pulmonary arterial hypertension: a pressure–volume relationship study," *American journal of respiratory and critical care medicine*, vol. 186, no. 2, pp. 181–189, 2012.

[154] B. A. Houston, R. Kalathiya, S. Hsu, R. S. Loungani, M. E. Davis, S. T. Coffin, N. Haglund, S. Maltais, M. Keebler, P. J. Leary, D. P. Judge, G. R. Stevens, J. Rickard, C. Sciortino, G. Whitman, A. S. Shah, S. D. Russell, and R. J. Tedford, "Right ventricular afterload sensitivity dramatically increases after left ventricular assist device implantation: A multi-center hemodynamic analysis," *The Journal of Heart and Lung Transplantation*, 2016.

[155] K. R. Walley, "Left ventricular function: time-varying elastance and left ventricular aortic coupling," *Critical care*, vol. 20, no. 1, p. 270, 2016.

[156] X. Zhao, L. Zhao, J. Xu, D. Li, H. Li, Y. Li, H. Chen, and Y. Zhang, "Aortic valve opening in mock-loop with continuous-flow left ventricular assist device," *The International Journal of Artificial Organs*, vol. 45, no. 10, pp. 809–816, 2022.

[157] T. Salesch, J. Gesenhues, M. Habigt, M. Mechelinck, M. Hein, and D. Abel, "Parameter optimization and validation of a cost efficient hybrid mock loop of the cardiovascular system," in *2021 European Control Conference (ECC)*, pp. 762–768, IEEE, 2021.

[158] F. Castagna, E. J. Stöhr, A. Pinsino, J. R. Cockcroft, J. Willey, A. Reshad Garan, V. K. Topkara, P. C. Colombo, M. Yuzefpolskaya, and B. J. McDonnell, "The unique blood pressures and pulsatility of lvad patients: current

challenges and future opportunities," *Current hypertension reports*, vol. 19, pp. 1–7, 2017.

[159] P. N. Mohite, A. Sabashnikov, A. R. Simon, A. Weymann, N. P. Patil, B. Unsoeld, C. Bireta, and A. F. Popov, "Does circulite synergy assist device as partial ventricular support have a place in modern management of advanced heart failure?," *Expert review of medical devices*, vol. 12, no. 1, pp. 49–60, 2015.

[160] C. Gross, F. Moscato, T. Schlöglhofer, M. Maw, B. Meyns, C. Marko, D. Wiedemann, D. Zimpfer, H. Schima, and L. Fresiello, "Lvad speed increase during exercise, which patients would benefit the most? a simulation study," *Artificial organs*, vol. 44, no. 3, pp. 239–247, 2020.

[161] E. Ortiz-Rangel, G. V. Guerrero-Ramírez, C. D. García-Beltrán, M. Guerrero-Lara, M. Adam-Medina, C. M. Astorga-Zaragoza, J. Reyes-Reyes, and R. Posada-Gómez, "Dynamic modeling and simulation of the human cardiovascular system with pda," *Biomedical Signal Processing and Control*, vol. 71, p. 103151, 2022.

[162] T. Li, H. Li, W. Cui, N. Xie, X. Li, and Y. Wang, "Design and intelligent control of mock circulation system to reproduce patient-specific physiological indexes," *Biomedical Signal Processing and Control*, vol. 78, p. 103987, 2022.

[163] M. Maw, C. Gross, T. Schloeglhofer, K. Dimitrov, D. Zimpfer, F. Moscato, and H. Schima, "Development of suction detection algorithms for a left ventricular assist device from patient data," *Biomedical Signal Processing and Control*, vol. 69, p. 102910, 2021.

[164] Y. Wu and Q. Zheng, "Adrc or adaptive controller–a simulation study on artificial blood pump," *Computers in biology and medicine*, vol. 66, pp. 135–143, 2015.

[165] W. P. H. M. Carrol JD, Shroff S and R. Sl, "Arterial mechanical properties in dilated cardiomyopathy. aging and the response to nitroprusside," *J Clin Invest*, pp. 1002–1009, 1991.

[166] L. Stevenson, D. Bellil, M. Grover-Mckay, R. C. Brunken, M. Schwaiger, J. H. Tillisch, and H. R. Schelbert, "Effects of afterload reduction (diuretics and vasodilators) on left ventricular volume and mitral regurgitation in severe congestive heart failure secondary to ischemic or idiopathic dilated cardiomyopathy," *The American Journal of Cardiology*, vol. 60, no. 8, pp. 654–658, 1987.

[167] J. MERILLON, G. FONTENIER, J. LERALLUT, M. JAFFRIN, J. CHASTRE, P. ASSAYAG, G. MOTTE, and R. GOURGON, "Aortic input impedance in heart failure: comparison with normal subjects and its changes during vasodilator therapy*," *European Heart Journal*, vol. 5, pp. 447–455, 06 1984.

[168] G. Cotter, Y. Moshkovitz, E. Kaluski, O. Milo, Y. Nobikov, A. Schneeweiss, R. Krakover, and Z. Vered, "The role of cardiac power and systemic vascular resistance in the pathophysiology and diagnosis of patients with acute congestive heart failure," *European journal of heart failure*, vol. 5, pp. 443–51, 08 2003.

[169] A. Y. Her, J.-Y. Kim, E.-Y. Choi, S.-A. Kim, R. S. Jae, C. Y. Shim, S.-M. Kang, J.-W. Ha, and N. Chung, "Value of ventricular stiffness index and ventriculoarterial interaction in patients with nonischemic dilated cardiomyopathy," *Circulation Journal*, vol. 73, no. 9, pp. 1683–1690, 2009.

[170] D. Chemla, J.-L. Hébert, C. Coirault, K. Zamani, I. Suard, P. Colin, and Y. Lecarpentier, "Total arterial compliance estimated by stroke volume-to-aortic pulse pressure ratio in humans," *American journal of physiology-Heart and circulatory physiology*, vol. 274, no. 2, pp. H500–H505, 1998.

# Appendix A

Table A.1: Parameters of the CVS model collected from published heart failure patients' data including respective references etiologies and demographic data (subject to availability).

| **Parameter** | **No. of Patients** | **Values** | **Etiology** | **Age** | **Male (%)** | **Ref.** |
|---|---|---|---|---|---|---|
| $E_{es}$ (mmHg/ml) | 9 | 0.7 ± 0.5 | Idiopathic | 52 ± 9.0 | 78 | [114] |
| | 33 | 0.84 ± 0.09 | Idiopathic | 53 ± 2.0 | 78 | [124] |
| | 31 | 1.17 ± 0.18 | Ischemic (n=5)<br>Non-ischemic (n=32) | - | - | [125] |
| | 92 | 0.55 ± 0.23 | Ischemic (n=750)<br>Idiopathic (n=42) | 58 | 84 | [126] |
| | 42 | 0.63 ± 0.36 | Ischemic (n=21)<br>Idiopathic (n=21) | 60 | 88 | |
| $E_{es,pooled}$ (mmHg/ml) | 254 | 0.71 ± 0.33 | | | | |
| $R_s$ (mmHg s /ml) | 25 | 1.62 ± 0.56 | Idiopathic (n=22)<br>Alcoholic (n=22)<br>Adriamycin[2] (n=1) | 42 ± 15 | 76 | [165] |
| | 15 | 1.47 ± 0.53 | Idiopathic (n=9)<br>Ischemic (n=6) | 56 ± 10 | 60 | [166] |
| | 11 | 1.47 ± 0.08 | Alcoholic (n=7)<br>Idiopathic (n=4) | 55 ± 7 | 100 | [127] |
| | 12 | 1.55 ± 0.6 | Non-obstructive | 48 ± 12 | 100 | [167] |

| | | | | | | |
|---|---|---|---|---|---|---|
| | 102 | 1.60 ± 0.62 | Ischemic | 67 ± 9 | 85 | [128] |
| | 222 | 1.79 ± 1.07 | Idiopathic | 61 ± 12 | 73 | |
| | 10 | 1.10 ± 0.31 | Non-ischemic | 43 ± 12 | 80 | [129] |
| | 56 | 1.43 ± 0.26 | Ischemic (79%) | 69 ± 10 | 80 | [168] |
| $R_{s,pooled}$ (mmHg s/ml) | 453 | 1.65 ± 0.85 | | | | |
| $C_2$ (ml/mmHg) | 25 | 0.85 ± 0.54 | Idiopathic (n=22) Alcoholic (n=2) Adriamycin[3] (n=1) | 42 ± 15 | 76 | [165] |
| | 25 | 1.20 ± 0.35 | Non-ischemic | 58 ± 11 | 52 | [169] |
| | 10 | 1.58 ± 0.72 | Non-ischemic | 43 ± 12 | 80 | [129] |
| | 10 | 1.48 ± 0.75 | Idiopathic | - | - | [170] |
| $C_{2,pooled}$ (ml/mmHg) | 70 | 1.17 ± 0.6 | | | | |
| $R_p$ (mmHg) s/ml) | 306 | 0.1238 ± 0.0986 | Ischemic/idiopathic[4] | 55 ± 11 | 68 | [130] |
| $C_5$ (ml/mmHg) | | 3.1 ± 1.9 | | | | |
| a (mmHg) | 9 | 0.02 ± 0.03 | Idiopathic | 52 ± 9.0 | 78 | [114] |
| b | | 0.031 ± 0.013 | | | | |
| $R_{ML}$ (mmHg s/ml) | | 0.0004 ± 0.002 | | | | |

Table A.2: PV Data for heart failure patients from the literature.

| **No. of Patients** | **EF (%)** | **LVEDV (ml)** | **LVESV (ml)** | **$LVP_{peak}$ (mmHg)** | **Ref.** |
|---|---|---|---|---|---|
| 9 | 20 ± 8 | 310 ± 77 | 249 ± 69 | 122 ± 16 | [114] |
| 6 | 26.6 ± 4.7 | 234.9 ± 16.8 | 171.7 ± 16.8 | 117 ± 16.9 | [131] |
| 102 | 28 ± 7 | 180.2 ± 56.4 | 129.2 ± 47.3 | 104 ± 18 | [128] |
| 222 | 28 ± 9 | 171.1 ± 69.2 | 121.9 ± 56.4 | 107 ± 19 | |
| 33 | 27 ± 9 | 217 ± 77 | 163 ± 73 | | [132] |
| 31 | 25 ± 3.4 | 299.2 ± 27.5 | | 126 ± 4.9 | [125] |
| 23 | 33 ± 2 | 216 ± 12 | | | [124] |
| 10 | 26.2 ± 8 | 227.5 ± 64.5 | 171.5 ± 66 | | [133] |
| 68 | 31.0 ± 6.6 | 227.6 ± 52 | 159.6 ± 43.9 | | [134] |
| 60 | 30.1 ± 4.1 | 226.7 ± 34.3 | 157.6 ± 27.2 | | [135] |
| 50 | 31.1 ± 4.2 | 218.8 ± 28.2 | 148.3 ± 26.4 | | |
| 129 | 25 ± 10 | 237 ± 62 | 166 ± 61 | | [126] |
| 62 | 32 ± 10 | 273 ± 98 | 210 ± 96 | | |
| 40 | 19 ± 5.5 | 246.2 ± 54.1 | | | [136] |
| 40 | 14.5 ± 5.3 | | | | [137] |
| 146 | 26.4 ± 7.4 | | | | [138] |
| 13 | 20 ± 7 | | | | [139] |
| 20 | 21 ± 10 | | | | |
| 25 | 21 ± 8 | | | | |
| 11 | 18 ± 5 | | | | [127] |
| 12 | 32 ± 8 | 222 ± 47 | 148 ± 49 | 132 ± 23 | [140] |
| 306 | 23 ± 7 | | | | [130] |
| 10 | 25 ± 10 | | | | [129] |

| Pooled | | | | | |
|---|---|---|---|---|---|
| 1428 | 25.9 ± 8.5 | 214.9 ± 71.8 | 150.2 ± 63.4 | 109 ± 19.4 | - |